Exhumation of the Ronda peridotite during hyper-extension: New structural and thermal constraints from the Nieves Unit (western Betic Cordillera, Spain)

Eloïse Bessière, Romain Augier, Laurent Jolivet, Jacques Précigout, Adrien Romagny

Tectonics®

RESEARCH ARTICLE
10.1029/2020TC006271

Key Points:

- Foliations and lineation of the Nieves Unit and Ronda peridotite are parallel to their contact. While T_{max} isograds are oblique to this one
- Ophicalcites and magnetite mineralizations are observed, characteristic of low-temperature conditions during a hyper-extensional context
- The contact between the Nieves Unit and Ronda peridotite is a major detachment, in the line with the Los Reales contact, named the NLRD

Supporting Information:

Supporting Information may be found in the online version of this article.

Correspondence to:

E. Bessière,
eloise.bessiere@gmail.com

Citation:

Bessière, E., Augier, R., Jolivet, L., Précigout, J., & Romagny, A. (2021). Exhumation of the Ronda peridotite during hyper-extension: New structural and thermal constraints from the Nieves Unit (western Betic Cordillera, Spain). *Tectonics*, *40*, e2020TC006271. https://doi.org/10.1029/2020TC006271

Received 24 APR 2020
Accepted 28 AUG 2021

Exhumation of the Ronda Peridotite During Hyper-Extension: New Structural and Thermal Constraints From the Nieves Unit (Western Betic Cordillera, Spain)

Eloïse Bessière[1,2], Romain Augier[1], Laurent Jolivet[2], Jacques Précigout[1], and Adrien Romagny[2]

[1]Institut des Sciences de la Terre d'Orléans (ISTO), Université d'Orléans, CNRS, BRGM, Orléans, France, [2]Institut des Sciences de la Terre de Paris (ISTeP), Sorbonne Université, CNRS-INSU, Paris, France

Abstract The Ronda peridotite (Betic Cordillera, Southern Spain) is the largest alpine-type peridotite massif worldwide. Yet, the emplacement mechanism of these mantle rocks is still a highly debated topic. In this study, we aim at better constraining their context of exhumation by focusing on the Nieves Unit, which is mostly composed of Mesozoic metasediments displaying H*T* metamorphism and deformation along the contact with peridotite. The topmost parts of the peridotites and the bottom parts of the Nieves Unit share the same planar/linear fabric parallel to the contact accompanied by component of sinistral kinematic indicators. Raman Spectroscopy on Carbonaceous Material geothermometry then shows a contraction of peak-temperature conditions within metasediments of the Nieves Unit, as well as a north-eastward decrease along strike, highlighting a strong thinning of the unit and a significant obliquity of the isograds to the contact with the peridotites. Local magnetite ores and ophicalcite bodies are finally observed nearby the contact, suggesting a hyper-extension context for the mantle exhumation. Indeed, the Nieves Unit, the Ronda peridotite and the Jubrique Unit, where a strong thinning has also been documented, are all in contact at a triple junction between the western contact of the peridotite and the Nieves/Jubrique contact. Altogether, these features support the idea that the western shear zone limiting the peridotites from the Nieves and Jubrique units is a tilted large-scale extensional detachment that has exhumed mantle rocks from beneath the continental basement (Jubrique Unit) and its Mesozoic cover (Nieves Unit) during an episode of hyper-extension.

1. Introduction

First order non-cylindricity or coexistence of interacting large-scale thrust and extensional shear zones are common features in small orogens hosted in the Mediterranean realm. The tight Betic-Rif arc is typical of this situation where Africa-Eurasia plate convergence strongly interferes with 3-D subduction dynamics to produce a complex crustal-scale tectono-metamorphic evolution (Augier et al., 2005; Azañón & Goffe, 1997; Booth-Rea et al., 2015; Chalouan et al., 2008; Crespo-Blanc et al., 2016; Faccenna et al., 2004; Frizon de Lamotte et al., 1991; García-Dueñas et al., 1992; Gómez-Pugnaire et al., 2019; Jolivet et al., 2003, 2008; Lonergan & White, 1997; Michard et al., 2006; Platt et al., 2013; Spakman & Wortel, 2004; van Hinsbergen et al., 2014; Williams & Platt, 2018). The present-day structure of the two orogenic segments, the Rif and Betic Cordillera on either side of the Alboran Sea, has been described in detail after a century of research. Yet, some first-order questions remain pending, such as the emplacement mechanism of the Ronda and Beni Bousera sub-continental peridotite massifs in the western orogen. These massifs form the largest bodies of sub-continental mantle exposed onshore at the Earth's surface, outcropping over more than 300 km^2 (Obata, 1980). Although these alpine-type peridotites have been thoroughly studied for almost a century (Blumenthal, 1927; de Orueta, 1917), the contribution of the different processes responsible for their exhumation from mantle depth and their emplacement onto the Iberian continental crust are still largely debated. Large ultramafic bodies are most often parts of ophiolite nappes, which belong to an obducted or subducted oceanic lithosphere before obduction. In contrast, the emplacement of sub-continental mantle rocks at shallow crustal levels is understood either as (a) a consequence of subduction and collision processes (Jabaloy-Sánchez et al., 2015; Mazzoli et al., 2013; Mazzoli & Martín-Algarra, 2011; Tubía et al., 1997, 2004, 2009) and/or (b) a consequence of hyper-extension tectonics during a pre-orogenic stage or a genuine syn-orogenic stage and the subsequent involvement of the exhumed mantle material into the

Alpine orogenic structure (Brune et al., 2014; Frasca et al., 2017; Gueydan et al., 2019; Lagabrielle & Bodinier, 2008; Lagabrielle et al., 2010; Masini et al., 2014; Manatschal et al., 2011; Michard et al., 2002, 2006; Pedrera et al., 2020; Précigout et al., 2013).

So far, no consensus exists on the respective contributions of pre-orogenic and syn-orogenic processes to explain the exhumation of the Ronda and Beni Bousera peridotite bodies from mantle depth to their current position, including their final emplacement on crustal rocks. Several models have been yet proposed, such as (a) mantle diapirism (Loomis, 1975; Tubía et al., 2004; Weijermars, 1991; Weijermars et al., 1985; Zeck et al., 1990), (b) development of a mantle core complex (Doblas & Oyarzun, 1989), (c) Mesozoic hyper-extension (Pedrera et al., 2020), (d) extrusion of a mantle wedge during transpressional tectonics (Darot, 1974; Mazzoli & Martín-Algarra, 2011; Tubía & Cuevas, 1986; Tubía et al., 1997, 2013; Vauchez & Nicolas, 1991), (e) detachment faulting during extensional collapse of the Betic-Rif belt (Platt et al., 2003; Van der Wal & Vissers, 1993), or (f) tectonic inversion of a thinned back-arc lithosphere during slab roll-back (Booth-Rea et al., 2005; Frasca et al., 2017; Garrido et al., 2011; Gueydan et al., 2019; Hidas et al., 2013; Précigout et al., 2013).

Discriminating between these possible emplacement modes, with a probable combination of several processes, requires that the tectonic timing of each stage is well constrained. Depending on the emplacement model, proposed ages of the exhumation of the Ronda or Beni Bousera peridotites from mantle depths in fact scan a long period: (a) Paleozoic (Kornprobst, 1976; Rossetti et al., 2010, 2020; Ruiz-Cruz & Sanz de Galdeano, 2014), (b) Mesozoic (Michard et al., 2002; Pedrera et al., 2020; van Hinsbergen et al., 2014; Vissers et al., 1995) or (c) Oligo-Miocene (Frasca et al., 2015; Garrido et al., 2011; Gueydan et al., 2015; Hidas et al., 2013; Marchesi et al., 2012; Précigout et al., 2013). However, most available radiometric age constraints for the tectonic evolution of the Western Betic-Rif orogen in the literature cluster around 22–20 Ma. Such an exclusive Miocene history, including the final emplacement of the peridotite into the upper crust, seems unlikely to encompass the entire process of exhumation (Frasca et al., 2016; Garrido et al., 2011; Gueydan et al., 2015; Lenoir, 2001; Marchesi et al., 2012; Mazzoli & Martín-Algarra, 2011; Platt & Vissers, 1989; Tubía et al., 1997, 2004, 2013).

Figure 1 illustrates the differences between some published, either commonly accepted or recent models in terms of mechanisms, geodynamic setting and timing. There is little in common between models favoring a Miocene or Mesozoic exhumation by hyper-extension and those involving Miocene exhumation within a subduction zone. The extensional models of Précigout et al. (2013), Frasca et al. (2017) or Pedrera et al. (2020) both involve exhumation by hyper-extension, but the timing and geodynamic contexts are entirely different (respectively Miocene late-orogenic back-arc extension vs. Mesozoic pre-orogenic rifting). Such a diversity of models on a single mountain belt has no equivalent elsewhere and this puzzling situation in such an emblematic mountain belt where sub-continental mantle has been exhumed deserves reassessment. A better understanding of the emplacement mechanism(s) of the Ronda peridotite would shed light on mantle exhumation, as well as on the dynamics of tight arcs formed by slab retreat in general. The lack of consensus in this region is partly due to the 3-D complexity of the finite geometry of the Betic-Rif orogen, where extensional detachments and low-angle thrust faults are found at close distance (Chalouan & Michard, 2004; García-Dueñas et al., 1992; Jabaloy et al., 1993; Lonergan & Platt, 1995; Martínez-Martínez et al., 2002; Pedrera et al., 2020; Platt, 1986; Platt et al., 2005; Platt & Vissers, 1989; Vissers et al., 1995) and to the clustering of many radiochronologic ages around 22–20 Ma (Augier et al., 2005; Esteban et al., 2011; Frasca et al., 2017; Homonnay et al., 2018; Loomis, 1975; Michard et al., 2006; Monié et al., 1991, 1994; Platt et al., 2003, 2005, 2006; Platt & Whitehouse, 1999; Priem et al., 1979; Sánchez-Rodríguez & Gebauer, 2000; Sánchez-Vizcaíno et al., 2001; Sosson et al., 1998; Tubía & Ibarguchi, 1991; Whitehouse & Platt, 2003; Zeck & Williams, 2001), which has not been explained so far. The Ronda peridotite is associated with high-temperature (H*T*) crustal metamorphic rocks cropping out in tectonic windows such as the Guadaiza tectonic window or along the western contact, the Jubrique Unit or the Nieves Unit, which structural and metamorphic characteristics have been used to produce the various models published so far (Figure 1). Several recent studies have indeed documented the H*T* metamorphism observed in these units, including the Blanca-type units, the Jubrique Unit and the Nieves Unit (i.e., the Betic part of the Dorsale Calcaire Complex; Acosta-Vigil et al., 2014; Barich et al., 2014; Massonne, 2014; Mazzoli et al., 2013; Negro et al., 2006; Ruiz-Cruz & Sanz de Galdeano, 2014). Two of these studies (Mazzoli et al., 2013; Mazzoli & Martín-Algarra, 2011)

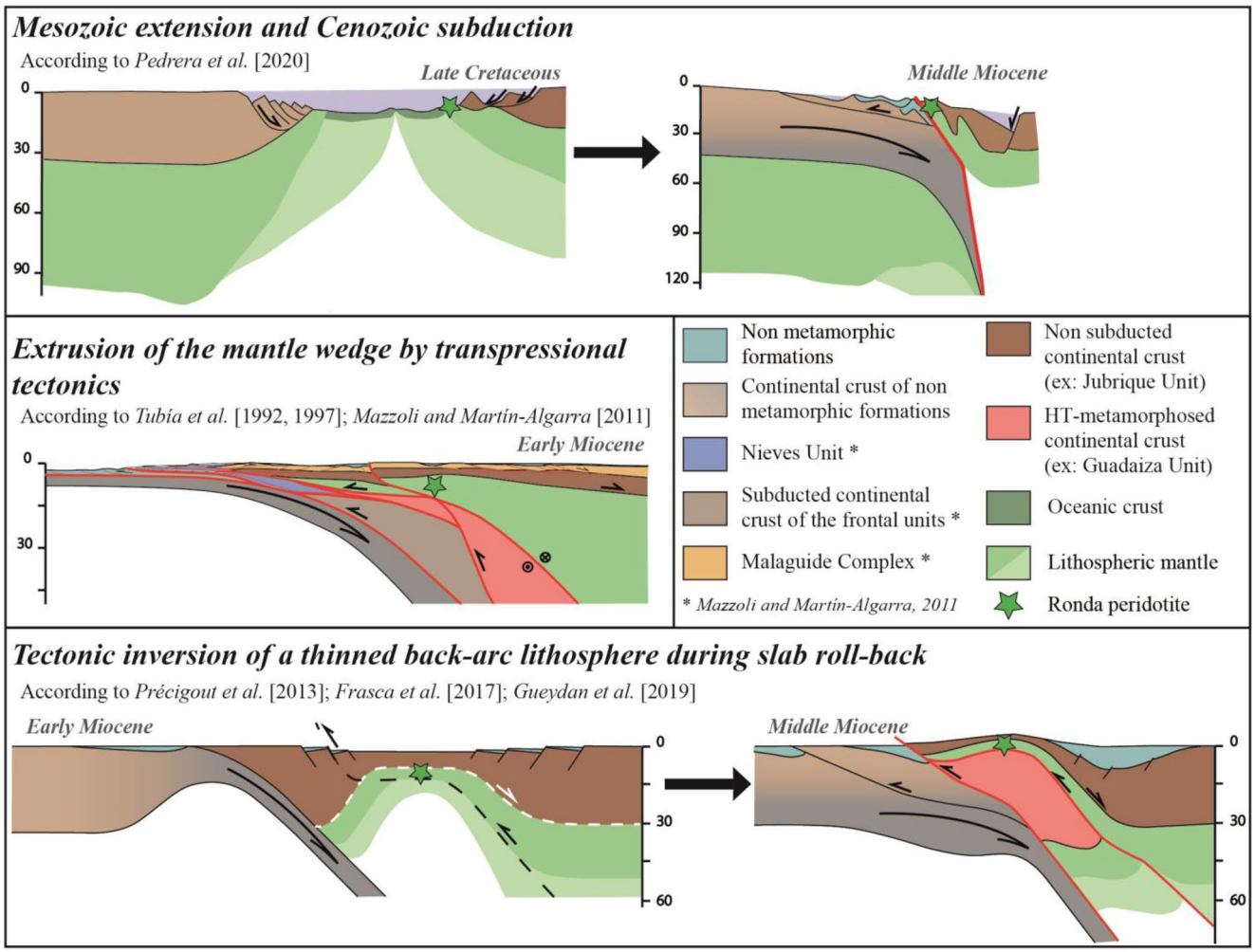

Figure 1. Previous models proposed to account for the exhumation and the emplacement of the Ronda peridotite from mantle depth. (a) Exhumation of the sub-continental mantle during the Mesozoic from mantle depth and emplacement during the Cenozoic through tectonic inversion processes (Pedrera et al., 2020); (b) Extrusion of a mantle wedge in a transpression context (Mazzoli & Martín-Algarra, 2011; Tubía et al., 1992, 1997); (c) Exhumation of the sub-continental mantle during the Miocene in a back-arc environment at the rear of a retreating slab subsequently emplaced over the Iberian margin by tectonic inversion (Frasca et al., 2017; Gueydan et al., 2019; Précigout et al., 2013).

described a cross-section through the metamorphic part of Nieves Unit, indeed a key element to better understand the exhumation process of mantle rocks in this area. The westward high-temperature thrusting model for the contact of the Ronda peridotite and the sediments of the nearby Nieves unit would suggest NW-SE stretching lineations while our own field observations show NE-SW stretching lineations trending parallel to the contact. This alone shows that at least a part of the existing model is inconsistent with part of the observations. Then, the hyper-extension hypothesis has been proposed based on observations along the contact between crustal units and the peridotite, but the contact with the sediments has never been explored in that respect.

In order to discriminate between all the proposed models and answer the question of the exhumation mechanism of these sub-continental peridotites, this paper is thus focused on the metasediments of the Nieves Unit. Indeed, this less studied unit, showing a *HT* metamorphism directly related to the Ronda peridotite emplacement is key in this debate. According to the several proposed models, the tectono-metamorphic records in the Nieves Unit will be completely different. This paper, first summarizes the available data, and then reports the result of a new field investigation including detailed field mapping, structural geology combined with a detailed mapping of peak-temperature conditions by Raman spectroscopy on carbonaceous material (RSCM) geothermometry. Our new investigations along the contact of the Ronda peridotite with

the Nieves Unit lead us reconsidering the emplacement mechanism of the Ronda peridotite and to argue in favor of a hyper-extension model.

2. Geological and Geodynamic Settings

2.1. The Western Mediterranean and the Betic-Rif Orogen

The Betic-Rif orogen in southern Spain and northern Morocco corresponds to the westernmost parts of the Alpine arcuate mountain belt that encircles the western Mediterranean basin (Figure 2a; e.g., Lonergan, 1993). This segment results from complex interrelations between the overall Africa/Iberia convergence since late Cretaceous times and 3-D dynamics of the Tethyan oceanic slabs, both responsible for the current arcuate shape of the belt (Andrieux et al., 1971; Dercourt et al., 1986, 1993; Do Couto et al., 2016; Faccenna et al., 2004; Jolivet et al., 2008; Lonergan & White, 1997; Stampfli, 2000). The Betic Cordillera is classically divided into unmetamorphosed External Zones and metamorphic Internal Zones (Figure 2a; Egeler & Simon, 1969a, 1969b; Garcia-Castellanos et al., 2002), separated by an internal-external boundary zone mostly composed of allochthonous flyschs, similarly to other Alpine mountain belts in the Mediterranean realm (Figure 2b; Vissers et al., 1995).

The External Zones correspond to the tectonic inversion of the African and Iberian paleo-passive margins composed of thick Triassic to Miocene sedimentary series (Crespo-Blanc & Frizon de Lamotte, 2006; Flinch et al., 1996; García-Hernández et al., 1980; Pedrera et al., 2020; Platt et al., 2003). Thanks to several decollements rooted in the Triassic evaporites, a fold-and-thrust belt formed coevally with the Guadalquivir (Spain) and Gharb (Morocco) foreland basins during the Miocene (Allerton et al., 1993; Chalouan & Michard, 2004; Garcia-Castellanos et al., 2002; Pedrera et al., 2020; Sanz de Galdeano & Vera, 1992). The Flyschs Complex is composed by upper Jurassic to lower Miocene distal turbiditic deposits and radiolarites, evidence of deep depositional environments over a thinned continental crust or directly over an oceanic crust (Figure 2; Didon et al., 1973; Durand-Delga, 1980; Durand-Delga et al., 2000; Guerrera et al., 1993, 2005; Sanz de Galdeano & Vera, 1992).

The Internal Zones correspond to structural culminations exhumed below extensional shear zones of regional extent, reworking the pre-existing nappe structure (Figure 2b; e.g., Martínez-Martínez & Azañón, 1997; Platt, 1986; Vissers et al., 1995). They are traditionally divided into three main metamorphic complexes, from bottom (or most internal) to top: (a) the Nevado-Filabride Complex, (b) the Alpujárride-Sebtide Complex and (c) the Malaguide-Ghomaride Complex (Blumenthal, 1927; Chalouan, 1986; Kornprobst & Durand-Delga, 1985; Torres-Roldán, 1979), each separated by crustal-scale low-angle ductile-to-brittle extensional shear zones mostly described in the Betics (Agard et al., 2011; Augier, Agard, & et al., 2005; Augier et al., 2015; Augier, Jolivet, & Robin, 2005; Behr & Platt, 2012; Crespo-Blanc et al., 1994; Galindo-Zaldívar et al., 1989; García-Dueñas & Balanyá, 1986; García-Dueñas et al., 1986, 1992; Jabaloy et al., 1993; Lonergan & Platt, 1995; Martínez-Martínez et al., 2002; Platt, 1986; Platt & Behrmann, 1986; Platt et al., 2005; Platt & Vissers, 1989; Vissers et al., 1995). The Filabres Shear Zone and Malaguide-Alpujárride Contact separate the Nevado-Filabride Complex from the Alpujárride Complex (García-Dueñas et al., 1992) and the Alpujárride Complex from the Malaguide Complex, respectively (Figure 2b; Vissers et al., 1995).

The Alpujárride-Sebtide Complex is the largest complex outcropping in the Internal Zones of the Betic-Rif belt that mostly forms the basement of the Alboran domain (e.g., Platt et al., 1998) including the mantle peridotite bodies of Ronda, Alpujata and Carratraca in the Betics and Beni Bousera in the Rif (Balanyá et al., 1997; Cuevas et al., 1990; Esteban et al., 2004; Frasca et al., 2016; Garrido et al., 2011; Gueydan et al., 2015; Lenoir, 2001; Marchesi et al., 2012; Mazzoli & Martín-Algarra, 2011; Platt & Vissers, 1989; Sanz de Galdeano, 2017; Tubía et al., 1997, 2004, 2013). The division of this complex is based on stratigraphic, metamorphic and structural criteria (Aldaya et al., 1979, 1991; Azañón et al., 1998; Tubía et al., 1992). It is composed of a common stratigraphic succession of variable thicknesses, including from base to top: Paleozoic dark graphitic micaschists and gneiss locally partially molten (Lafuste & Pavillon, 1976; Zeck et al., 1989), Permian meta-conglomerates, Permo-Triassic meta-quartzites and micaschists, and Triassic marbles and dolomites (Kozur et al., 1974). Following the syn-to post metamorphic stacking of these units, this metamorphic complex has been subsequently shredded in several sub-units by the activity of low-angle extensional shear zones, low-angle normal (Azañón et al., 1997; Azañón & Crespo-Blanc, 2000; Crespo-Blanc, 1995;

10.1029/2020TC006271

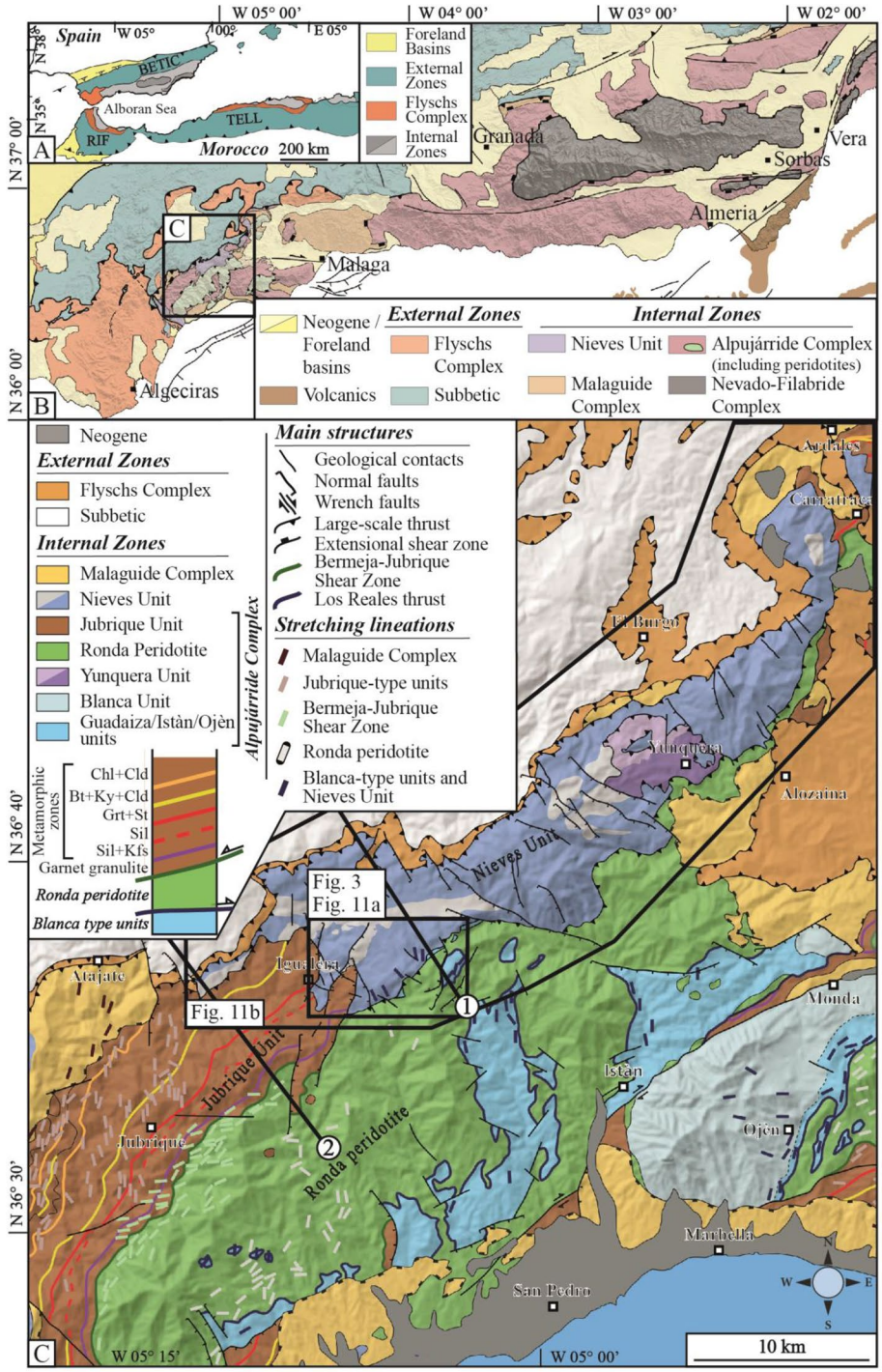

Figure 2. Geological map of the Betic Cordillera and of the study area showing the major tectonic features and the main geological subdivisions. (a) Simplified geological map of the Gibraltar arc and the western termination of the Mediterranean orogenic system. (b) Geological map of the southern parts of the Betic Cordillera, modified after Do Couto et al. (2016). The study area is located on the western termination of the Ronda peridotite massif, in the western Sierra de Nieves area. (c) Geological map of the western part of the Betic Cordillera showing the main geological formations, the major contacts and metamorphic features and a synthesis of the stretching lineations, after Balanyá et al. (1997); Negro et al. (2006); Esteban et al. (2008); Mazzoli and Martín-Algarra (2011); Précigout et al. (2013); Tubía et al. (2013); Pedrera et al. (2015); Williams and Platt (2018). Mineral abbreviations are after Whitney and Evans (2010).

Crespo-Blanc et al., 1994; García-Dueñas et al., 1992; Martínez-Martínez & Azañón, 1997) and high angle normal faults (e.g., Booth-Rea et al., 2003; Crespo-Blanc & Campos, 2001; García-Dueñas et al., 1992). Some of these faults produce important omissions overprinting former geometries and thermal structures (Booth-Rea et al., 2003; Crespo-Blanc & Campos, 2001).

2.2. The Sierra Bermeja Area

The western Alpujárride Complex (Figure 2) is made up of several tectonic units, which are as follows in ascending order: (a) the Guadaiza, Istan and Ojén units, belonging to the so-called Blanca group (e.g., Balanyá et al., 1997); and (b) the ultramafic slices of the Ronda region and the Jubrique Unit, which constitutes the highest Alpujárride unit directly located below the Malaguide Complex. The Sierra Bermeja area encompasses the Jubrique Unit, the Guadaiza Unit, the Ronda peridotite and the Nieves Unit (Figure 2c). In their current position, the Jubrique Unit and the Ronda peridotite compose the hangingwall of the so-called Los Reales Nappe that overthrusts the Blanca group and Flyschs Complex, while the Jubrique Unit and the Ronda peridotite are separated by the so-called Bermeja-Jubrique Shear Zone inherited from a large-scale exhumation stage (Figure 2; Balanyá et al., 1997; Lundeen, 1978; Précigout et al., 2013; Reuber et al., 1982). The tectono-metamorphic record in the Nieves Unit, as well as the relationships between the Nieves Unit, the Jubrique Unit and the Ronda peridotite, constitute the main scope of this study.

2.2.1. Jubrique Unit

The Jubrique Unit is a complete and extremely condensed crustal-section displaying H*T* migmatites and granulites that grade upward into low-grade metasediments structurally overlying the Ronda peridotite (Balanyá et al., 1997; Negro et al., 2006). From bottom to top, this crustal sequence is composed by: (a) granulitic gneisses and kinzigites, (b) migmatitic gneisses, (c) Paleozoic metapelitic gneiss and micaschists and (d) Permian-Triassic low-grade phyllites with few quartzitic levels and minor marbles (Balanyá et al., 1997; Loomis, 1972). The highly tectonized and serpentinized contact between the crustal sequence and ultramafic massif of the Ronda peridotite is characterized as a HT ductile crustal-scale shear zone, the Bermeja-Jubrique Shear Zone (BJSZ), corresponding to a flat detachment zone on the paleo-Moho (Figure 2c; Balanyá et al., 1997; Lundeen, 1978; Précigout et al., 2013; Reuber et al., 1982). The upper contact of the Jubrique Unit corresponds to the Malaguide/Alpujárride contact, a major low-angle normal fault with ENE displacement, active in the early Miocene (Lonergan & Platt, 1995). A penetrative mylonitic foliation in both the Jubrique Unit and the Ronda peridotite is parallel to lithological contacts (Figure 2c; Balanyá et al., 1997; Barich et al., 2014; Précigout et al., 2013). Foliation planes dip toward the NW-NNW in the north and toward the west in the south and the stretching lineation trend is N-S in most of the unit (Figure 2c; Balanyá et al., 1997; Ruiz-Cruz & Sanz de Galdeano, 2014; Williams & Platt, 2018). Closer to the contact with the Ronda peridotite, in the deep parts of the Jubrique Unit, the migmatitic gneiss show a strong NE-SW stretching lineation (Figure 2c) parallel to the strike of the BJSZ (Balanyá et al., 1997). More recent studies of Précigout et al., (2013) and of Johanesen and Platt (2015) also show that this NE-SW intense stretching in the top of the peridotite and the base of the Jubrique Unit is associated with a preferred top-to-the SW sense of shear (Johanesen & Platt, 2015), compatible with the overall bending of foliation trajectories toward the contact and associated shear zones (Précigout et al., 2013). From the contact with the Ronda peridotite to the top of the crustal sequence, metamorphic grades present a steep gradient of *P-T* conditions from around 12–14 kbar and ~780°C in felsic granulites, to 7–9 kbar and 400°C in phyllites in contact with the low-grade Malaguide Complex (Balanyá et al., 1997; Loomis, 1972; Massonne, 2014; Negro et al., 2006; Torres-Roldán, 1979) and metamorphic isograds are roughly parallel to the contact with the Ronda peridotite (Figure 2c; Balanyá et al., 1997). The steep pressure-temperature gradient through this crustal sequence shows that the Jubrique Unit has undergone a drastic thinning coeval with an almost isothermal decompression, classically associated with the clustering of most radiochronological ages between 23 and 19 Ma (Argles et al., 1999; Balanyá et al., 1997; Barich et al., 2014; Platt et al., 2003; Priem et al., 1979). According to Balanyá et al. (1997), the Jubrique Unit may have been reduced to 1/3 of its initial thickness.

2.2.2. Ronda Peridotite

The Ronda peridotites *lato sensu* compose the basal portion of the upper Alpujárride-Sebtide sequence. They form a series of ultramafic massifs that overthrusted the Alpujárride units cropping out as tectonic

windows such as the Guadaiza window (Figure 2c). Their "hot" emplacement is marked by a dynamo-thermal metamorphic aureole formed at the expense of the Alpujárride footwall rocks made of the Blanca group units (Cuevas et al., 2006; Esteban et al., 2008). The timing of H*T* metamorphism is constrained by U/Pb dating of zircons either directly from the metamorphic sole (the lithoclastic gneiss; Lundeen, 1987) or from synkinematic leucogranite dykes that emanate from the aureole and intrude the overlying peridotites, providing ages of 18.8 ± 4.9 Ma (Sánchez-Rodríguez & Gebauer, 2000) and 21.8 ± 0.5 Ma (Esteban et al., 2007). The basal contact of the peridotite is associated with a thin H*T* shear zone with a top-to-the-N sense of shear in the Guadaiza and Istán tectonic windows (Acosta-Vigil et al., 2014; Esteban et al., 2008) and a top-to-the-ENE sense of shear in the Ojén tectonic window (Tubía et al., 1997, 2013) drawing a large-scale curved pattern. Using U/Pb ages on zircon closely associated with the H*T* metamorphic facies, several concordant ages at ca. 20 Ma were ascribed to a H*T* event recorded by the lower parts of the Jubrique Unit (Platt & Whitehouse, 1999). Numerical models of the thermal evolution of a cooling crust suggest that these rocks were at a depth of about 52 km at ca. 27 Ma when extension started in the Alboran Domain and reached about 16 km some 20 Ma ago. $^{40}Ar/^{39}Ar$ ages in the same region are also around 20 Ma, suggesting very-high late exhumation rates for the peridotite (Bessière et al., 2021; Frasca et al., 2017; Monié et al., 1994; Sosson et al., 1998). However, well constrained U/Pb ages on zircon at ca. 290–300 Ma ages were recently obtained on the H*T* metamorphism gneissic envelope of the Beni Bousera and the Ronda peridotites, suggesting that the H*T* metamorphism is probably partly inherited from the Variscan orogeny (Barich et al., 2014, 2016; Gómez-Pugnaire et al., 2019; Massonne, 2014; Rossetti et al., 2020). The timing of partial melting appears therefore still not consensual.

The Ronda peridotite *s.s.*, and more specifically its western part, was the subject of several detailed studies (Garrido et al., 2011; Lenoir, 2001; Obata, 1980; Précigout et al., 2007, 2013; Soustelle et al., 2009; Van der Wal & Bodinier, 1996; Van der Wal & Vissers, 1993, 1996). It is characterized by a 1.5–2 km thick unit of variably serpentinized lherzolite and harzburgite with minor dunite. The mean composition of the Ronda peridotite includes ~70% of forsterite, ~20% of enstatite, ~5% of diopside, and ~5% of spinel (Garrido et al., 2011; Obata, 1980; Précigout et al., 2007). Based on structural and petrological features (Dickey, 1970; Garrido et al., 2011; Hernández-Pacheco, 1967; Lundeen, 1978; Obata, 1977, 1980; Obata & Lundeen, 1979; Tubía, 1994; Van der Wal & Vissers, 1996), the following domain sequence has been described as follows, from top to bottom: (a) garnet/spinel mylonite, (b) spinel tectonite, (c) spinel granular (coarse-grained) peridotite, and (d) plagioclase tectonite (Obata, 1980; Van der Wal & Vissers, 1996). Pervasive pyroxenite layers and a few bands/lenses of mafic rocks are also present (Morishita et al., 2001). The foliation is oriented N50°E and dips 80°NW in average, with the development of a progressive strain gradient from the spinel tectonite to the mylonitic domain (Précigout et al., 2013). In these two domains, the stretching lineation is nearly horizontal and presents a consistent NE-SW orientation associated with a left-lateral kinematics (Argles et al., 1999; Balanyá et al., 1997; Précigout et al., 2013; Van der Wal & Vissers, 1996). Boudins and isoclinal folds are locally observed in the spinel tectonite and Grt/Spl mylonite with NE-SW axes slightly dipping toward the NE (Garrido & Bodinier, 1999; Précigout et al., 2007), as observed in the bottom parts of the Jubrique Unit (Z5 and Z6 of Balanyá et al., 1997). The spinel tectonite to granular peridotite transition is characterized by a strong coarsening of grain-size associated with the disappearance of the tectonic foliation, giving rise to the so-called "recrystallization front" (Lenoir, 2001; Vauchez & Garrido, 2001). This "front" results from either static recrystallization ("asthenopherization") of a previously deformed lithosphere (Van der Wal & Vissers, 1996) or an overprint by crystal-plastic deformation in the spinel tectonite zone (Johanesen et al., 2014). The plagioclase tectonite domain is marked by a penetrative foliation in the lherzolite, while the harzburgite and dunite show a less penetrative foliation, generally striking N110°–130° and dipping 40°–60°N, with an associated lineation trending N45°E and plunging 45°N (Précigout et al., 2013). In addition, the pyroxenite layers are affected by hectometric folds in this domain, the axial plane of which is parallel to the foliation. Metric folds are also observed, but they are reworked by the plagioclase-bearing foliation (Van der Wal & Vissers, 1996; Précigout et al., 2013). The km-scale fold affecting the sole of the Jubrique-Ronda peridotite massif shows a reverse limb cross-cut by mylonitic shear zones developed in the plagioclase stability field, testifying for thrusts cutting the km-scale fold (Hidas et al., 2013). While Lu/Hf and U/Th/Pb isochrons yield ages between 300 ± 8 and 88.6 ± 3.1 Ma, U/Pb on zircons yield ages scattered between more than 1,800 Ma to ca. 21 Ma, including numerous ages between 180 and 131 Ma in the Ronda and Beni Bousera peridotites (Blichert-Toft, 1999; González-Jiménez et al., 2017; Sánchez-Rodríguez &

Gebauer, 2000). This led Sánchez-Rodríguez and Gebauer (2000) to conclude that the protolith of the pyroxenite layers has been formed during lower Jurassic to lower Cretaceous times reflecting partial-melting and melt extraction in the mantle during Mesozoic rifting of the alpine Tethys domain. Interestingly, these ages fall into the same range of ca. 180–185 Ma ages based on U/Pb on zircons in the mafic protolith of the Ojén eclogites (Sánchez-Rodríguez & Gebauer, 2000). Similar conclusions have been reached about the mafic eclogites from the Nevado-Filabride Complex (Puga et al., 2011). A Late Oligocene-Miocene HT event is recorded in the rim of zircons with ages around 25–20 Ma, close to the age of undeformed anatectic granites cross-cutting both the peridotite bodies and some crustal units in the Betics and Rif (Frasca et al., 2017; Marchesi et al., 2012; Rossetti et al., 2010; Sánchez-Rodríguez & Gebauer, 2000; Varas-Reus et al., 2017). For further discussions about the timing of exhumation of the Ronda peridotite s.l., the readers may also refer to Bessière et al. (2021).

2.2.3. Nieves Unit

The Nieves Unit (Dürr, 1967) is composed of Tethyan carbonate platform deposits, including limestones, dolostones, marls and condensed pelagic successions of Norian to Cretaceous ages, completed by the Nava Breccia unconformably deposited on top of the sedimentary sequence (Blumenthal, 1933; Dürr, 1963, 1967; Martín-Algarra, 1987; Martín-Algarra et al., 1998; Martín-Algarra & Estévez, 1984; O'Dogherty et al., 2001). The Nieves Unit has been traditionally linked to the evolution of the Internal Zones, as suggested by paleomagnetic data (Berndt et al., 2015; Crespo-Blanc et al., 2016; Feinberg et al., 1996; Osete et al., 1988; Platzman et al., 1993; Platzman & Lowrie, 1992; Villasante-Marcos et al., 2003;) as the probable detached sedimentary cover from more internal units (Didon et al., 1973; Chalouan et al., 2008). It has been interpreted as the cover of the Malaguide Complex (Dürr, 1963; Michard et al., 2002) or the Alpujarride-Sebtide Complex (Chalouan & Michard, 2004). Generally considered as non-metamorphic and little deformed in upper crustal levels, the Nieves Unit however presents strong metamorphic recrystallisations and an intense ductile deformation in the vicinity of the contact with the Ronda peridotite. There, carbonate rocks are turned into marbles and present H*T* parageneses including forsterite + diopside + clinohumite + spinel equilibrated at temperatures of ca. 600–700°C (Mazzoli et al., 2013). Metamorphic conditions drastically decrease upward to temperatures as low as 330°C over only ca. 2 km (Mazzoli et al., 2013) that can be compared to the extreme metamorphic field gradient within the adjacent Jubrique Unit. So far, this steep gradient has been related to the H*T* metamorphic aureole developed below the Ronda peridotite within the Blanca group units (e.g., Lundeen, 1978; Mazzoli et al., 2013; Mazzoli & Martín-Algarra, 2011; Tubía et al., 1997). However, the shape of metamorphic isograds in map view within the Nieves Unit is not known and has only been studied along a single NW-SE section (i.e., the A-397 road-cut; Mazzoli et al., 2013). Furthermore, deformation dominated by isoclinal folding presents a strong gradient toward the contact with the Ronda peridotite. Both fold axes and the main regional foliation are generally steeply dipping toward the NW, but also locally to the SE in the vicinity of the Ronda peridotite (Martín-Algarra, 1987; Mazzoli & Martín-Algarra, 2011). According to Mazzoli et al. (2013), the stretching lineation, marked by elongated calcite and dolomite is oriented NW-SE and is associated with top-to-the-NW sense of shear. These authors envisioned the tectono-metamorphic record of the Nieves Unit as the results of the emplacement of the Los Reales Nappe, the basal part of a large-scale mantle extrusion wedge (Gueydan et al., 2019; Mazzoli et al., 2013). In this scheme, the Nieves unit appears as a "frontal unit" equivalent to the Guadaiza unit metamorphosed and sheared in the footwall of a large-scale thrust (Balanyá et al., 1997). However, kinematics of the emplacement in the frontal parts is in conflict with kinematics that is exposed in the tectonic windows below the Los Reales nappe (Esteban et al., 2008; Williams & Platt, 2018). In this area, the metamorphic sole shows a clear and consistent N-S lineation associated with a top-to-the-N shear sense recorded in the field of partial-melting (Esteban et al., 2008).

3. Field Observations: Large-Scale Structure and Strain Markers

A detailed field survey was conducted over an area of ca. 7 × 4 km including mostly rocks of the Nieves Unit and the Ronda peridotite, the contact of which is exposed over more than 7 km along-strike. In Figure 3, we provide a detailed map and aerial image analysis in order to complement the existing maps (IGME; Martín-Algarra, 1987; Mazzoli et al., 2013; Pedrera et al., 2015). Mapping was complemented by structural observations presented in the next section.

10.1029/2020TC006271

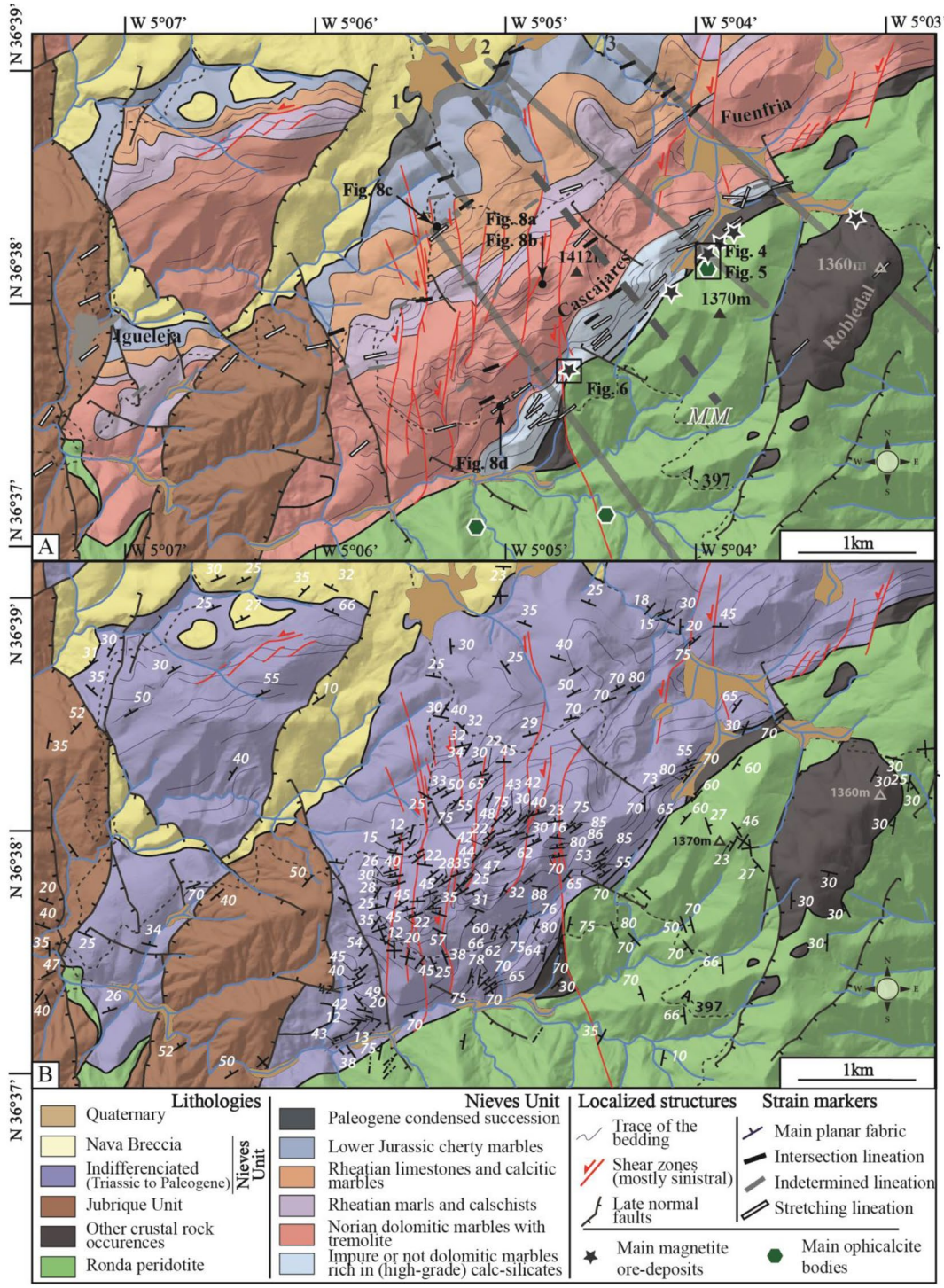

Figure 3. A new tectonic map of the studied area. (a) Lineations map. Indicated are the sections presented in Figure 12. (b) Main planar fabrics map. Data are mostly from this study measurements and a compilation of existing data (IGME; Dürr, 1967). Faults and lithological outlines are from new fields observations and a compilation of existing maps (IGME; Mazzoli et al., 2013; Mazzoli & Martín-Algarra, 2011; Pedrera et al., 2015). Litho-stratigraphy is based on Mazzoli et al. (2013). Traces of lithologic boundary are shown to allow constraining either the geometry of the localized shear zones or their apparent sinitral offset. The main ophicalcite bodies, the magnetite mineralized zones (old mines) and other ore deposits are located. Also indicated is the position of the pictures of Figures 4–6 and 8.

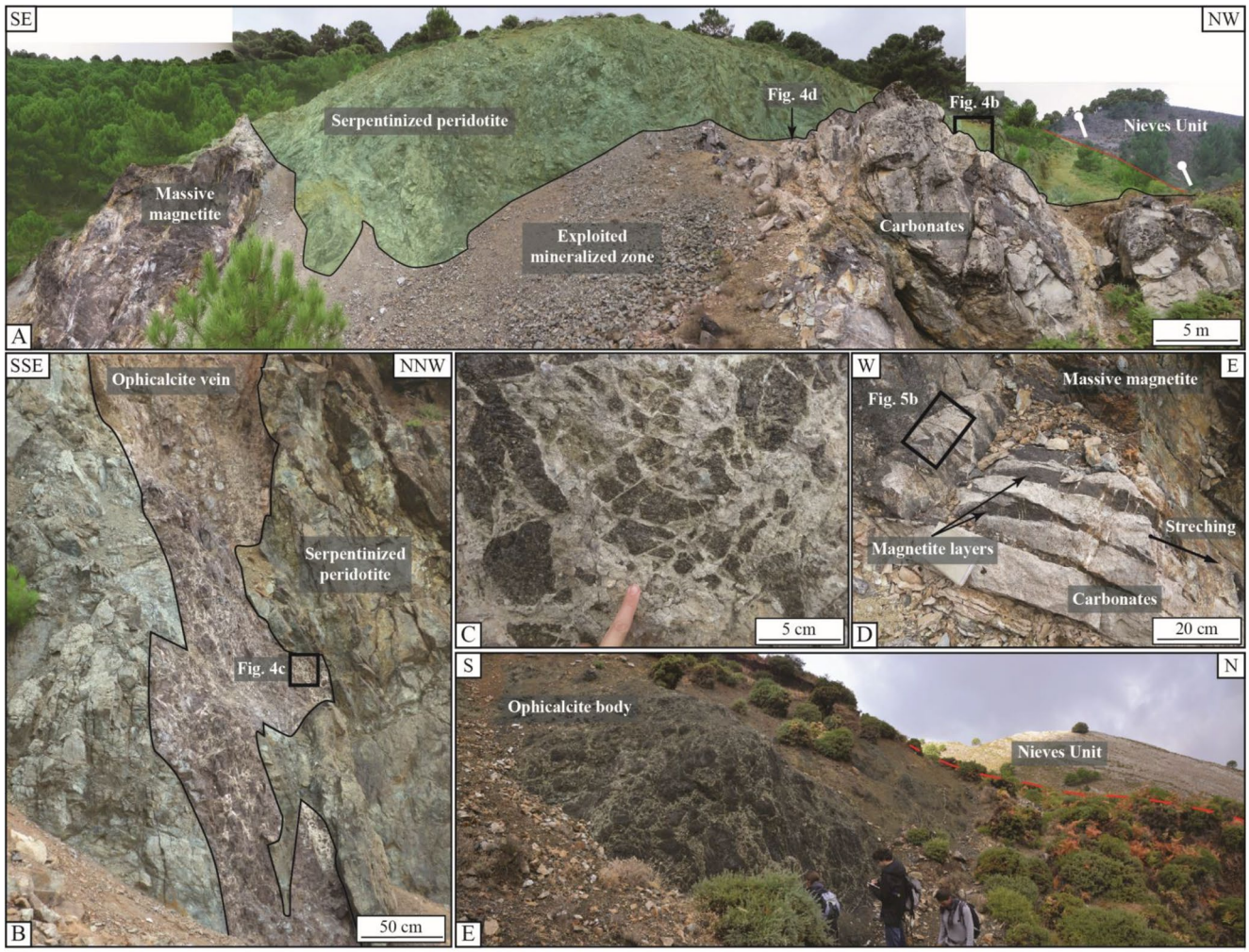

Figure 4. Detailed field relationships between the Nieves Unit and the Ronda peridotite in the eastern mine area (Puerto de Robledal). (a) Up to 180° panorama of the massive-magnetite mining area. The main foliation of the peridotite is parallel to either the contact or the internal main planar fabrics of the carbonate rocks from the Nieves Unit. It is worth mentioning that the Nieves Unit is here lying structurally above the Ronda peridotite. Besides, rocks are ductily deformed without significant brittle reworking. (b) Small-scale, non-mappable ophicalcite body within the serpentinized peridotites. (c) Close-up view of the ophicalcites. (d) Magnetite layers intercalated within the calcite marbles from the Nieves Unit. Only a ductile and fluid-enhanced deposits are present. Magnetite-rich layers are truncated in the direction of the stretching lineation and strongly folded (e) Large-scale ophicalcite body located between the Nieves Unit and the serpentinized peridotite. Again, the Nieves Unit whose main planar fabrics appear clearly in the landscape is lying above the Ronda peridotite.

3.1. Main Complements to the Geological Map

The main lithofacies subdivisions proposed on the IGME maps (Spanish Geological Survey) (del Olmo Sanz et al., 1981, 1987; Piles Mateo et al., 1973) and other existing maps were drawn within the Nieves Unit irrespectively of the metamorphic grade or finite strain experienced by the rocks (Martín-Algarra, 1987). These main lithologies include carbonate rocks often turned into massive calcite and dolomite marbles, together with local chert layers and minor amounts of calcschists, with protoliths dated from the upper Triassic and lower Jurassic (Martín-Algarra, 1987). The geological outlines were marginally modified in the vicinity of the contact between the Nieves Unit and the Ronda peridotite (Figure 3). Indeed, we distinguish mappable bodies or punctual occurrences of massive magnetite deposits and ophicalcites that developed at the direct contact (Figures 4–6). In addition, the structural position of crustal rocks units, including paragneisses, orthogneisses and migmatites, was reconsidered with respect to the Ronda peridotite (Figure 7). These rocks that mostly crop out in the Robledal area now appear as a klippe lying on top of the peridotite body (Figures 3 and 7). Other structural elements having a map-scale expression such as oblique shear zones or traces of the bedding also complete the map (Figure 3), together with a dense array of late brittle faults that

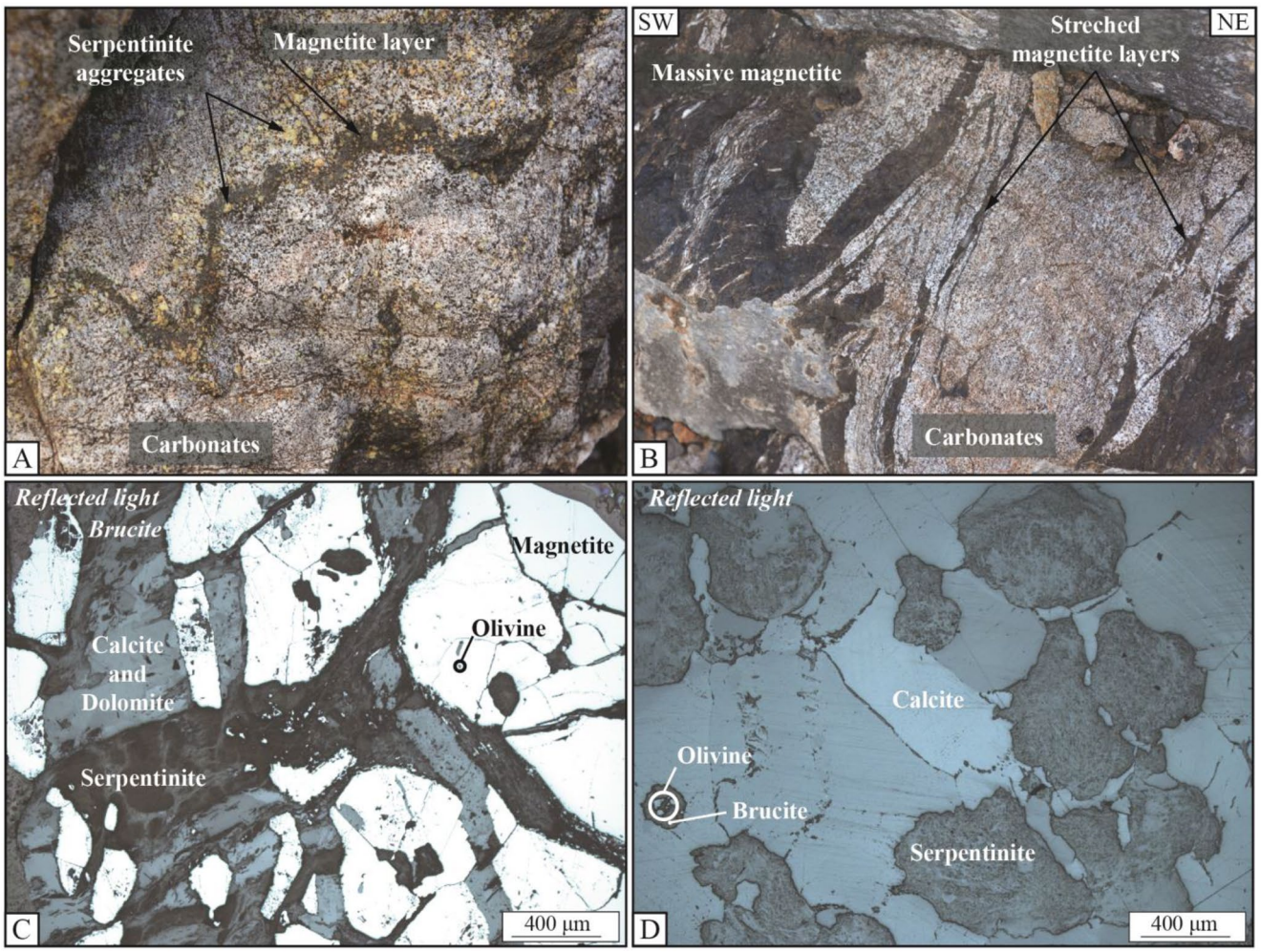

Figure 5. Field and microscopic observations of the magnetite layers in the eastern magnetite mine area (Puerto de Robledal). (a) Folded magnetite layers containing serpentinite aggregates within both the dark layers or the carbonates rocks. (b) Massive magnetite layers are truncated and ductily folded by continuous deformation. Samples presented in insets c and d are coming from that part of the outcrop. (c and d) Microscopic observations of samples from the mineralized zones in reflected-light mode. Note that the growth of both brucite and magnetite post-dates and overprint metamorphic olivine.

were reported using new field mapping and a complication of existing maps (Mazzoli et al., 2013; Pedrera et al., 2015).

3.1.1. Main Magnetite Ore-Deposits and Ophicalcites

Magnetite deposits of past economic interest occur along the main contact between the Nieves Unit and the Ronda peridotite (Figures 3–6). These mining areas provide good conditions of observation and expose the geometrical relationships between the magnetite ore deposits and bounding units. Two ancient mines were observed in this study (Figures 4 and 6). In both mining areas, the peridotite appears much more pervasively serpentinized than the bulk of the Ronda peridotite. Interestingly, the contact between the marbles and the Ronda peridotite, as well as the main foliation, are very steeply dipping to the NW indicating that, in the present state, the Nieves Unit and ore deposits are structurally above the Ronda peridotite (Figure 3). This strong planar fabric is accompanied on both sides of the contact by a locally well-developed NE-SW gently dipping common stretching lineation. Magnetite mineralizations occur as magnetite-rich layers parallel to the main planar fabric. The main ore body is located in the eastern mine area, close to the Robledal pass (Figure 3) where magnetite was exploited in galleries parallel to the contact between the marbles and the Ronda peridotite.

10.1029/2020TC006271

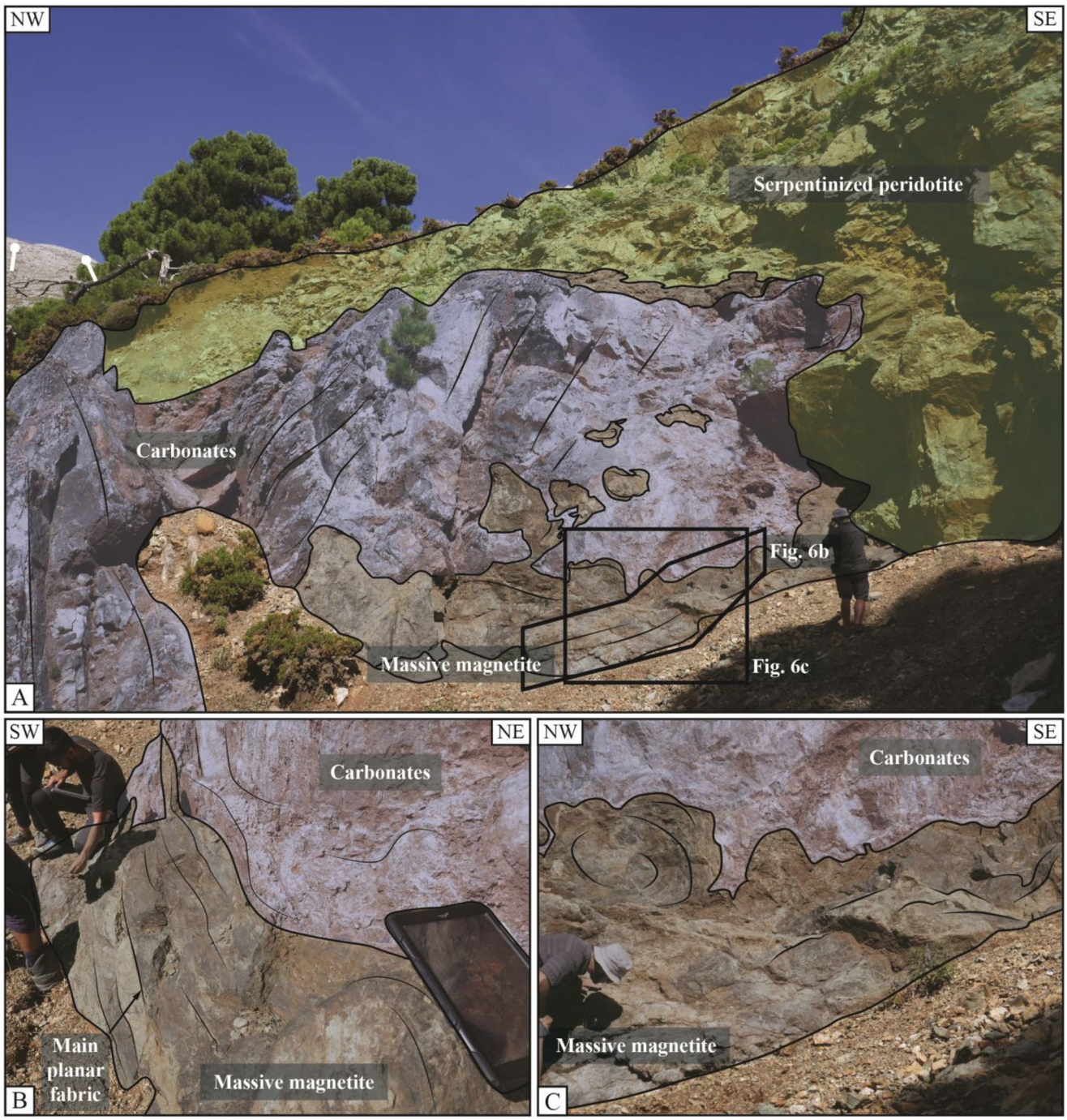

Figure 6. Detailed field relationships between the Nieves Unit and the Ronda peridotite in the western magnetite mine area (Puerto de Robledal). (a) General view of the southeastern wall of the western magnetite mining area. (b) Close-up view on the verticalized magnetite mineralized zone. (c) Close-up view the magnetite mineralized zone and especially on the still attached pieces of magnetite on the vertical marbles few decimeters above the contact with the Ronda peridotite.

Mineralizations are dominated by magnetite, associated with calcite, dolomite, serpentine, brucite and occasionally talc. Relics of former olivine, sometimes organized in layers, are also observed (Figure 5). In the western magnetite mine, the contact between the serpentinized peridotite is decorated with a 50 cm-thick mineralized zone rich in magnetite or a banded ore alternating magnetite-rich layers and calcite-rich layers (Figure 6). The serpentinite is brecciated over a thickness of several meters up from the contact with the

10.1029/2020TC006271

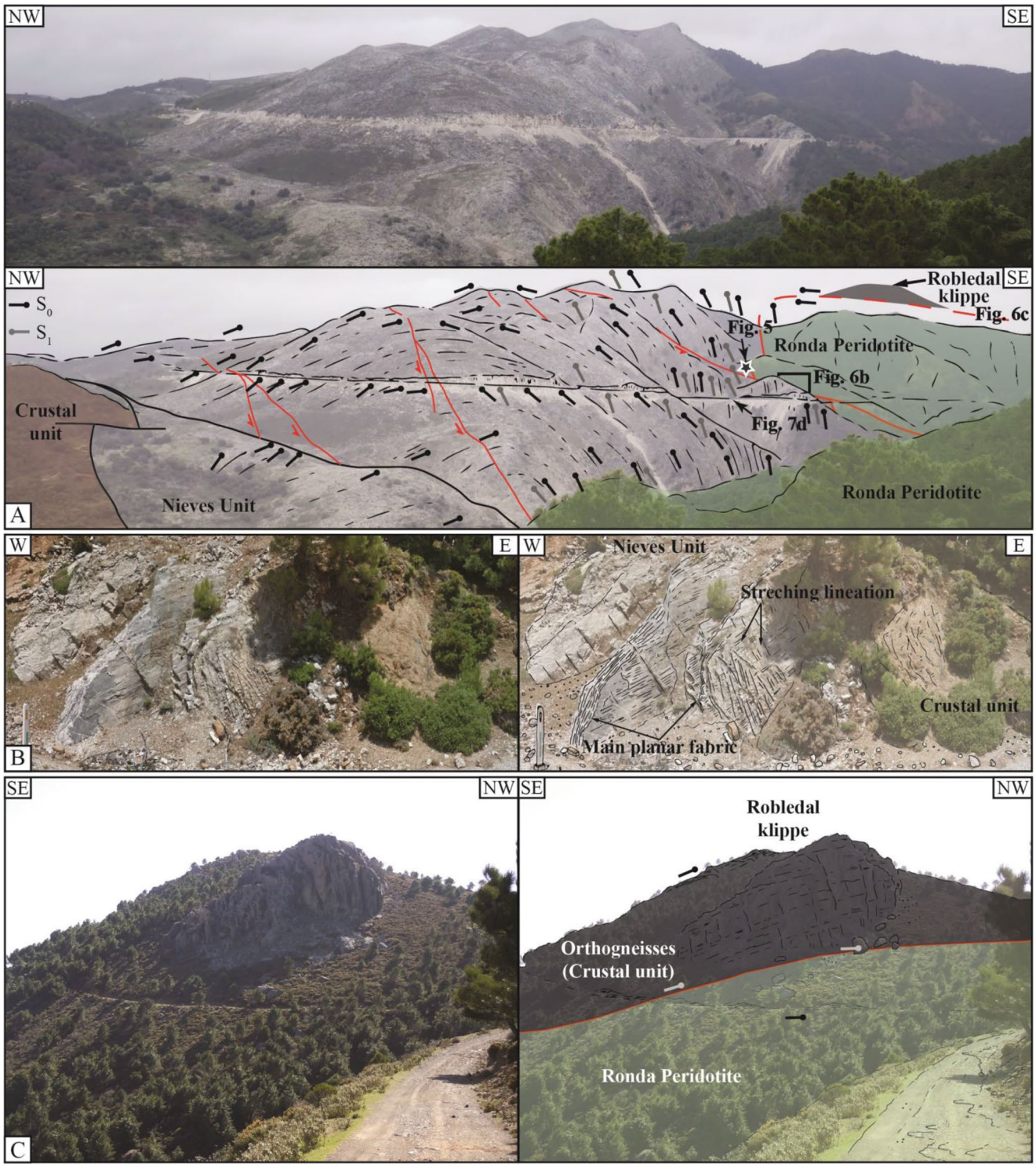

Figure 7.

marbles. Marbles do not show a significant magnetite content away from the contact. In contrast, the eastern mine shows a thicker ore body that extends parallel to the contact over more than 500 m. Magnetite mineralization occurs dispersed in the foliated, folded marble with variable concentration of magnetite grains and green-colored altered olivine grains, usually transformed into orange-color iddingsite (Figures 4 and 5).

Marbles and magnetite layers are foliated, truncated and folded indicating that ductile shearing continued after mineralization (Figures 5a and 5b). In thin-sections, the H*T* olivine-rich metamorphic paragenesis described by Mazzoli et al. (2013) were observed in various states of preservation. Still fresh and perfectly preserved in the lower parts of the Nieves Unit close to the contact with the Ronda peridotite, olivine however disappears almost totally in the contact zone. The paragenesis is here destabilized and overprinted by the ore body that typically forms after peak-temperature conditions, including talc, the association magnetite-serpentine and brucite. Representative electron-probe micro-analyses of the minerals involved in these retrograde parageneses are presented in Table 1. A relative chronology of the different events in the mineralization can be proposed: (a) H*T* metamorphism with the crystallization of olivine and the other HT minerals; (b) crystallization of magnetite coeval with serpentinite, calcite and dolomite grains clearly post-dating olivine that is scarcely preserved as inclusions within the magnetite grains or in the core of some brucite grains (Figures 5c and 5d); (c) massive and penetrative formation of brucite and serpentine that cross-cuts the previously formed crystals, mainly magnetite and calcite; and (d) injection of hydromagnesite veins in the later stages of fluid circulation (Table 1, Figures 5c and 5d). In any case, magnetite mineralizations appear at least partly syn-kinematic, coeval with ductile deformation, but they clearly post-date peak-metamorphic conditions. In addition, ophicalcite veins and genuine bodies have been observed along the contact between the Nieves Unit and the Ronda peridotite and within the peridotite along oblique shear zones cross-cutting the contact (Figures 3 and 4). Ophicalcites are composed of angular, centimeter to decimeter clasts of serpentinites or partly serpentinized peridotites cemented by a calcitic matrix (Figures 4b, 4c and 4e).

3.1.2. Occurrences and Structural Position of Crustal Rocks Over the Mapped Area

New patches from few meters to few tens of meters of sillimanite-biotite paragneisses, orthogneisses, and locally migmatites were added on the map along the contact, but also within the outcropping area of the Ronda peridotite (Figure 3). Most of these patches occur along the contact between the carbonate rocks from the Nieves Unit and the Ronda peridotite, such as observed along road A-397 (Figure 7b). Althought these rocks are often pervasively weathered, they present a strong ductile deformation characterized by a subvertical foliation and a spectacular NE-SW gently dipping stretching lineation (Figure 7b). Other patches and particularly the largest body of felsic rocks cropping out in the Robledal area (Figure 3) to the SE of the study area, present drastically different geometries. In the Robledal area, feldsic rocks crop out over a 1.5×1 km area forming a topographic high surrounded by the Ronda peridotite (Figures 3, 7c and 7d). This body mostly consists of orthogneiss and high-grade rocks resting on top of the peridotites. Both the gneiss and peridotite show a flat to very gently SE dipping foliation parallel to the contact and crudely following the elevation contours (Figures 3b and 7c). These rocks thus do not crop out within a large-scale tectonic window as recently proposed by Mazzoli et al. (2013) on the basis of their lithological affinity with the feldsic rocks present within the Guadaiza window, but they instead occur as a tectonic klippe overlying the Ronda peridotite.

3.2. Strain Markers

We studied more than 700 stations to document strain markers of the study area, including planar and linear fabrics, folds, kinematic indicators and localized structures such as shear zones and brittle faults.

Figure 7. Structural relationships between of the Nieves Unit, the Ronda peridotite and other crustal units. (a) Internal structure of the Nieves Unit at large scale. To the SE, shown is the contact with the main body of the Ronda peridotite. This contact is overturned in this area displaying a reverse succession marbles from the Nieves Unit, high-grade rocks from the crustal units and more or less serpentinized peridotite from the Ronda peridotite from bottom to top. The Robledal klippe crops out only ca. 1 km to the SE. (b) Close-up view of the contact between the Ronda peridotite and the Nieves Unit here separated by a thin, strongly deformed lense of high-grade gneisses. Foliation is steeply dipping to the SE. Foliation planes are decorated by a strong stretching lineation, indicating that the relative motion across the contact is sub-horizontal. Stretching is also marked by a set of lineation-orthogonal veins and joints (see statistics on Figure 9). (c) Mesoscale relationships between the crustal rocks and the Ronda peridotite in the Robledal area. The upper parts of the hill are made of heterogeneous orthogneisses while the dirt road is mostly cut within serpentinized peridotite. The main planar fabrics for both types of rocks are very gently dipping toward the SE. Although limited by a late normal-sinistral fault to the NW, the orthogneisses appear structurally above the Ronda peridotite and therefore appear as a tectonic klippe of crustal rocks lying above the mantle rocks.

Table 1
Chemical Compositions of the Major Observed Minerals in the Nieves Unit and in the Mineralized Zone (wt %)

	RDA1601				RDA1609		RDA1740	
Sample phase	Olivine	Phlogopite	Diopside	Spinel	Titanite	Magnetite	Serpentine	
SiO_2	41.89	40.97	54.25	0.25	29.69	0,00	40.16	38.13
TiO_2	0	0.58	0.1	0.05	37.62	0,00	0	0.05
Al_2O_3	0	13.42	0.57	70.06	2.13	0.006	0.011	0.11
FeO	1.82	0.23	0.1	1.27	0.50	81.93	1.38	2.59
MnO	0	0	0	0.04	0.02	0,00	0.12	0.15
MgO	56.4	27.60	18.39	27.39	0.01	0,00	42.15	39.26
CaO	0.04	0.13	25.65	0.02	28.66	0.02	0.04	0.076
Na_2O	0.02	0.56	0.04	0.01	0,00	0.03	0	0
K_2O	0.01	9.97	0	0	0,00	0,00	0	0
Cr_2O_3	0	0	0	0.03	0.07	0,00	0	0
NiO	0.04	0.07	0.07	0	0,00	0.10	0.18	0
UO_2	/	/	/	/	/	/	/	/
Total	100.21	93.53	99.17	99.12	98.69	82.08	84.04	80.36

	RDA1625						RDA1670			
Sample phase	Magnetite	Olivine		Brucite	Serpentine		Serpentine	Hydro-magnesite		
SiO_2	0,66	37,23	36,98	0,03	38,80	33,55	39,33	0,31	0,57	0,96
TiO_2	0,00	0,39	0,47	0,00	0,63	0,00	0,00	0,00	0,06	0,00
Al_2O_3	0,02	0,00	0,00	0,11	0,08	3,70	1,45	0,00	0,01	0,00
FeO	92,31	1,05	0,89	7,45	0,87	2,17	2,17	0,10	0,13	0,01
MnO	0,00	0,10	0,00	0,02	0,09	0,07	0,00	0,00	0,03	0,02
MgO	0,51	57,90	57,40	75,92	42,39	41,72	40,60	49,89	47,92	51,47
CaO	0,22	0,07	0,05	0,06	0,09	0,02	0,01	0,03	0,03	0,00
Na_2O	0,05	0,00	0,00	0,00	0,00	0,00	0,07	0,00	0,00	0,01
K_2O	0,04	0,01	0,00	0,00	0,04	0,00	0,04	0,00	0,04	0,00
Cr_2O_3	0,00	0,01	0,00	0,00	0,05	0,00	0,03	0,00	0,00	0,00
NiO	0,07	0,12	0,00	0,11	0,00	0,07	0,00	0,00	0,00	0,00
UO_2	0	0	0,004	/	0,058	0	0	/	/	/
Total	93,88	96,86	95,79	83,70	83,09	81,30	83,74	50,33	48,79	52,47

Map-scale structural features are given in Figure 3 and illustrated in Figures 7b and 8. The compilation of field measurements is presented on the maps of Figure 3 and as different stereograms of Figure 9.

3.2.1. Planar Fabrics

At first glance, the primary compositional layering (S_0) of the Mesozoic series remains the main planar fabric in the Nieves Unit. It is particularly clear to the north of the study area where the dominant anisotropy corresponds to the alternation of low-grade calcschists and dark recrystallized limestones and dolostones (Figure 3). Moving south, the compositional layering is increasingly involved and reworked into recumbent isoclinal folds observed at almost all scales (Figures 3 and 8). These folds deform all lithologies and are best expressed in alternating calcite and dolomite marbles showing various degrees of transposition of S_0 into S_1. In the vicinity of the contact with the Ronda peridotite, the transposition of S_0 into S_1 is almost complete and a few occurrences of the initial relationships between S_0 and S_1 only appear in fold hinges that are sometimes detached (Figure 8d). The main planar fabric observed in these folded layers thus corresponds to a composite S_0/S_1 fabric as mentioned by Mazzoli et al. (2013). This main composite S_0/S_1 fabric therefore

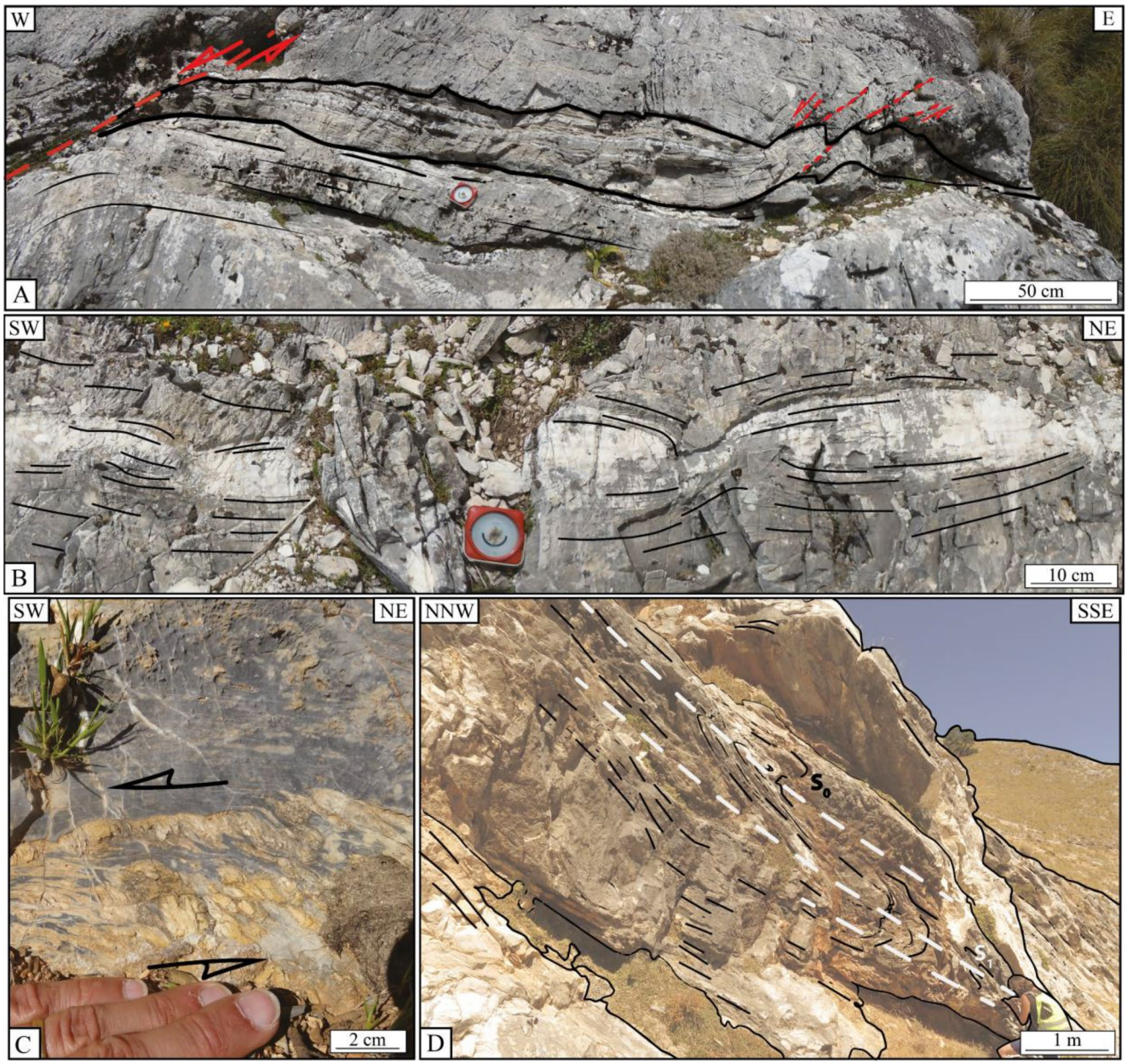

Figure 8. Field examples of the ductile deformation within the Nieves Unit. (a) Attitude of the main planar fabrics of the Nieves Unit in the vicinity of a sinitral small scale shear zone. The main planar fabric is oriented N80 away from the shear zones and is bent and locally transposed into the shear planes oriented between N170 and N20. (b) Asymmetric boudinage of calcitic layers within a more dolomitic matrix, indicating a component of sinistral shear close to the contact with the Ronda peridotite (c) Small-scale sinistral shear criteria indicating a preferred sinitral sense of shear in the Nieves Unit. (d) Series of isoclinal folds allowing the local distinction between S0 and S1.

tends to increase in intensity toward the contact with the Ronda peridotite defining a strong first-order strain gradient that is locally further complicated by more local strain localization in weak and/or alternating lithologies. Based on field observations and structural measurements (Figure 3 and Figures 7–9), the larger-scale structures are defined by series of upright folds that can be followed over kilometers (Figures 3 and 7). For example, a large-scale antiform of S_0 can be observed along the road A-397 between km 17 and km 19 (Figures 7a and 9c). However, the axial trace of this antiform is rapidly lost along-strike, passing laterally to a large-scale synform. This shows the non-cylindrical geometry of these folds and the probable presence of large-scale SE-NW-striking boudins of dolomite-rich rocks similar to those observed at small-scale (Figure 8b).

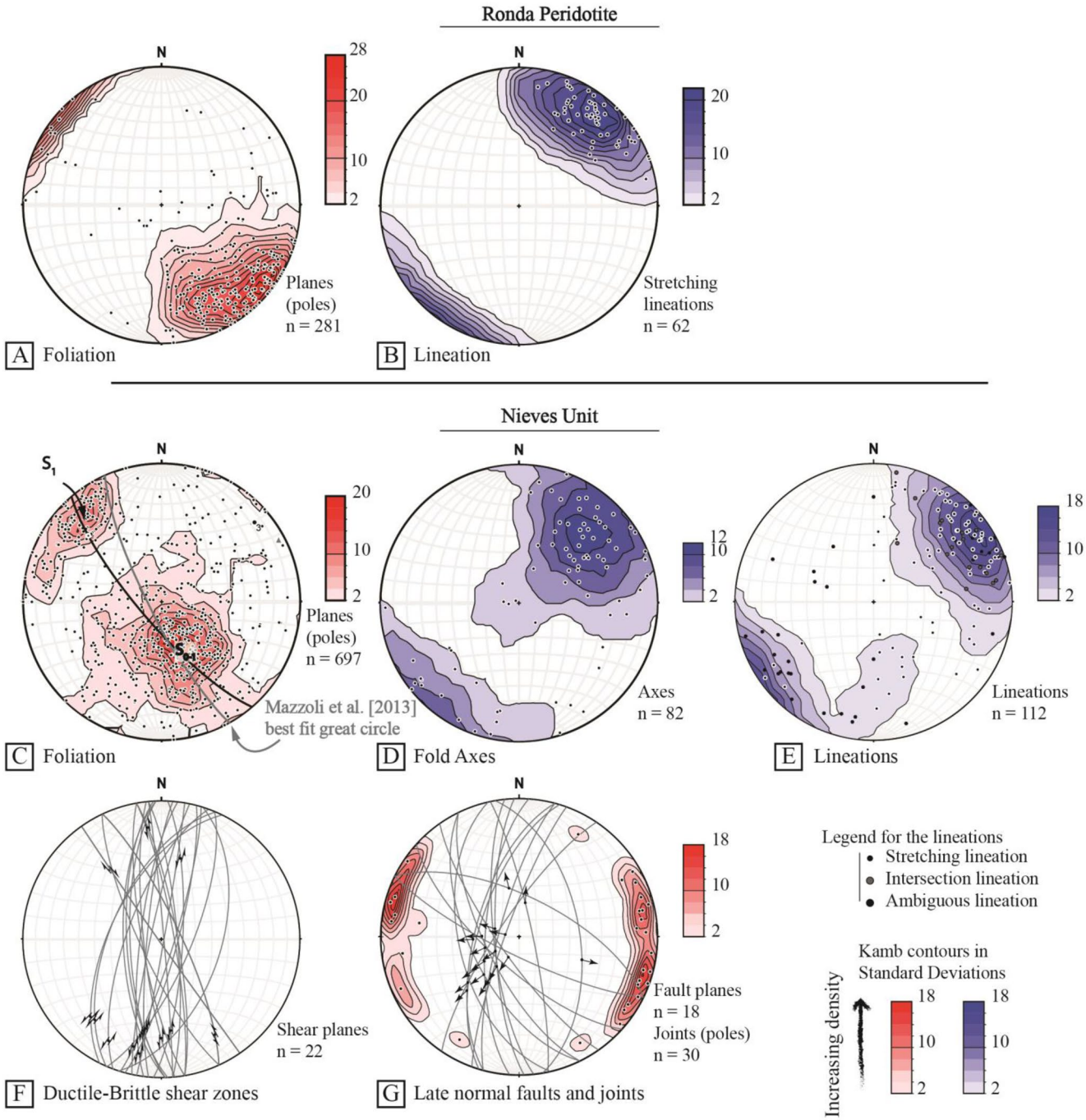

Figure 9. Lower-hemisphere equal-area projection of the structural data. Data for the Ronda peridotite are from this study and compiled from Précigout et al. (2013), while data from the Nieves Unit are all coming from this study. (a) Poles of foliation in the Ronda peridotite. (b) Stretching lineations in the Ronda peridotite. (c) Poles of foliation in the Nieves Unit. Results are compared to the work of Mazzoli et al. (2013). (d) Lineations (stretching, intersection or ambiguous lineations) in the Nieves Unit and (e) Fold axes measured in the Nieves Unit. Note the strong similarity in the strike of the stretching lineations measured either in the Ronda peridotite or the Nieves Unit that are parallel to the trace of the western contact of the Ronda peridotite. (f) Ductile-brittle shear zones in the Nieves Unit. (g) Late normal faults and joints from the Nieves Unit.

As collected in pole figures, almost 700 planes were measured in the study area including S_0, S_1 and composite planes S_0/S_1 (Figures 3 and 9c). Despite a significant dispersion of the main planar fabrics, their average attitude indicates that both bedding and schistosity strike parallel to the contact with the Ronda peridotite. In low-strain domains, that is, the northwest of the studied area, S_0 shows a gently NW-dipping monocline

consistent with the overall northward bedding of the stratigraphic succession. Conversely, toward the southeast, S_1 and the composite fabric appear generally with a steep, often close to vertical dip directed either to the NW or to the SE (Figures 7a, 8d and 9c). Foliation within the Ronda peridotite is not always clearly expressed, but the compilation of existing data and new measurements show that the foliation plane consistently dips toward the NW with various angles, from very steep close to the contact with the Nieves unit to gentle in the vicinity of the crustal units and the topographic highs (Figure 9a). Interestingly, as observed in details in the field, statistics show that the attitudes of the ductile fabric respectively developed in the Nieves Unit and the Ronda peridotite are parallel to each other and parallel to the trace of the contact.

3.2.2. Lineations

Stretching lineations are unevenly distributed following the distribution of the intensity of the composite S_0/S_1 fabric and is therefore locally difficult to observe over the studied area. Nevertheless, unambiguous stretching lineations were observed over ca. 400–500 m toward the contact of the Ronda peridotite and the crustal rocks. Along the road A-397, a spectacular and very persavive gently SW-dipping stretching lineation is displayed over the foliation planes, either within the last 50 m of marbles belonging to the Nieves Unit or within a thin lense of crustal rocks intercalated along the contact with the Ronda peridotite (Figure 7b). As observed in the old mining areas, quarries and road cuts, the stretching lineation is marked by different markers, such as the elongation of calcite or dolomite grains or the preferred orientation of tremolite crystals. Evidence of stretching is also marked by a single set of joints and tension gashes arranged perpendicular to the stretching lineation affecting the marbles and locally the ore deposits (Figures 7b and 9). Higher in the metamorphic succession, stretching lineation is defined by the direction of strain shadows at the tips of dolomite marble boudins, chert clasts, calcsilicate aggregates or even phlogopite-tremolite aggregates. A clear stretching lineation is also well expressed within the aggregates. There, the stretching lineation becomes heterogeneously developed and more ambiguous as it interferes with a strong intersection lineation, particularly when S_0 is incompletely transposed into S_1. The two types of lineation have been separated when possible (Figures 3a and 7d). The trend of the stretching lineation shows a weak dispersion (Figures 3a and 9d) centered on an average value of N 48°E parallel to the trace of the main contact. Plunge is generally shallow and dominantly dipping toward the NE (26° toward the NE; Figure 9d).

In the Ronda peridotite, the stretching lineation is not a common deformation feature. However, it can be easily measured in the garnet/spinel-mylonite at the vicinity of the contact with both the Nieves Unit and the crustal rocks of the Jubrique Unit. Interestingly, the stretching lineation is there also dominantly trending NE-SW with a preferred plunge toward the NE (Figure 9b), fairly consistent with the orientation of the stretching lineation observed in the Nieves Unit.

The stretching lineation measured in the crustal rocks of the Robledal klippe is also oriented NE-SW as already reported by Esteban et al. (2008). In the rocks of the Robledal klippe, the stretching lineation carried by a very gently dipping high-grade foliation (Figure 7c) is marked by strain shadows developed around feldspath clasts and the elongation of quartz.

3.2.3. Folding

In the study area, most folds correspond to recumbent tight to isoclinal folds that transpose the primary compositional layering accompanying the development of an axial planar S_1 foliation, as shown by Mazzoli et al. (2013). At first glance, fold axes show variable directions and plunges that define a single axial plane quite comparable to the mean S_1 oriented N 50°E along strike and steeply dipping to the SE (Figures 7a, 8d and 9e). However, a SW-NE preferred orientation of axes appears with shallow to gently dipping plunges (Figures 8d and 9e), consistent with the geometries deduced from the large-scale traces of S_0 (Figures 3a and 9c). Axial planes are therefore mostly parallel to the regional trend of S_1 and to the contact with the Ronda peridotite. In addition, fold axes are mainly colinear with the stretching lineation. This peculiar orientation of folds indicates a strong component of simple shear associated with NE-SW stretching. This observation is consistent with the contraction of metamorphic isograds within the Nieves Unit (Mazzoli et al., 2013) and the Jubrique Unit (Balanyá et al., 1997) within a non-coaxial flow. Late open folds with NE–SW-trending axes deform and partially overprint all planar fabrics S_1, S_0/S_1, and $S_{0,}$ including at the contact between the Nieves Unit and the Ronda peridotite. Development and amplification of S_1 planar fabric

being coeval with the main metamorphic event, these late folds correspond to post-metamorphic features developed at low-grade conditions as suggested by Mazzoli et al. (2013).

3.2.4. Preferred Sense of Shear

In massive lithologies of the Nieves Unit, the deformation shows intense folding, particularly visible in the YZ plane showing the flattening component of finite strain. In layered, alternating lithologies, the dolomitic and chert layers are boudinaged into a weaker calcitic matrix (Figures 8a and 8b). Boudinage occurs at various scales, from a few centimeters to hundreds of meters with the development of well-defined L-S tectonites, particularly clear in the vicinity of the contact with the Ronda peridotite. Asymmetric boudinage at different scales and the development of shear bands also occur in the more strained zones, particularly over the last ca. 250 m toward the contact with the Ronda peridotite. Asymmetry of the different markers suggest consistently a sinistral sense of shear in the current position of the rocks (Figures 8a and 8c). Associated with flattening, asymmetric boudinage indicates a component of non-coaxial flow during deformation, also observed in the Jubrique Unit (Balanyá et al., 1997; Précigout et al., 2013). Moreover, large-scale sinistral shear zones are specifically described in the next section. These cartographic traces of these shear zones are mapped as simple lines because deformation along them is highly localized at that scale.

3.2.5. Oblique Shear Zones

The structure of the Nieves Unit is cross-cut by a series of high-angle structures oblique on the layering and the main foliation with typical length ranging from several hundreds of meters to a few kilometres (Figures 3 and 9). Two main types of structures have been distinguished, including brittle-ductile shear zones mechanically consistent with the activity of the Jubrique/Nieves contact and late brittle faults. Brittle-ductile shear zones show straight to slightly curved traces and strike around N170° to N20°E (Figure 9). Mostly restricted to the Nieves Unit, some of these brittle-ductile shear zones bend into or cross-cut the contact between the Nieves Unit and the Ronda peridotite. The horizontal apparent offset cannot always be confidently retrieved. However, using the displacement of marker layers present on either side of the shear zones, the apparent offset may reach ca. 400 m (Figure 3). The damage zone of the larger structures generally does not crop out and corresponds to topographic lows filled by recent scree deposits. Kinematics of each shear zone was deduced by the analysis of apparent offset of fold axes on satellite images, as synthetized on Figure 3. The damage zone of smaller ductile shear zones corresponds to tens of decimeters highly deformed zones over which the main schistosity is bent and locally transposed into the shear planes (Figure 8), ensuring a consistent sinistral sense of shear.

3.2.6. Late Normal Faults

Ductile-britte shear zones are cut or locally reactivated by a series of brittle faults. Some of these faults can followed over 3–5 km (Figure 3). There, while horizontal displacements appear small and not reproducible from one structure to another, vertical displacements sometimes reach several hundred of meters; 300–500 m for the Igualera fault zone as proposed by Pedrera et al. (2015). To the west of the area, the faults are arranged as an hort and graben structure, pervasively overprinting the contact between the Jubrique Unit and Nieves Unit (Figure 3). The preferred orientation of the fault planes is around N150°E to N20°E (Figure 3). Small-scale brittle structures mostly correspond to N-S to NW-SE straight planes with dip angles higher than 50°–60° with dominantly normal to normal-sinistral fault kinematics. Faults are accompanied by a pervasive array of subvertical joints and tension gashes filled with calcite, and iron hydroxides as already mentioned by Pedrera et al. (2015).

4. Raman Spectroscopy on Carbonaceous Material (RSCM) Geothermometry

In order to characterize the finite thermal structure of Nieves Unit, peak-metamorphic temperatures were quantitatively estimated using RSCM geothermometry (Figure 10; Beyssac, Goffé, et al., 2020; Beyssac, Rouzaud, et al., 2002). To gather a representative data set for the RSCM approach, metasedimentary rocks were collected either across the metamorphic succession of the Nieves Unit with a high-resolution cartographic approach, or along the contact with the Ronda peridotite (Figure S1). Due to the scarcity or even the lack of carbonaceous material in some particularly pure marble layers, several samples were abandoned, particularly those from the base of the Norian dolomitic marble formation. Detailed results, including R2 ratio,

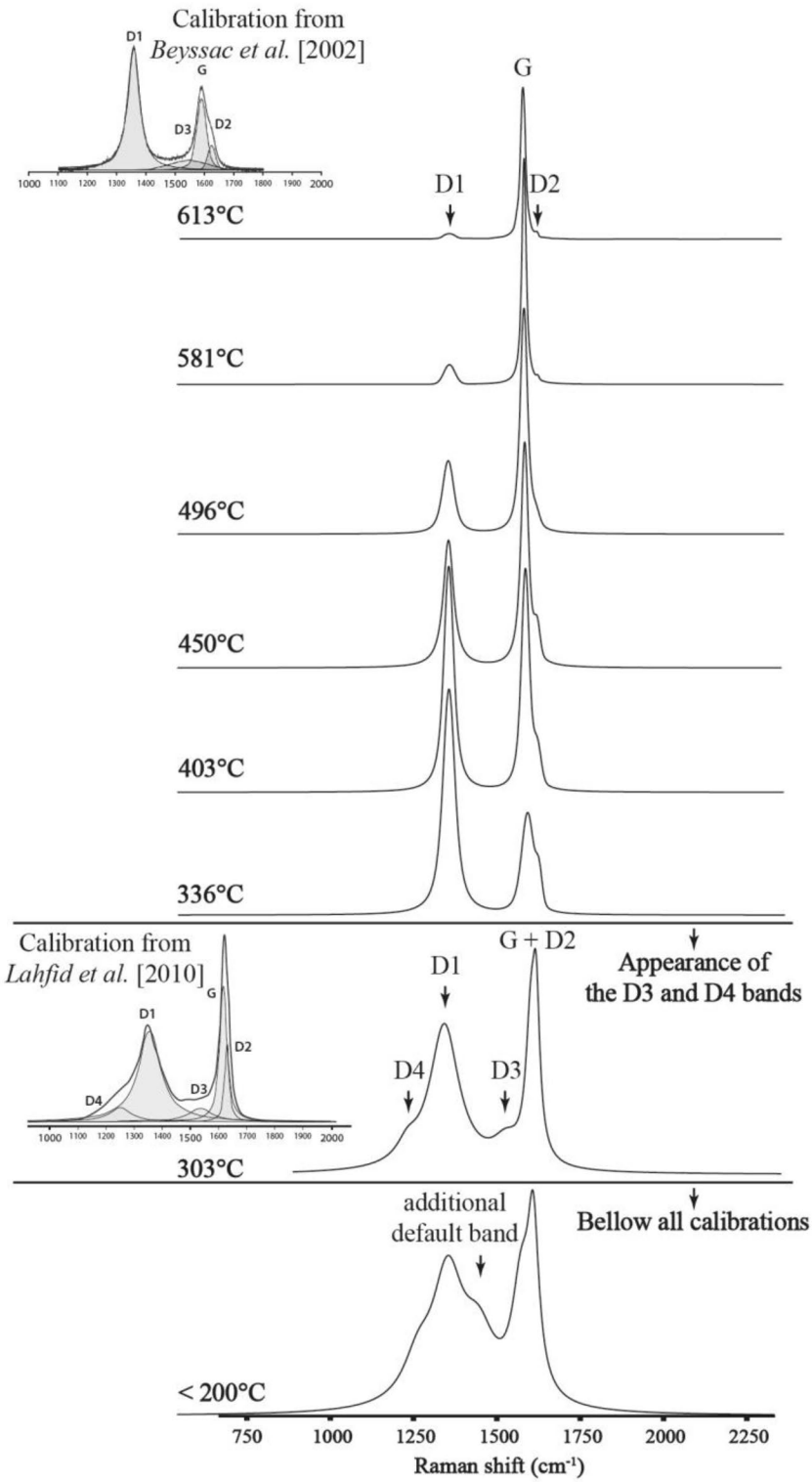

Figure 10. Representative spectra obtained from samples collected within the Nieves Unit. Given is the corresponding temperature for each type spectrum. Appearance of a D4 shoulder appears to correspond to structural organization of the CM and therefore a temperature below the lower bounds of the calibration proposed by Beyssac, Rouzaud, et al. (2002), that is, 330°C. For these samples, the RA1 correlation proposed by Lahfid et al. (2010) for low temperature was used. Some samples (see Table 2) returned spectra typical for very immature CM that experienced very low metamorphic conditions falling below ca. 200°C.

number of spectra, T_{max}, and standard deviation are presented for the 74 samples in Table 2. RSCM data were also reported on two maps at different scales (Figure 11) and along three representative geological cross-sections orthogonal to the main structures presented in Figure 12.

Carbonaceous material (CM) often occurs as a minor component within (meta-)sediments, which have undergone successively carbonization and graphitization processes during diagenesis and metamorphism. These processes participate to irreversible chemical and structural transformations accompanying the progressive evolution from poorly organized CM to graphite (Wopenka & Pasteris, 1993). The RSCM method is based upon the quantitative estimate of the degree of structural organisation of CM, which has been proven a reliable indicator of metamorphic temperature (T) (Aoya et al., 2010; Beyssac, Rouzaud, et al., 2002; Lahfid et al., 2010). Because of the irreversible character of graphitization, the CM structure thus appears relevant to determine maximal paleo-T conditions (noted RSCM T_{max} thereafter) even in strongly retrogressed metasedimentary rocks (Angiboust et al., 2011; Augier, Agard, & et al., 2005; Beaudoin et al., 2015; Beyssac, Goffé, et al., 2002; Gabalda et al., 2009). RSCM T_{max} can be determined with accuracies of ±50°C in the range ca. 350°–650°C and ±25°C in the range ca. 200°–330°C, depending on the precision and dispersion of petrological data used for the calibration of the geothermometers (Beyssac, Rouzaud, et al., 2002; Lahfid et al., 2010). Relative uncertainties on RSCM T_{max} on a single section or a map, are however much smaller, around 10°–15°C and slight variations in RSCM T_{max} of that order of magnitude may be detected (Beyssac et al., 2004, 2007; Vitale Brovarone et al., 2013). Moreover, a good consistency between RSCM T_{max} data and average P–T estimates is generally observed (Angiboust et al., 2011; Augier et al., 2015; Bellanger et al., 2015; Delchini et al., 2016; Laurent et al., 2018; Plunder et al., 2012).

Raman spectra were obtained using a Renishaw inVia Reflex system (BRGM-ISTO) equipped with an argon laser source of 514,5 nm. Laser was focused on the CM particles using a Leica DM2500 microscope specially adapted for the system using a ×100 lense (NA = 0.90). RSCM analyses were conducted on polished thin sections cut in the structural X-Z plane (i.e., orthogonal to foliation and parallel to lineation). To avoid defects on the CM related to thin-section preparation (Beyssac, Rouzaud, et al., 2002), the analyses were all performed below the surface of the section by focusing the laser beam beneath a transparent crystal (i.e., dominantly calcite, dolomite and occasionally other calcsilicates). To bring out and possibly smooth out the inner structural heterogeneity of CM within samples, 13 to 33 spectra were routinely recorded for each sample (Table 2). Resulting spectra were then processed using the software Peakfit (Beyssac, Rouzaud, et al., 2002).

5. RSCM Results and Thermal Structure of the Nieves Unit

Metasediments selected from Nieves Unit show significant variations in the structural organization of CM, as indicated by the variations in the shapes of spectra (Figure 10). We first document an upward decrease of the CM structural organization away from the contact with the Ronda peridotite (Figures 11 and 12), which correlates well with the metamorphic zones defined along the NW-SE section studied by Mazzoli et al., (2013). Interestingly, a general decrease of the CM structural order also occurs at a larger scale along the contact with the Ronda peridotite from SW to NE (Figures 11 and 12). Samples selected to the SW of the study, close to the contact, exhibit graphite-type spectra, almost devoid of defect bands (Figure 10). Upward the metamorphic sequence, spectra then show an overall common increase of D1 and D2 defect bands relative to the G graphite band and, locally, the appearance of the D3 defect band (Figure 10), highlighting a general increase of the structural disorder within the graphitic structure (e.g., Beyssac, Rouzaud, et al., 2002). In both the uppermost parts of the metamorphic sequence and the NE end of the study area along the contact, spectra all present a prominent D3 band, a very large D1 band and the appearance of a D4 band (Figure 10), indicating even less organized CM. This overall evolution can be interpreted as the result of a general T_{max} decrease (Beyssac, Rouzaud, et al., 2002; Lahfid et al., 2010). Poorly organized CM corresponds to T below the lower boundary of the R2 calibration (Beyssac, Rouzaud, et al., 2002) and sometimes even falls below the lower boundary RA1 correlation at less than ca. 200°C (Lahfid et al., 2010).

All RSCM T_{max} obtained are located on geological maps and cross-sections in Figures 11 and 12. Detailed calculation (R2, number of spectra, temperature and standard deviation) is presented in Table 2. T_{max} present generally unimodal temperature distributions that show quite low dispersion (Table 2). Conversely,

10.1029/2020TC006271

Table 2
Detailed RSCM T_{max} Results for the Rocks of the Nieves Unit

Sample	X	Y	Elevation (m)	N of recorded spectra	N of used spectra	Beyssac/Lahfid				
						Meth.	mean R2	SD for R2	mean T (°C)	SD for T	SE
RDA1601	36.6261	−5.0780	1,040	30	19	B	0.174	0.028	563.47	12.68	2.9
RDA1602	36.6261	−5.0781	1,040	24	17	B	0.090	0.026	600.94	11.72	2.8
RDA1603	36.6261	−5.0782	1,040	33	28	B	0.186	0.028	558.12	12.34	2.3
RDA1609	36.6270	−5.0803	1,036	15	12	B	0.207	0.02	548.96	8.8	2.5
RDA1613	36.6442	−5.0889	1,128	25	22	B	0.657	0.015	348.49	6.53	1.4
RDA1614	36.6395	−5.0897	1,130	20	20	B	0.623	0.024	363.74	10.83	2.4
RDA1615	36.6332	−5.0926	1,082	24	13	B	0.264	0.030	523.31	13.42	3.7
RDA1623	36.6579	−4.9739	653	21	17	B	0.432	0.025	448.76	11.29	2.7
RDA1636	36.6742	−4.9661	924	19	19	B	0.338	0.02	490.43	9.03	2.1
RDA1642	36.6908	−4.9329	450	20	19	B	0.408	0.025	459.51	11.03	2.5
RDA1644	36.7432	−4.8968	728	18	18	L	0.634	0.017	314.12	9.85	2.3
RDA1647	36.7481	−4.9131	831	5	5	L	–	–	<200	–	–
RDA1655b	36.8677	−4.8279	655	5	5	L	–	–	<200	–	–
RDA1668	36.6269	−5.1206	776	13	6	B	0.375	0.017	474.33	7.67	3.1
RDA1704	36.6383	−5.0674	1,225	26	22	B	0.144	0.03	576.79	13.15	2.8
RDA1707	36.6415	−5.0605	1,190	21	14	B	0.196	0.031	553.89	13.81	3.7
RDA1708	36.6420	−5.0591	1,151	24	22	B	0.168	0.02	566.1	9.22	2.0
RDA1709A	36.6474	−5.0668	1,108	18	15	B	0.65	0.026	350.44	11.58	3.0
RDA1710	36.6483	−5.0680	1,104	17	17	B	0.617	0.02	366.51	9.05	2.2
RDA1711	36.6487	−5.0691	1,100	17	17	B	0.683	0.016	336.95	7.13	1.7
RDA1712	36.6494	−5.0694	1,094	24	23	B	0.674	0.040	341.11	17.89	3.7
RDA1713	36.6496	−5.0708	1,094	22	17	B	0.615	0.037	367.12	16.28	4.0
RDA1714	36.6504	−5.0728	1,088	23	16	B	0.628	0.034	361.38	15.28	3.8
RDA1716	36.6504	−5.0837	1,134	19	18	B	0.611	0.019	368.99	8.37	2.0
RDA1717	36.6448	−5.0897	1,125	21	17	B	0.656	0.029	349.03	12.93	3.1
RDA1718	36.6424	−5.0885	1,131	21	19	B	0.682	0.024	337.33	10.81	2.5
RDA1719	36.6379	−5.0900	1,122	20	15	B	0.40	0.023	461.41	10.22	2.6
RDA1720	36.6363	−5.0904	1,113	26	18	B	0.264	0.040	523.32	18.08	4.3
RDA1721	36.6337	−5.0903	1,096	22	14	B	0.349	0.02	485.53	8.77	2.3
RDA1722	36.6337	−5.0924	1,087	23	16	B	0.355	0.025	482.86	11.02	2.8
RDA1723	36.6323	−5.0929	1,076	21	14	B	0.332	0.024	493.14	10.87	2.9
RDA1725	36.6293	−5.0944	1,054	26	18	B	0.166	0.026	567.25	11.65	2.8
RDA1726	36.6258	−5.0934	1,041	24	21	B	0.269	0.017	521.32	7.66	1.7
RDA1728	36.6415	−5.0892	1,159	18	18	B	0.617	0.032	366.32	14.44	3.4
RDA1729	36.6406	−5.0868	1,188	19	17	B	0.605	0.035	371.66	15.76	3.8
RDA1730	36.6407	−5.0812	1,213	20	15	B	0.605	0.032	371.58	14.34	3.7
RDA1731	36.6419	−5.0776	1,228	26	24	B	0.495	0.028	420.9	12.47	2.6
RDA1732	36.6432	−5.0743	1,257	24	16	B	0.495	0.132	405.39	15.11	3.8
RDA1735	36.637	−5.0702	1,293	24	15	B	0.181	0.029	560.23	12.76	3.3
RDA1736	36.6306	−5.0778	1,148	28	21	B	0.302	0.034	506.79	15.79	3.5
RDA1738	36.6311	−5.0750	1,209	13	9	B	0.146	0.022	576.23	9.71	3.2

Table 2
Continued

Sample	X	Y	Elevation (m)	N of recorded spectra	N of used spectra	Beyssac/Lahfid					
						Meth.	mean R2	SD for R2	mean T (°C)	SD for T	SE
RDA1745	36.6341	−5.0832	1,306	19	15	B	0.255	0.03	527.55	13.67	3.5
RDA1746	36.6371	−5.0850	1,219	20	14	B	0.363	0.039	479.67	17.35	4.6
RDA1747	36.6375	−5.0854	1,210	27	25	B	0.298	0.023	508.34	10.16	2.0
RDA1750	36.6288	−5.0977	993	19	13	B	0.305	0.024	505.11	10.66	3.0
RDA1751	36.6317	−5.0981	978	16	12	B	0.381	0.018	471.36	8.17	2.4
RDA1752	36.6292	−5.1119	913	25	23	B	0.672	0.008	341.76	3.51	0.7
RDA1753	36.6273	−5.1153	810	20	14	B	0.407	0.035	459.81	15.79	4.2
RDA1754	36.6240	−5.1220	710	22	18	B	0.246	0.033	531.36	14.78	3.5
RDA1755	36.6419	−5.1200	852	25	21	L	0.005	0.62	307.71	7.22	1.6
RDA1756	36.6466	−5.1182	880	21	13	L	0.006	0.625	311.71	9.11	2.5
RDA1757	36.6504	−5.1109	913	24	24	L	0.618	0.007	302.15	8.48	1.7
RDA1758	36.6458	−5.0913	1,110	22	22	B	0.642	0.011	355.28	5.03	1.1
RDA1759	36.6693	−5.1243	982	5	5	L	–	–	<200	–	-
RDA1761	36.6671	−5.1104	1,052	25	19	L	0.613	0.009	296.29	11.67	2.7
RDA1762	36.6676	−5.1123	1,044	20	20	L	–	–	<200	–	–
RDA1764	36.6384	−5.0893	1,123	22	18	B	0.329	0.029	494.43	12.93	3.1
RDA1765	36.6387	−5.0894	1,125	19	17	B	0.545	0.026	398.29	11.55	2.8
RDA1766	36.6386	−5.0894	1,123	24	19	B	0.24	0.02	534.34	9.33	2.1
RDA1769	36.6441	−5.0704	1,189	19	16	B	0.49	0.03	422.67	13.63	3.4
RDA1770	36.6439	−5.0722	1,207	22	22	B	0.546	0.035	398.25	15.6	3.3
RDA1771	36.6443	−5.0746	1,268	19	17	B	0.575	0.024	384.91	10.72	2.6
RDA1772	36.6446	−5.0759	1,281	22	21	B	0.581	0.02	382.39	8.69	1.9
RDA1773	36.6452	−5.0772	1,264	18	18	B	0.604	0.009	372.12	3.97	0.9
RDA1775	36.6476	−5.0799	1,231	14	14	B	0.646	0.008	353.8	3.39	0.9
RDA1779	36.6383	−5.0894	1,123	21	19	B	0.476	0.024	429.02	10.75	2.5
RDA1780	36.6383	−5.0894	1,124	18	14	B	0.391	0.043	467.01	19.1	5.1
RDA1781	36.6382	−5.0899	1,121	20	17	B	0.589	0.028	379.13	12.45	3.0
RDA1782	36.6690	−5.1150	1,012	5	5	L	–	–	<200	–	–
RDA1783	36.6655	−5.1157	1,010	5	5	L	–	–	<200	–	–
RDA1802	36.6895	−4.9587	735	30	29	B	0.296	0.033	509.36	14.5	2.7
RDA1805	36.6585	−5.0119	727	18	16	B	0.163	0.028	568.34	12.33	3.1
RDA1809	36.6225	−5.0845	905	21	12	B	0.175	0.032	563.35	14.32	4.1
RDA1827	36.6558	−5.0344	863	17	17	B	0.339	0.025	490.17	10.93	2.7

Note. Reported are the name samples, *XY* coordinates and the respective elevation. The number of recorded and used spectra, as well as the calibration that has been applied. The parameters RA1 (Lahfid et al., 2010) and R2 (Beyssac, Rouzaud, et al., 2002) are used to calculate the temperatures from ~220°C to ~320°C and from ~320°C to ~600°C, respectively with the Lahfid et al. (2010) and Beyssac, Rouzaud, et al. (2002) calibrations (L and B). The parameters and calculated temperatures are presented with a mean value and the associated Standard Deviation (SD). The Standard Errors (SE) are presented for all the calculated temperatures and correspond to the SD divided by the square root of the number of the used spectra.

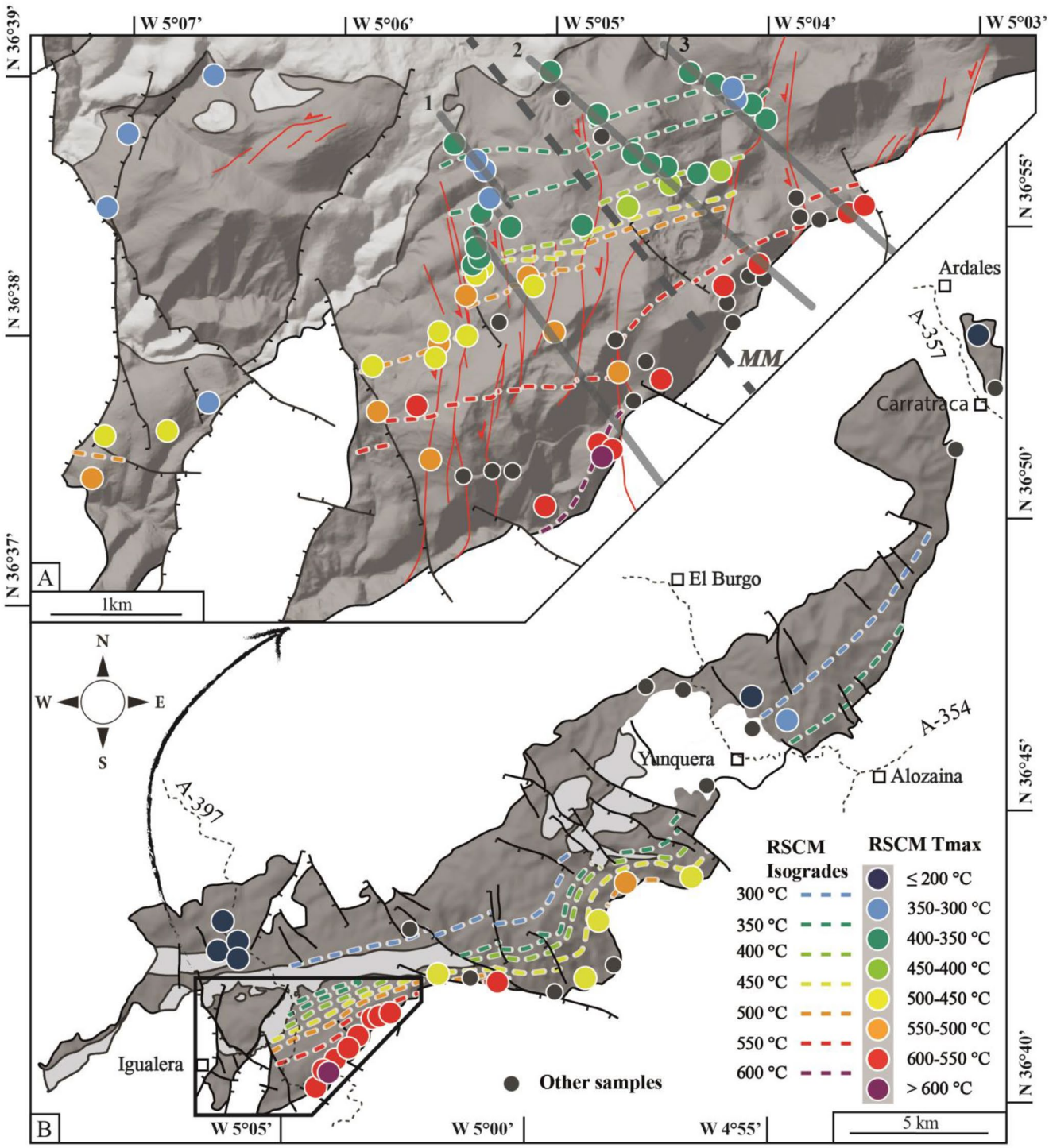

Figure 11. Finite thermal structure of the Nieves Unit as evidenced by Raman spectroscopy on carbonaceous material (RSCM) geothermometry. (a) RSCM peak-metamorphic temperatures distribution over the studied area. Given are the interpolated RSCM isograds. (b) Map of the entirely Nieves Unit showing the RSCM peak-metamorphic temperatures for the rest of the unit. Note that the temperatures show either a drastic NW-SE decrease perpendicular to the main structure associated with a very large-scale SW-NE decrease along the contact with the Ronda peridotite. Cross-sections presented in Figure 12 are located in this figure by gray lines.

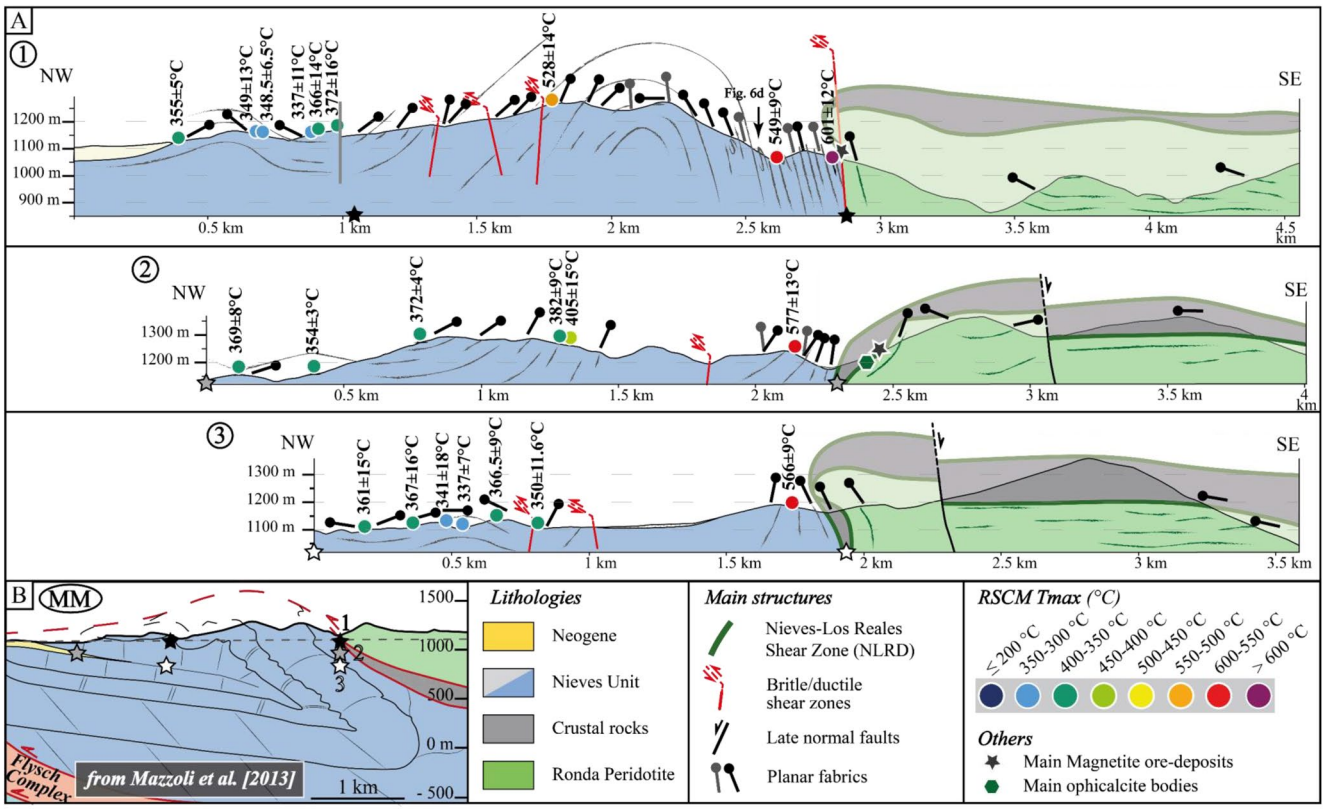

Figure 12. Geological cross-sections of the study area. (a) Detailed cross-sections focused on the internal geometry and the thermal structure of the metamorphic zone of the Nieves Unit and the contact between the Nieves Unit and the Ronda peridotite, as well as the crustal units. Geometries are constrained by structural measurements (see Figure 3) and observations at all scales, particularly for the geometry of the contact between the Nieves Unit and Ronda peridotite. Results of RSCM peak-metamorphism temperatures are reported according to their locations on the cross-sections. In all cross-sections, vertical and horizontal distances are the same. (b) Cross-section over the large-scale section proposed by Mazzoli et al. (2013). This section is referenced "*MM*" on Figure 3 and on Figure 11. Stars correspond to point of references allowing the comparison between the *MM* cross-section and ours, that is, the black stars are the cross-section 1, the gray stars are referencing to the cross-section 2 and the white stars correspond to the cross-section 3.

CM-poor samples display higher dispersions possibly in response to the presence of an inherited component of CM or the effect of brittle deformation (Beyssac, Rouzaud, et al., 2002; Kirilova et al., 2018; Nakamura et al., 2015). The distribution of T_{max} embraces a wide range of temperatures from less than 200°C to more than 600°C, either at the small-scale of the high-resolution map of the western parts of the Nieves Unit (Figure 11) or at much larger scale along the contact with the Ronda peridotite from the SW to the NE (Figure 11).

Despite gaps related to the lack of CM in the Norian dolomite marbles, Figures 11 and 12 show that a steep metamorphic gradient is observed along any structure-perpendicular section, as proposed by Mazzoli et al. (2013). Along the road A-397, between km 17 and km 21, RSCM T_{max} drastically decreases from 600°C down to ca. 350°C over about 2.2 km across the main foliation, and thus against the contact with the peridotite (Figures 11–13). The apparent field thermal gradient may then be as steep as 120°C/km, indicating a strong contraction of the RSCM isograds. This decreasing evolution is consistent, in a broad sense, with published petrological investigation including thermobarometric modeling, whereas the precise position and spacing of thermal zones, defined by Mazzoli et al. (2013), seem slightly different (Figure 11). Indeed, the RSCM isograds highlight a larger temperature decrease. This trend is confirmed by additional samples (RDA1762, RDA1782, and RDA1783) located further north and yielding very poorly organized CM, corresponding to RSCM T_{max} lower than 200°C (Figure 11). Interpolation of RSCM T_{max} isovalues obtained by the RSCM method is shown on Figure 11 as RSCM isograds. The distribution of RSCM isograds appears quite similar on lateral sections allowing reasonable constraints on the geometry. The thermal structure is not cylindrical as RSCM isograds are oblique to the contact with the Ronda peridotite. Despite local and small

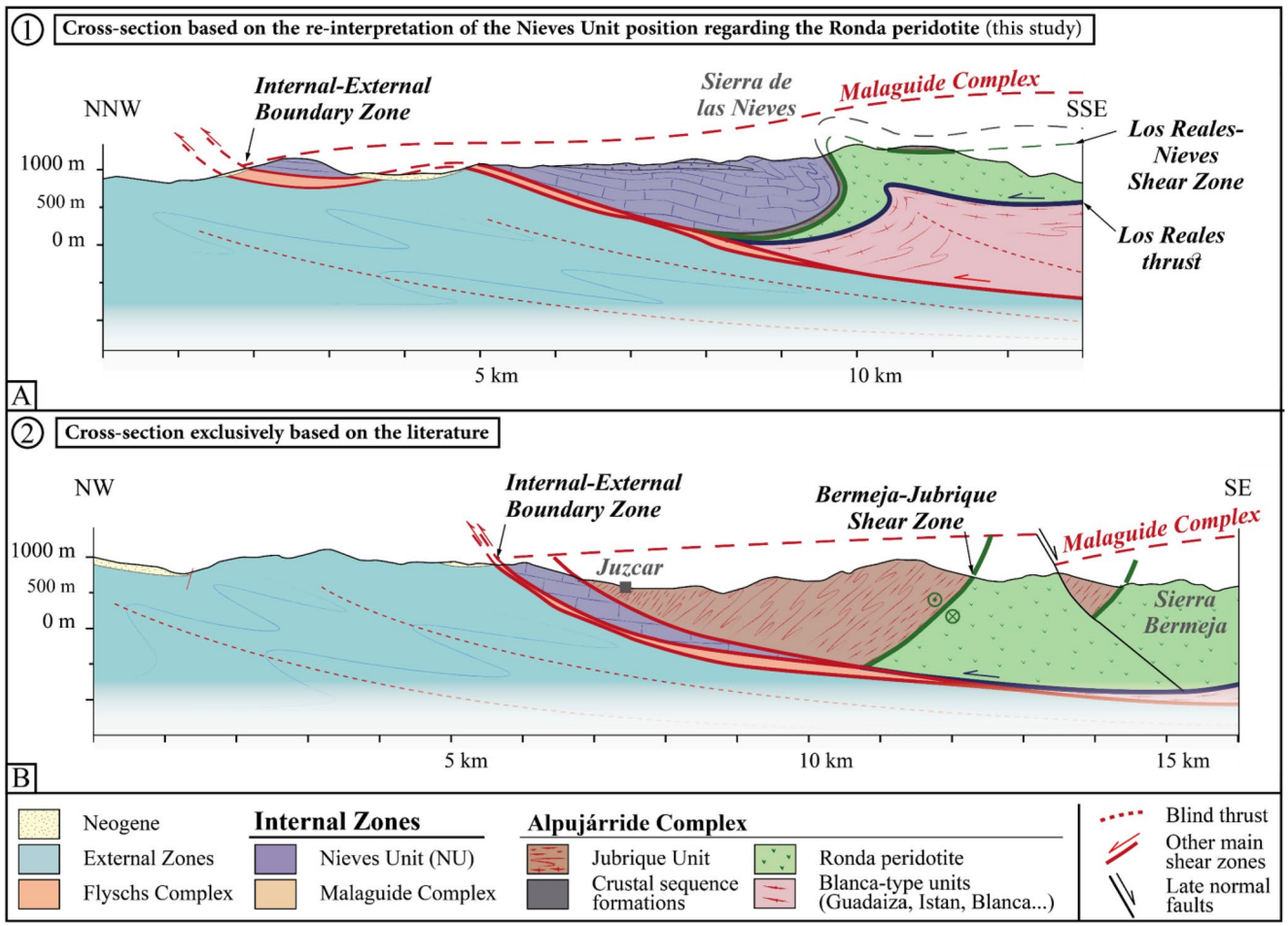

Figure 13. General cross-sections showing the geological structuration of the enlarged studied area. (a) According to the general geological re-interpretations of the relationships between the Ronda peridotite and the Nieves Unit (see location on Figure 2). Cross-section modified after Platt et al. (2003, 2013); Esteban et al. (2008); Tubía et al. (2013) and Acosta-Vigil et al. (2014). (b) According to the commonly accepted geological interpretations of the relationships between the Ronda peridotite and the neighboring units (see location on Figure 2). Cross-section modified after Platt et al. (2003, 2013); Esteban et al. (2008); Tubía et al. (2013) and Acosta-Vigil et al. (2014).

variations that may be due to the effect of topography and the offset related to localized structures such as shear zones or faults, RSCM T_{max} shows a general decrease from ca. 600°C to around 300°C over ca. 30 km along the contact (Figure 11). Rocks of the Nieves Unit therefore experienced highly variable metamorphic temperatures along the contact with the Ronda peridotite from NE to SW and are involved in a large-scale lateral temperature gradient.

Effects of late folding on the former finite thermal structure cannot be confidently retrieved as the data set does not appears dense enough along a single cross-section to accurately constrain the obliquity of the RSCM isograds and the fold geometries. It is however noteworthy that higher temperatures are locally observed in the core of the late antiform while lower temperatures occupy the synforms in the vicinity of the Nava Breccia deposits (Figures 10 and 11), suggesting that RSCM isograds appear slightly affected by late folding.

6. Discussion

6.1. Geometry Versus Thermal Structure of the Nieves Unit

As described above, the strain gradient observed within the Nieves Unit when approaching the contact with the peridotite reveals a sinistral ductile shear zone, similarly to the one observed in the Ronda peridotite

(Figures 3, 7 and 8). A single ductile fabric including a steep NE-SW foliation and a NE-SW lineation is developed across the thick zone across the contact (Figure 12). Minor brittle deformation can be locally observed (Mazzoli & Martín-Algarra, 2011), but the two well-exposed old mines and numerous outcrops including fresh road cuts show a ductile contact (Figures 3–8). Therefore, any late brittle movement along the contact was local, minor and does not modify the former geometrical relations produced during ductile deformation and mineralization. In addition, part of the left-lateral oblique shear zones that affect the foliation of the Nieves Unit marbles are rooted in the contact with the peridotite, even though a few of them may offset the contact (Figure 3 and S1). The observed faults locally impact the strike of the main composite fabric, which is bent from N40°–N50°E, its preferred direction for the whole studied area, to N170°E–N20°E when approaching the shear zones (Figure 3 and S1). This implies that the nucleation of these structures occurred in ductile conditions without significant reactivation in the brittle field. Despite these local disturbances, the strikes of bedding, schistosity and stretching lineation are parallel to the trace of the contact with the Ronda peridotite (Figures 3, 9 and 12). Besides, an increasing component of ductile shearing is recorded when approaching the contact with the peridotite (Figures 3 and 8).

These results markedly contrast with the study of Mazzoli et al. (2013) in three important ways: (a) the trend of stretching lineations shows that most of the relative displacement between the Nieves Unit and the Ronda peridotite appears almost parallel to the NE-SW trace of the contact and not toward the NW as implied by the thrust model; (b) the strike of foliation and trend of stretching lineation seem continuous across the contact with the peridotite, suggesting that the Nieves Unit and the Ronda peridotite underwent the same deformation event in the ductile field and then behave as a single, coherent block afterward; and (c) therefore, the contact between the Nieves Unit and the Ronda peridotite appears as a genuine ductile shear zone showing a sinistral kinematics in the present geometry (Figures 3, 7, 8, 9 and 12). This point is discussed specifically in Section 6.3.

The thermal structure of the Nieves Unit shows a very steep thermal gradient from 600°C, close to the contact, down to less than 350°C only 2.2 km apart (Figures 11 and 12). Temperatures even drop down below 200°C north of the Nava breccia, farther north (Figure 11). Despite minor variations, these results were already reached by the previous study of Mazzoli et al. (2013), but are extended here from a single section to a map, allowing an accurate mapping of the RSCM isograds. At that scale, the traces of the isograds appear oblique to the contact with the peridotite and RSCM T_{max} decreases from ca. 600°C to less than 200°C over ca. 5 km along the contact (Figure 11). By extending further to the NE along the contact between the Nieves Unit and the Ronda peridotite over ca. 30 km, temperatures significantly decrease down ~300°C (Figures 11 and 12). This large-scale evolution of the metamorphic temperatures along the contact with the Ronda peridotite seems to extend further SW on the other side of the large-scale triple junction formed by the Ronda peridotite, the crustal rocks of the Jubrique Unit and the Nieves Unit on the map with the existence of high-grade metamorphism in the lower parts of the Jubrique Unit. In this area, temperature conditions in the field of partial melting reached temperature as high as 780°C (Acosta-Vigil et al., 2014; Balanyá et al., 1997; Barich et al., 2014; Negro et al., 2006; Platt et al., 2003). In parallel, the petrology of the peridotites also shows a significant evolution parallel to the contact. High-pressure mylonitized peridotites are found further SW in contact with the kinzigites of the Jubrique Unit (Précigout et al., 2013), while low-pressure plagioclase tectonite crops out to the NE in contact with the Nieves Unit (Obata, 1980).

Based on this large-scale consistency of the thermal structure in both the Jubrique Unit and Nieves Unit along the western bound of the Ronda peridotite, it appears therefore tempting to propose as a working hypothesis that this contact corresponds to a single tectonic contact extending to the NE the so-called Bermeja-Jubrique Shear Zone (BJSZ; Balanyá et al., 1997). This proposition is consistent with the continuity of the peridotite on each side of the triple junction.

6.2. Magnetite Mineralizations and Ophicalcites

Magnetite mineralizations occur along the contact between the Nieves Unit and the Ronda peridotite as discrete, localized deposits (Figures 3, 4 and 6). Field relationships between ore deposits and deformation show that ore deposition occurred in the ductile field (Figure 5). Observations of fractured and brecciated serpentinized peridotites (centimeter-to meter-scale), which are traversed and cemented by a

locally dense array of calcite veins, have been reported in this study within the contact zone and in the top-most parts of the Ronda peridotite (Figure 4). This type of rocks corresponds to the ophicalcites or ophiolitic *mélange* definition (Brongniart, 1813), which corresponds to the ophicalcites first type of Lemoine et al., (1987) described in the French Alps or to the "*tectonically controlled*" type of Clerc et al. (2013) described in the Pyrenees (France).

These rocks are commonly associated and related to mantle exhumation (Clerc et al., 2013; Lagabrielle et al., 2010; Lemoine et al., 1987). They are characterized by a rock *mélange* formed by carbonatized serpentine and/or serpentinized peridotite blocks. Ophicalcites formation is related to fluid circulation and low-temperature alteration of serpentine. This process occurs in various geological settings like (a) slow-spreading ridges and oceanic transform faults (Mével, 2003), (b) ocean-continent transition (OCT) zones in passive margins (Agrinier et al., 1988; Milliken & Morgan, 1996; Schwarzenbach et al., 2013) or (c) modern alteration at ambient temperature in outcropping peridotites (Kelemen & Matter, 2008; Streit et al., 2012). Mantle rocks exposed to sea water in OCT of passive margins or mid-oceanic ridges is at shallow depth and low-temperature (Clerc et al., 2013; Jammes et al., 2009; Lagabrielle & Bodinier, 2008; Lagabrielle et al., 2010; Picazo et al., 2012). In fact, the depth of formation cannot exceed 3–4 km in the case of (ultra-) slow-spreading ridges (Cannat et al., 2010).

Considering the formation modalities of ophicalcites in a hyper-extension context, when ultramafic rocks are exposed to sea water, serpentinization reactions occur and produce serpentine ± brucite ± talc ± magnetite (Klein et al., 2013). This reaction is controlled by several parameters, the most important one being temperature (Klein et al., 2009, 2013, 2014; Martin & Fyfe, 1970; Malvoisin, Brunet, et al., 2012; Malvoisin, Carlut, & Brunet, 2012; Mayhew et al., 2013; McCollom & Bach, 2009; McCollom et al., 2016; Moody, 1976). Brucite and talc formation also depends on the composition of ultramafic rocks, with the relative proportion between olivine and orthopyroxene as a limiting factor. Depending on the water/rock (w/r) ratio, mineral assemblages can evolve from a brucite-serpentine-clinopyroxene-wustite assemblage for w/r ratio <0.3, to a talc-serpentine assemblage for a w/r ratio >130–140. Using thermodynamic modeling, Klein et al. (2013) showed that a w/r ratio >10 is required to produce magnetite for a peridotite composition similar to the composition of the Ronda peridotite. It is also shown in that study that the production of serpentine embraces a quite large temperature range from 400°C to very low temperatures (Klein et al., 2013). Conversely, peak-production conditions for associated magnetite and a Fe-poor serpentine is much more restrictive and are bracketed in a narrow temperature range of 350°C down to 270°C. Table 1 shows that chemical composition of serpentinite associated with magnetite in the studied area is indeed Fe-poor, with Fe content <3%. Interestingly, the modeled paragenetic succession from 400°C to ambient temperatures corresponds to the observed succession including minor production of talc, the association magnetite + Fe-poor serpentine and then brucite. To summarize, the magnetite ore deposition along the contact associated with ductile deformation shows that a large amount of water interacted with the exhuming mantle and that the contact remained ductile until rather low temperature, 350°C or even less before it was frozen and only locally cut by high-angle brittle-ductile shear zones.

6.3. The Nieves Unit/Ronda Peridotite Contact: Thrust or Detachment?

Drastic contraction of the metamorphic isotherms in the Jubrique Unit has long been interpreted as the result of syn-metamorphic thinning and stretching of the Alpujárride lithologic sequence coeval with intense shearing along the BJSZ (Balanyá et al., 1997; Negro et al., 2006). Shearing is recorded across the pluri-hectometric thickness of H*T*-mylonites developed at the expense of both lower crustal rocks of the Jubrique Unit and mantle rocks of the Ronda peridotite (Balanyá et al., 1997; Précigout et al., 2013; Van der Wal & Vissers, 1996). There, rocks are marked by a strong, gently dipping NE-SW stretching lineation while the bulk of the Jubrique Unit is characterized by a more N-S stretching (Figure 14; Williams & Platt, 2018). Kinematic indicators that are ambiguous and partly conflicting in the crustal rocks of the Jubrique Unit involved in the BJSZ (Balanyá et al., 1997) are conversely very clear in the peridotite drawing large-scale sigmoids (Précigout et al., 2013) and therefore pointing to a sinistral overall shear sense. Based on the bending of foliation trajectories in the peridotite toward the contact with the Jubrique Unit, Précigout et al. (2013) concluded that this contact is, in its current position, a left-lateral shear zone. This was more recently con-

10.1029/2020TC006271

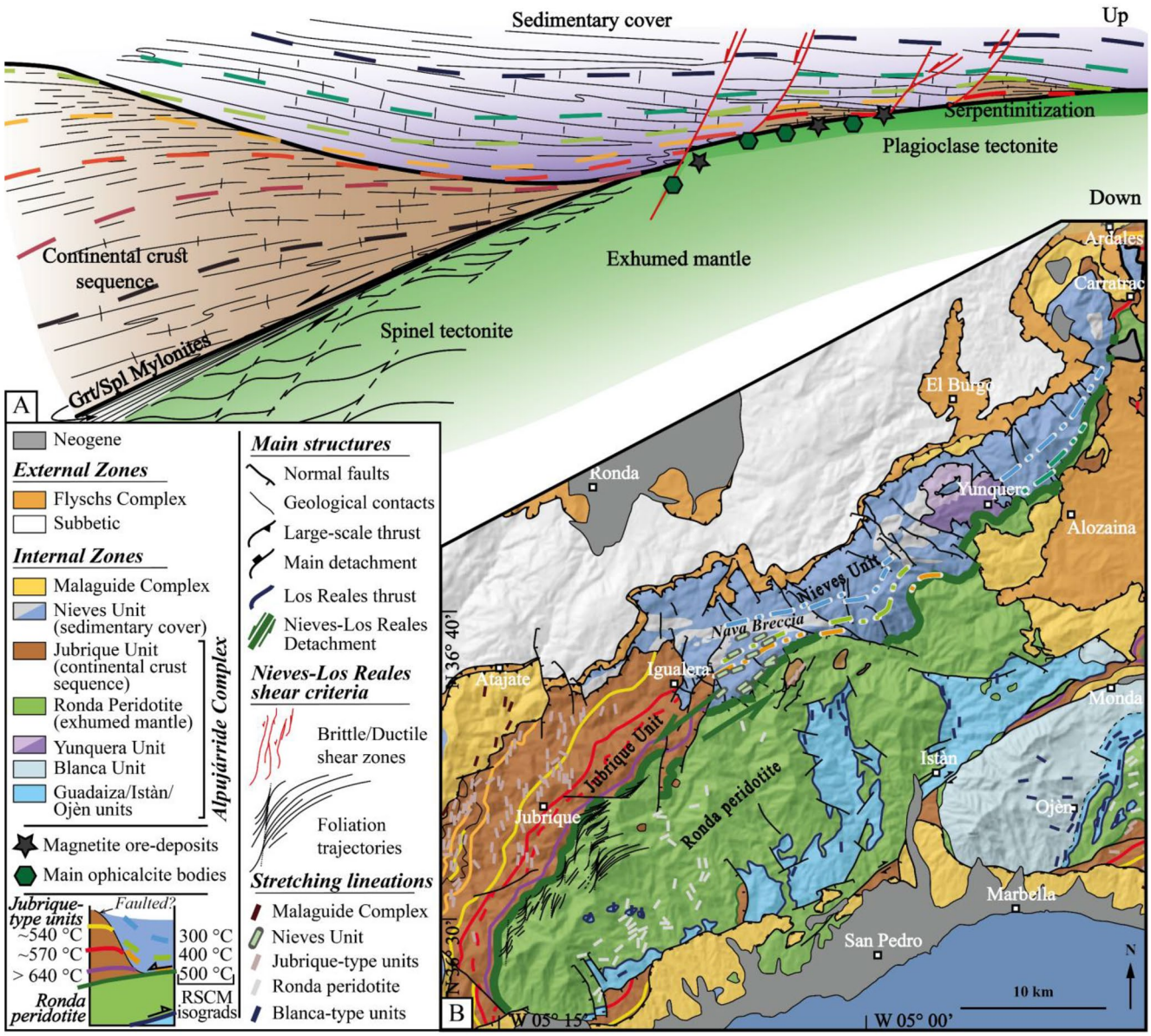

Figure 14. Proposed cross-section of the Nieves-Los Reales Detachment in a restored position during the hyper-extension stage. (a) Presumed relationships between the Ronda peridotite in the footwall of the Nieves-Los Reales Detachment and the Jubrique Unit/Nieves Unit in the hanging wall block. The hanging wall block is formed by a dramatically thinned crustal sequence, the Jubrique Unit, and its probable sedimentary cover, the Nieves Unit. Formation of ophicalcite bodies and massive magnetite deposits occurred late in the evolution of the system. (b) Detailed geological map of the western part of the Internal Zones of the Betic Cordillera highlighting the present-day relationships between the main metamorphic units and the position of the Nieves-Los Reales Detachment defined in this study. The metamorphic features are the same as in Figure 2 and refer to Balanyá et al. (1997); Negro et al. (2006); Esteban et al. (2008); Précigout et al. (2013); Tubía et al. (2013); Pedrera et al. (2015); Williams and Platt (2018).

firmed by Johanesen and Platt (2015) through a study of the peridotite fabric showing top-to-the-SW sense of shear during ductile deformation. According to the restored position of both the metamorphic isograds and the main planar fabrics, attenuation of the Jubrique Unit appears related to an intense vertical ductile thinning coeval with the activity of the BJSZ as a major top to the SW shear zone (Frasca et al., 2017; Hidas et al., 2013; Johanesen & Platt, 2015; Van der Wal & Vissers 1996; Vissers 2012). The extensional character of this shear zone is widely recognized and considered as a major detachment/decollement zone developed during continental extension (Afiri et al., 2011; Balanyá et al., 1997; Frasca et al., 2016; Garrido et al., 2011; Platt et al., 2003; Précigout et al., 2013).

However, few hundreds of meter along-strike toward the NE, the contact between the Nieves Unit and Ronda peridotite has been instead interpreted as the emergence of a major thrust bounding the Los Reales nappe (Figures 1 and 13b; Martín-Algarra, 1987; Mazzoli et al., 2013; Mazzoli & Martín-Algarra, 2011). According to these studies, both deformation and metamorphism developed within the Nieves Unit is envisioned as the result of the emplacement of the hot peridotite body over the Nieves Unit by the top-to-the-NW thrusting. Yet, this interpretation can be simply questioned based on the cartographic continuity of the western contact of the Ronda peridotite with the crustal rocks of the Jubrique Unit and Nieves Unit (Figure 1). In this section, we thus explore a possible re-interpretation of the contact between the Nieves Unit and Ronda peridotite as a NE-ward extension of the BJSZ along the peridotite/Nieves contact beyond the triple junction that marks the boundary between basement rocks of the Jubrique Unit and sedimentary cover of the Nieves Unit (Figures 13 and 14). The progressive NE-ward decrease of temperature along the contact shows that the northeastern part was active in a higher structural position (Figures 11 and 12).

The debate on the significance of the high-*T* metamorphism and the associated deformation therefore primarily hinges either on the relative structural position of the Nieves Unit at large-scale with respect to the Ronda peridotite or the geometry and kinematics of the contact. The main arguments are summarized below:

1. Structural observations of the contact between the Nieves Unit and the Ronda peridotite highlight this contact as steep, locally vertical, but rarely overturned (Figures 3, 12 and 13a). Crustal rocks sandwiched in the contact zone also occur with a steep attitude. However, crustal rocks also occur above the peridotites with a very gently dipping contact and flat to very gently SE dipping foliation in both units Figures 3 and 12). For instance, we show here that the large felsic rocks body located to the SE of the study area in the Robledal area (Figures 7c and 7d) rests as a tectonic klippe on top of the Ronda peridotite. These rocks therefore correspond to remnants of tectonic units preserved above the Ronda peridotite just as the Jubrique Unit (Balanyá et al., 1997; García-Dueñas et al., 1992; Johanesen & Platt, 2015; Platt et al., 2013; Précigout et al., 2013). Consequently, these rocks do not crop out within a large-scale tectonic window as proposed by Mazzoli et al. (2013) and can therefore not be used as evidence of the allochtony of the Ronda peridotite with respect to crustal rocks at variance with the Guadaiza tectonic window (Acosta-Vigil et al., 2014; Esteban et al., 2004, 2008, 2013; Frasca et al., 2015, 2017; Martín-Algarra & Estévez, 1984; Mazzoli et al., 2013; Mazzoli & Martín-Algarra, 2011; Platt et al., 2003, 2013; Sánchez-Rodríguez & Gebauer, 2000; Sanz de Galdeano & Andreo, 1995; Tubía & Cuevas, 1986; Tubía & Ibarguchi, 1991, Tubía et al., 1992, 1997, 2013). Stretching lineations retrieved from the crustal rocks in the Robledal area moreover show a NE-SW orientation inconsistent with the N-S lineation that regionally characterizes the stretching into the metamorphic sole developed during the thrusting of the Ronda peridotite (Esteban et al., 2008; Williams & Platt, 2018).
2. The consistency of ductile finite strain markers, NE-SW foliation and NE-SW stretching lineation (Figures 3, 7, 9 and 12), across the contact strongly argue for the preservation of a former ductile shear zone passively integrated into the Betics orogenic wedge (Figures 8 and 13a), in contrast to the classical juxtaposion of the Ronda peridotite onto the Nieves Unit by a single NW-directed thrust (Nieves Unit position with respect of the Ronda peridotite in the cross-section 2 of Figure 13b; Martín-Algarra, 1987; Mazzoli et al., 2013; Mazzoli & Martín-Algarra, 2011).
3. Kinematics of the ductile deformation located in the vicinity of the contact between the Nieves Unit and Ronda peridotite corresponds to left-lateral shearing (Figures 3, 7 and 8). Activity of this shear zone is accompanied, and partly post-dated, by the development of an array of smaller-scale brittle-ductile shear zones cutting across the Nieves Unit with a consistent sinistral component (Figures 3 and S1). This picture is currently disrupted by a dense array of late brittle normal faults, particularly obliterating the contact between the Nieves Unit and Jubrique Unit (Figure 3).
4. Metamorphic isograds, as shown by the mapping of RSCM T_{max}, are oblique to the contact with strong decrease of RSCM T_{max} toward the NE within the Nieves Unit from ca. 600°C to ca. 300°C over ca. 30 km along the contact (Figure 11). Conversely, temperatures drastically increase toward the SW to reach temperatures as high as 780°C in the lower parts of the Jubrique Unit (Balanyá et al., 1997). This obliquity between the large-scale geometries and the thermal structure is a common feature of major extensional shear zones, such as described for the Malaguide/Alpujarride Contact (e.g., Vissers et al., 1995) or the Mecina/Filabres shear zone roofing the Nevado Filabride Complex (e.g., Martínez-Martínez & Azañón, 1997).

We therefore propose that the shear zone described between the Nieves Unit and the Ronda peridotite forms a geometrically, kinematically and mechanically linked single structure with the BJSZ. Rotating back the whole system about a horizontal axis rotation using metamorphic isograds (Jubrique Unit; Balanyá et al., 1997; Negro et al., 2006) or RSCM isograds (Nieves Unit, this study), this shear zone becomes a SW-directed gently dipping extensional detachment characterized by a common top-to-the-SW kinematics (Figure 14). The gneiss of the Robledal klippe lying on top of the system and characterized by gently dipping foliation escaped significant rotation and shows the initial position of the shear zone before late thrusting. In our model, mantle rocks have been exhumed and juxtaposed with the sedimentary cover of the Nieves Unit along the same extensional shear zone, previously only recognized along the contact between the Jubrique Unit and the Ronda peridotite, giving rise to H*T* metamorphism as in the Pyrenean examples of sub-continental mantle exhumation (Clerc et al., 2015; Lagabrielle et al., 2010). Occurrence of massive fluid circulation at shallow depth also accounts for the formation of ophicalcites and magnetite deposits during exhumation (Clerc et al., 2013; Klein et al., 2013). The Nieves/Jubrique units and the Ronda peridotite therefore respectively constitute the hangingwall and footwall of a large-scale detachment, which we term the *Nieves-Los Reales Detachment*, called hereafter the NLRD (Figures 13 and 14). On Figure 14, we sketch a restored image of the NLRD at the time of extension and hyperextension. The main shear zone exhumes sub-continental mantle rocks from below the Jubrique Unit, and then the sedimentary cover of the Nieves Unit. Small rafts of crustal units are abandoned along the detachment, as exemplified by the Robledal klippe, or along the contact between the Nieves Unit and the Ronda peridotite. This crustal-scale detachment responsible for the exhumation of mantle rocks can be followed over more than 50 km parallel to the movement and therefore appears as a first order structure of the Alpujárride Complex. Another implicit yet important outcome of this study concerns the relationships between the Jubrique Unit and the Nieves Unit. In the lights of this study, these units both form the hanging wall unit of the NLRD, sharing, despite minor differences the same tectonometamorphic evolution including a drastic contraction either of the metamorphic sequence in the Jubrique Unit or the metasedimentary succession in the Nieves Unit acquired during exhumation. It appears therefore tempting to propose the Nieves Unit to represent the probably partly detached sedimentary cover of the upper Alpujàride units as proposed by Chalouan and Michard (2004).

6.4. Late Tectonic Inversion and Overthrusting

Despite the preservation of what appears as a first-order extensional feature in the heart of the Betics, it is beyond doubt that a major episode of thrusting accounts for the final emplacement of the Los Reales nappe and more generally of the Internal Zones onto the Iberian margin around 20 Ma ago (Balanyá & García-Dueñas, 1987; Guerrera et al., 2005; Gueydan et al., 2019; Platt et al., 2013; Williams & Platt, 2018). Classical studies deduced this large-scale thrusting of the Los Reales nappe based on large-scale tectonic windows, such as the Guadaiza or the Istán windows in which basement and cover rocks from the western Alpujarride complex (i.e., the Blanca group units) appear tectonically overlain by the Ronda peridotite. Thrusting of hot mantle rocks is in this case attested by the development of a deformed metamorphic sole known as the dynamothermal aureole (Acosta-Vigil et al., 2014; Bartoli et al., 2013, 2016; Esteban et al., 2008; Tubía & Cuevas, 1986; Tubía et al., 1997). The contact zone then corresponds to a migmatitic breccia, produced by partial melting and deformation during the emplacement of the peridotite in early Miocene (Esteban et al., 2011). Note however that this view has been recently challenged by Sanz de Galdeano and Ruiz Cruz (2016) who interpret these same formations as metasedimentary breccias of Triassic age. Nevertheless, this main thrust does not breach the surface along the western contact of the peridotite, cutting the NLRD, but further to the northwest along the western front of the Nieves Unit, that is, along the Internal-External Boundary Zone, it is marked by the Flyschs Complex thrusted indifferently by the Malaguide and Alpujárride complexes as well as by the Nieves Unit (Figures 13 and 14). Instead, after the main increments of exhumation of the Ronda peridotite, the NLRD was frozen, passively folded and only locally cut by brittle faults, but it was not reactivated during the compressional stage, so that most ductile deformation has been preserved from the former, pre-thrusting event. During Miocene times, the late emplacement by thrusting onto the External Zones and Flyschs Complex of the Internal Zones had tectonic and structural consequences. The NLRD has been verticalized, and even locally overturned while the bulk of the Nieves Unit was affected by open to tight post-metamorphic folding as described by Mazzoli et al. (2013). Orientation of

these late folds axes is indeed consistent with the Miocene compressional episode, that is, the overall top-to-the-NW kinematics, and corresponds to that ended with the overthrusting of the Alpujárride Complex and the Nieves Unit on top of the External Zones.

7. Conclusion

Based on new field observations focused mainly on the Nieves Unit and the contact between the Nieves Unit and the Ronda peridotite, we here reconsider the tectonometamorphic evolution of the western Alpujárrides and particularly the sequence of geological events that resulted in its present-day complex finite structure. At first, the shear zone along the western rim of the peridotite body, that is, the contact with the Jubrique Unit is proposed to extend toward the NE as a single first order shear zone that bounds the Nieves Unit, named the *Nieves-Los Reales Detachment*. Together with kinematic indicators, foliation trajectories and trend of stretching lineations parallel to the trace of the contact argue for a left-lateral shear zone in the present-day geometry mostly characterized by ductile deformation. We also re-interpret the structural position of a crustal occurrence in the studied area as a klippe on top of the peridotite, which ensures the former relative position of the Jubrique/Nieves block in the hanging wall unit of the NLRD, instead of a tectonic window below the Los Reales nappe. Our field observations are complemented by an extensive RSCM data set in the Nieves Unit that constrain the finite thermal structure of the Nieves Unit. High-resolution RSCM T_{max} mapping focused on the western parts of the Nieves Unit allow refining the geometry of the metamorphic gradient developed in the vicinity of the Ronda peridotite. Field gradients that appear slightly affected by late folding reach values as extreme as ca. 120°C/km, highlighting a drastic contraction of the isotherms. Larger scale approach shows a conspicuous obliquity of the RSCM isograds to the contact with the Ronda peridotite. Occurence of ophicalcites and magnetite ores along the contact further show intense fluid circulations associated with the activity of the shear zone at lower temperature during the end of ductile deformation. This shear zone extends the Bermeja-Jubrique Shear Zone toward the NE and can be seen as its shallower equivalent. The NLRD is therefore similar to those described in hyper-extension contexts, such as the Pyrenean rift system exhuming sub-continental mantle from below crustal units and cover sequences. Because the ductile contact is still observed, we conclude that this contact has been frozen and not reworked after the end of extensional tectonics. Peridotites was thus exhumed to shallow crustal levels by a mechanism of hyper-extension before the final thrust-related emplacement in the whole Internal Zones of the Betic Cordillera during Early Miocene. Future work should nevertheless focus on the precise timing and the context of this hyper-extension event with respect to the tectonic history of the Western Betics.

Data Availability Statement

All the data set is provided in this paper and available here: https://zenodo.org/record/5175852#.YRJeJuc682w.

Acknowledgments
This work was funded by the OROGEN Project, including the French Geological Survey (BRGM), CNRS, and TOTAL. The authors thank I. di Carlo for the microprobe analysis achieved in ISTO laboratory. The authors also warmly thank M. Ducoux and G. Barré, from TOTAL and UPPA (Université de Pau et Pays de l'Adour), for very interesting and helpful discussions. Our gratitude is extended to the Editors, John Geissman and Margaret Rusmore, as well as the Associate Editors who provided additional helpful comments. The authors want to gratefully acknowledge Agustín Martín-Algarra, John Platt, Douwe van Hinsbergen, Guillermo Booth-Rea and two anonymous referees for their constructive comments and suggestions that contributed to improve the quality of the manuscript.

References

Acosta-Vigil, A., Rubatto, D., Bartoli, O., Cesare, B., Meli, S., Pedrera, A., et al. (2014). Age of anatexis in the crustal footwall of the Ronda peridotites, S Spain. *Lithos*, *210–211*, 147–167. https://doi.org/10.1016/j.lithos.2014.08.018

Afiri, A., Gueydan, F., Pitra, P., Essaifi, A., & Précigout, J. (2011). Oligo-Miocene exhumation of the Beni-Bousera peridotite through a lithosphere-scale extensional shear zone. *Geodinamica Acta*, *24*, 49–60. https://doi.org/10.3166/ga.24.49-60

Agard, P., Augier, R., & Monié, P. (2011). Shear band formation and strain localization on a regional scale: Evidence from anisotropic rocks below a major detachment (Betic Cordilleras, Spain). *Journal of Structural Geology*, *33*, 114–131. https://doi.org/10.1016/j.jsg.2010.11.011

Agrinier, P., Javoy, M., & Girardeau, J. (1988). Hydrothermal activity in a peculiar oceanic ridge: Oxygen and hydrogen isotope evidence in the Xigaze ophiolite (Tibet, China). *Chemical Geology*, *71*, 313–335. https://doi.org/10.1016/0009-2541(88)90057-5

Aldaya, F., Alvarez, F., Galindo-Zaldívar, J., González-Lodeiro, F., Jabaloy, A., & Navarro-Villá, F. (1991). The Malaguide-Alpujarride contact (Betic Cordilleras, Spain): A brittle extensional detachment. *Comptes rendus de l'Académie des sciences. Série 2, Mécanique, Physique, Chimie, Sciences de l'univers, Sciences de la Terre*, *313*, 1447–1453.

Aldaya, F., García-Dueñas, V., & Vilá, F. N. (1979). Los Mantos apujárrides del tercio central de las Cordilleras Béticas. Ensayo de la correlación tectónica de los Alpujárrides. *Acta Geológica Hispánica*, 154–166.

Allerton, S., Lonergan, L., Platt, J. P., Platzman, E. S., & McClelland, E. (1993). Palaeomagnetic rotations in the eastern Betic Cordillera, southern Spain. *Earth and Planetary Science Letters*, *119*, 225–241. https://doi.org/10.1016/0012-821x(93)90135-v

Andrieux, J., Fontbote, J.-M., & Mattauer, M. (1971). Sur un modele explicatif de l'arc de Gibraltar. *Earth and Planetary Science Letters*, *12*, 191–198. https://doi.org/10.1016/0012-821x(71)90077-x

Angiboust, S., Agard, P., Raimbourg, H., Yamato, P., & Huet, B. (2011). Subduction interface processes recorded by eclogite-facies shear zones (Monviso, W. Alps). *Lithos*, *127*, 222–238. https://doi.org/10.1016/j.lithos.2011.09.004

Aoya, M., Kouketsu, Y., Endo, S., Shimizu, H., Mizukami, T., Nakamura, D., & Wallis, S. (2010). Extending the applicability of the Raman carbonaceous-material geothermometer using data from contact metamorphic rocks. *Journal of Metamorphic Geology*, *28*, 895–914. https://doi.org/10.1111/j.1525-1314.2010.00896.x

Argles, T. W., Platt, J. P., & Waters, D. J. (1999). Attenuation and excision of a crustal section during extensional exhumation: The Carratraca Massif, Betic Cordillera, southern Spain. *Journal of the Geological Society*, *156*, 149–162. https://doi.org/10.1144/gsjgs.156.1.0149

Augier, R., Agard, P., Monie, P., Jolivet, L., Robin, C., & Booth-Rea, G. (2005). Exhumation, doming and slab retreat in the Betic Cordillera (SE Spain): In situ $^{40}Ar/^{39}Ar$ ages and *P-T-d-t* paths for the Nevado-Filabride complex. *Journal of Metamorphic Geology*, *23*, 357–381. https://doi.org/10.1111/j.1525-1314.2005.00581.x

Augier, R., Jolivet, L., Gadenne, L., Lahfid, A., & Driussi, O. (2015). Exhumation kinematics of the Cycladic Blueschists unit and back-arc extension, insight from the Southern Cyclades (Sikinos and Folegandros Islands, Greece). *Tectonics*, *34*, 152–185. https://doi.org/10.1002/2014tc003664

Augier, R., Jolivet, L., & Robin, C. (2005). Late Orogenic doming in the eastern Betic Cordilleras: Final exhumation of the Nevado-Filabride complex and its relation to basin genesis. *Tectonics*, *24*. https://doi.org/10.1029/2004tc001687

Azañón, J. M., & Crespo-Blanc, A. (2000). Exhumation during a continental collision inferred from the tectonometamorphic evolution of the Alpujarride Complex in the central Betics (Alboran Domain, SE Spain). *Tectonics*, *19*, 549–565. https://doi.org/10.1029/2000tc900005

Azañón, J. M., Crespo-blanc, A., & García-Dueñas, V. (1997). Continental collision, crustal thinning and nappe forming during the pre-Miocene evolution of the Alpujarride Complex (Alboran Domain, Betics). *Journal of Structural Geology*, *19*, 1055–1071.

Azañón, J. M., García-Dueñas, V., & Goffé, B. (1998). Exhumation of high-pressure metapelites and coeval crustal extension in the Alpujarride complex (Betic Cordillera). *Tectonophysics*, *285*, 231–252. https://doi.org/10.1016/s0040-1951(97)00273-4

Azañón, J. M., & Goffe, B. (1997). Ferro-and magnesiocarpholite assemblages as record of high-P, low-T metamorphism in the central Alpujarrides, Betic Cordillera (SE Spain). *European Journal of Mineralogy-Ohne Beihefte*, *9*(5), 1035–1052. https://doi.org/10.1127/ejm/9/5/1035

Balanyá, J. C., & García-Dueñas, V. (1987). Les directions structurales dans le Domaine d'Alborán de part et d'autre du Détroit de Gibraltar. *Comptes rendus de l'Académie des sciences. Série 2, Mécanique, Physique, Chimie, Sciences de l'univers, Sciences de la Terre*, *304*(15), 929–932.

Balanyá, J. C., García-Dueñas, V., Azañón, J. M., & Sánchez-Gómez, M. (1997). Alternating contractional and extensional events in the Alpujarride nappes of the Alboran Domain (Betics, Gibraltar Arc). *Tectonics*, *16*, 226–238. https://doi.org/10.1029/96tc03871

Barich, A., Acosta-Vigil, A., Garrido, C. J., Cesare, B., Tajčmanová, L., & Bartoli, O. (2014). Microstructures and petrology of melt inclusions in the anatectic sequence of Jubrique (Betic Cordillera, S Spain): Implications for crustal anatexis. *Lithos*, *206–207*, 303–320. https://doi.org/10.1016/j.lithos.2014.08.003

Barich, A., Acosta-Vigil, A., Garrido, C. J., Cesare, B., Tajčmanová, L., & Bartoli, O. (2016). Corrigendum to" Microstructures and petrology of melt inclusions in the anatectic sequence of Jubrique (Betic Cordillera, S Spain): Implications for crustal anatexis"[Lithos 206-207 (2014) 303-320]. *Litho*, *264*, 596–596. https://doi.org/10.1016/j.lithos.2016.08.033

Bartoli, O., Acosta-Vigil, A., Tajčmanová, L., Cesare, B., & Bodnar, R. J. (2016). Using nanogranitoids and phase equilibria modeling to unravel anatexis in the crustal footwall of the Ronda peridotites (Betic Cordillera, S Spain). *Lithos*, *256*, 282–299. https://doi.org/10.1016/j.lithos.2016.03.016

Bartoli, O., Tajčmanová, L., Cesare, B., & Acosta-Vigil, A. (2013). Phase equilibria constraints on melting of stromatic migmatites from Ronda (S. S pain): Insights on the formation of peritectic garnet. *Journal of Metamorphic Geology*, *31*(7), 775–789. https://doi.org/10.1111/jmg.12044

Beaudoin, A., Augier, R., Laurent, V., Jolivet, L., Lahfid, A., Bosse, V., et al. (2015). The Ikaria high-temperature metamorphic core complex (Cyclades, Greece): Geometry, kinematics and thermal structure. *Journal of Geodynamics*, *92*, 18–41. https://doi.org/10.1016/j.jog.2015.09.004

Behr, W. M., & Platt, J. P. (2012). Kinematic and thermal evolution during two-stage exhumation of a Mediterranean subduction complex. *Tectonics*, *31*. https://doi.org/10.1029/2012tc003121

Bellanger, M., Augier, R., Bellahsen, N., Jolivet, L., Monié, P., Baudin, T., & Beyssac, O. (2015). Shortening of the European Dauphinois margin (Oisans Massif, Western Alps): New insights from RSCM maximum temperature estimates and $^{40}Ar/^{39}Ar$ in situ dating. *Journal of Geodynamics*, *83*, 37–64. https://doi.org/10.1016/j.jog.2014.09.004

Berndt, T., Ruiz-Martínez, V. C., & Chalouan, A. (2015). New constraints on the evolution of the Gibraltar Arc from palaeomagnetic data of the Ceuta and Beni Bousera peridotites (Rif, northern Africa). *Journal of Geodynamics*, *84*, 19–39. https://doi.org/10.1016/j.jog.2014.09.014

Bessière, E., Jolivet, L., Augier, R., Scaillet, S., Précigout, J., Azañon, J.-M., et al. (2021). Lateral variations of pressure-temperature evolution in non-cylindrical orogens and 3-D subduction dynamics: The Betic-Rif cordillera example. *Bulletin de la Societe Geologique de France*, *192*(1), 8. https://doi.org/10.1051/bsgf/2021007

Beyssac, O., Bollinger, L., Avouac, J.-P., & Goffé, B. (2004). Thermal metamorphism in the lesser Himalaya of Nepal determined from Raman spectroscopy of carbonaceous material. *Earth and Planetary Science Letters*, *225*, 233–241. https://doi.org/10.1016/j.epsl.2004.05.023

Beyssac, O., Goffé, B., Chopin, C., & Rouzaud, J. N. (2002). Raman spectra of carbonaceous material in metasediments: A new geothermometer. *Journal of Metamorphic Geology*, *20*, 859–871. https://doi.org/10.1046/j.1525-1314.2002.00408.x

Beyssac, O., Rouzaud, J.-N., Goffé, B., Brunet, F., & Chopin, C. (2002). Graphitization in a high-pressure, low-temperature metamorphic gradient: A Raman microspectroscopy and HRTEM study. *Contributions to Mineralogy and Petrology*, *143*, 19–31. https://doi.org/10.1007/s00410-001-0324-7

Beyssac, O., Simoes, M., Avouac, J.-P., Farley, K. A., Chen, Y.-G., Chan, Y.-C., & Goffé, B. (2007). Late Cenozoic metamorphic evolution and exhumation of Taiwan. *Tectonics*, *26*. https://doi.org/10.1029/2006tc002064

Blichert-Toft, J. (1999). Lu-Hf Isotope systematics of garnet pyroxenites from Beni Bousera, Morocco: Implications for Basalt Origin. *Science*, *283*, 1303–1306. https://doi.org/10.1126/science.283.5406.1303

Blumenthal, M. (1927). Zum Bauplan betischer und penibetischer Decken im Norden der Provinz Málaga. *Geologische Rundschau*, *18*, 37–45. https://doi.org/10.1007/bf01802765

Blumenthal, M. (1933). Sur les rélations tectoniques entre les zones bétique, pénibétique et subbétique du SW. de l'Andalousie. *Comptes rendus de l'Académie des Sciences*, *197*, 1.

Booth-Rea, G., Azañón, J. M., García-Dueñas, V., Augier, R., & Sánchez-Gómez, M. (2003). A 'core-complex-like structure'formed by superimposed extension, folding and high-angle normal faulting. The Santi Petri dome (western Betics, Spain). *Comptes Rendus Geoscience*, *335*(2), 265–274. https://doi.org/10.1016/s1631-0713(03)00026-9

Booth-Rea, G., Azañón, J. M., Martínez-Martínez, J. M., Vidal, O., & García-Dueñas, V. (2005). Contrasting structural and P-T evolution of tectonic units in the southeastern Betics: Key for understanding the exhumation of the Alboran Domain HP/LT crustal rocks (western Mediterranean). *Tectonics*, *24*. https://doi.org/10.1029/2004tc001640

Booth-Rea, G., Martínez-Martínez, J. M., & Giaconia, F. (2015). Continental subduction, intracrustal shortening, and coeval upper-crustal extension: PT evolution of subducted south Iberian paleomargin metapelites (Betics, SE Spain). *Tectonophysics*, *663*, 122–139. https://doi.org/10.1016/j.tecto.2015.08.036

Brongniart, A. (1813). *Essai d'une classification minéralogique des roches mélangées*.

Brune, S., Heine, C., Pérez-Gussinyé, M., & Sobolev, S. V. (2014). Rift migration explains continental margin asymmetry and crustal hyper-extension. *Nature Communications*, *5*. https://doi.org/10.1038/ncomms5014

Cannat, M., Fontaine, F., & Escartín, J. (2010). Serpentinization and associated hydrogen and methane fluxes at slow spreading ridges. In Rona, P. A., Devey, C. W., Dyment, J., & Murton, B. J. (Eds.), *Geophysical Monograph* (pp. 241–264). Washington, DC: American Geophysical Union. https://doi.org/10.1029/2008gm000760

Chalouan, A. (1986). *Les nappes Ghomarides (Rif septentrional, Maroc), un terrain varisque dans la chaîne alpine*. (PhD Thesis). Université Louis Pasteur.

Chalouan, A., & Michard, A. (2004). The Alpine Rif Belt (Morocco): A case of mountain building in a subduction-subduction-transform fault triple junction. *Pure and Applied Geophysics*, *161*, 489–519. https://doi.org/10.1007/978-3-0348-7899-9_3

Chalouan, A., Michard, A., Kadiri, K. E., Negro, F., Lamotte, D. F., de Soto, J. I., & Saddiqi, O. (2008). The Rif Belt. In Michard, A. (Ed.), *Continental evolution: The geology of Morocco* (pp. 203–302). Berlin, Heidelberg: Springer Berlin Heidelberg. https://doi.org/10.1007/978-3-540-77076-3_5

Clerc, C., Boulvais, P., Lagabrielle, Y., & de Saint Blanquat, M. (2013). Ophicalcites from the northern Pyrenean belt: A field, petrographic and stable isotope study. *International Journal of Earth Sciences*, *103*, 141–163. https://doi.org/10.1007/s00531-013-0927-z

Clerc, C., Lahfid, A., Monié, P., Lagabrielle, Y., Chopin, C., Poujol, M., et al. (2015). HT metamorphism during extreme thinning of the continental crust: A reappraisal of the North Pyrenean passive paleomargin. *Solid Earth*, *6*, 643–668. https://doi.org/10.5194/se-6-643-2015

Crespo-Blanc, A. (1995). Interference pattern of Miocene extensional systems in the Alpujarride Complex (N of Sierra Nevada, Betic Cordillera). *Geogaceta*, *17*, 140–142. https://doi.org/10.1016/0191-8141(95)e0044-d

Crespo-Blanc, A., & Campos, J. (2001). Structure and kinematics of the South Iberian paleomargin and its relationship with the Flysch Trough units: Extensional tectonics within the Gibraltar Arc fold-and-thrust belt (western Betics). *Journal of Structural Geology*, *23*(10), 1615–1630. https://doi.org/10.1016/s0191-8141(01)00012-8

Crespo-Blanc, A., Comas, M., & Balanyá, J. C. (2016). Clues for a Tortonian reconstruction of the Gibraltar Arc: Structural pattern, deformation diachronism and block rotations. *Tectonophysics*, *683*, 308–324. https://doi.org/10.1016/j.tecto.2016.05.045

Crespo-Blanc, A., & Frizon de Lamotte, D. (2006). Structural evolution of the external zones derived from the Flysch trough and the South Iberian and Maghrebian paleomargins around the Gibraltar arc: A comparative study. *Bulletin de la Societe Geologique de France*, *177*, 267–282. https://doi.org/10.2113/gssgfbull.177.5.267

Crespo-Blanc, A., Orozco, M., & Garcia-Dueñas, V. (1994). Extension versus compression during the Miocene tectonic evolution of the Betic chain. Late folding of normal fault systems. *Tectonics*, *13*, 78–88. https://doi.org/10.1029/93tc02231

Cuevas, J., Aldaya, F., Navarro-Vilá, F., & Tubía, J. M. (1990). Structure of the Alpujarrides on the southern and eastern border of the Sierra de Lújar. *Estudios Geológicos*, 209–216.

Cuevas, J., Esteban, J. J., & Tubía, J. M. (2006). Tectonic implications of the granite dyke swarm in the Ronda peridotites (Betic Cordilleras, Southern Spain). *Journal of the Geological Society*, *163*(4), 631–640. https://doi.org/10.1144/0016-764905-038

Darot, M. (1974). Cinematics of extrusion from mantle for peridotites of Sierre Bermeja (Serrania Ronda, Spain). *Comptes Rendus Hebdomadaires des Seances de l Academie des Sciences Serie D*, *278*, 1673–1676.

de Orueta, D. (1917). *Estudio geológico y petrográfico de la Serranía de Ronda*. Imprenta de J. Palacios.

Delchini, S., Lahfid, A., Plunder, A., & Michard, A. (2016). Applicability of the RSCM geothermometry approach in a complex tectono-metamorphic context: The Jebilet massif case study (Variscan Belt, Morocco). *Lithos*, *256–257*, 1–12. https://doi.org/10.1016/j.lithos.2016.04.007

del Olmo Sanz, A., de Macía, J. G. P., Aldaya Valverde, F., Campos Fernández, J., Chacón Montero, J., García Dueñas, V., et al. (1987). *Mapa Geológico de España, 1:50.000, hoja 1064 (Cortes de la Frontera)*. Instituto Geológico y Minero de España.

del Olmo Sanz, A., Moreno Serrano, F., Campos Fernández, J., Estevez, A., García Dueñas, V., García Rossell, L., et al. (1981). *Mapa Geológico de España, 1:50.000, hoja 1051 (Ronda)*. Instituto Geológico y Minero de España.

Dercourt, J., Ricou, L. E., & Vrielynck, B. (1993). *Atlas Tethys palaeoenvironmental maps: Explanatory note*.

Dercourt, J., Zonenshain, L. P., Ricou, L.-E., Kazmin, V. G., Le Pichon, X., Knipper, A. L., et al. (1986). Geological evolution of the Tethys belt from the Atlantic to the Pamirs since the LIAS. *Tectonophysics*, *123*, 241–315. https://doi.org/10.1016/0040-1951(86)90199-x

Dickey, J. S. (1970). Partial fusion products in Alpine peridotites: Serrania De La Ronda and other examples. *Minerological Society of American Special Paper*, *3*, 33–49.

Didon, J., Durand-Delga, M., & Kornprobst, J. (1973). Homologies geologiques entre les deux rives du detroit de Gibraltar. *Bulletin de la Societé géologique de France*, *S7-XV*, 77–105. https://doi.org/10.2113/gssgfbull.s7-xv.2.77

Doblas, M., & Oyarzun, R. (1989). "Mantle core complexes" and Neogene extensional detachment tectonics in the western Betic Cordilleras, Spain: An alternative model for the emplacement of the Ronda peridotite. *Earth and Planetary Science Letters*, *93*, 76–84. https://doi.org/10.1016/0012-821x(89)90185-4

Do Couto, D., Gorini, C., Jolivet, L., Lebret, N., Augier, R., Gumiaux, C (2016). Tectonic and stratigraphic evolution of the Western Alboran Sea Basin in the last 25Myrs. *Tectonophysics*, *677–678*, 280–311. https://doi.org/10.1016/j.tecto.2016.03.020

Durand-Delga, M. (1980). Le cadre structural de la Méditerranée occidentale. *Georogie des chaines alpines issues de la Tethys*, 67–85.

Durand-Delga, M., Rossi, P., Olivier, P., & Puglisi, D. (2000). Situation structurale et nature ophiolitique de roches basiques jurassiques associées aux flyschs maghrébins du Rif (Maroc) et de Sicile (Italie). *Comptes Rendus de l'Académie des Sciences-Series IIA-Earth and Planetary Science*, *331*, 29–38. https://doi.org/10.1016/s1251-8050(00)01378-1

Dürr, S. H. (1963). *Geologie der Serrania de Ronda und ihrer südwestlichen Ausläufer*. (PhD Thesis). University of Bonn.

Dürr, S. H. (1967). *Geologie der Serrania de Ronda und ihrer südwestlichen Ausläufer*. (PhD Thesis). Instituto di Geologica.

Egeler, C. G., & Simon, O. J. (1969a). Orogenic evolution of the Betic Zone (Betic Cordilleras, Spain), with emphasis on the nappe structures. *Geologie en Mijnbouw*, *48*, 296–305.

Egeler, C. G., & Simon, O. J. (1969b). Sur la tectonique de la Zone Bétique (Cordillères Bétiques, Espagne). Étude basée sur la recherche dans le secteur compris entre Almería y Vélez Rubio. *Verh Kon Ned Akad Wet Afd Natuurk*, *25*.
Esteban, J. J., Cuevas, J., Tubía, J. M., Liati, A., Seward, D., & Gebauer, D. (2007). Timing and origin of zircon-bearing chlorite schists in the Ronda peridotites (Betic Cordilleras, Southern Spain). *Lithos*, *99*(1–2), 121–135. https://doi.org/10.1016/j.lithos.2007.06.006
Esteban, J. J., Cuevas, J., Tubía, J. M., Sergeev, S., & Larionov, A. (2011). A revised Aquitanian age for the emplacement of the Ronda peridotites (Betic Cordilleras, southern Spain). *Geological Magazine*, *148*, 183–187. https://doi.org/10.1017/s0016756810000737
Esteban, J. J., Cuevas, J., Vegas, N., & Tubía, J. M. (2008). Deformation and kinematics in a melt-bearing shear zone from the Western Betic Cordilleras (Southern Spain). *Journal of Structural Geology*, *30*, 380–393. https://doi.org/10.1016/j.jsg.2007.11.010
Esteban, J. J., Sánchez-Rodríguez, L., Seward, D., Cuevas, J., & Tubía, J. M. (2004). The late thermal history of the Ronda area, southern Spain. *Tectonophysics*, *389*, 81–92. https://doi.org/10.1016/j.tecto.2004.07.050
Esteban, J. J., Tubía, J. M., Cuevas, J., Seward, D., Larionov, A., Sergeev, S., & Navarro-Vilá, F. (2013). Insights into extensional events in the Betic Cordilleras, southern Spain: New fission-track and U–Pb SHRIMP analyses. *Tectonophysics*, *603*, 179–188. https://doi.org/10.1016/j.tecto.2013.05.027
Faccenna, C., Piromallo, C., Crespo-Blanc, A., Jolivet, L., & Rossetti, F. (2004). Lateral slab deformation and the origin of the western Mediterranean arcs. *Tectonics*, *23*. https://doi.org/10.1029/2002tc001488
Feinberg, H., Saddiqi, O., & Michard, A. (1996). New constraints on the bending of the Gibraltar Arc from palaeomagnetism of the Ronda peridotites (Betic Cordilleras, Spain). *Special Publication—Geological Society of London*, *105*, 43–52. https://doi.org/10.1144/gsl.sp.1996.105.01.04
Flinch, J. F., Bally, A. W., & Wu, S. (1996). Emplacement of a passive-margin evaporitic allochthon in the Betic Cordillera of Spain. *Geology*, *24*, 67. https://doi.org/10.1130/0091-7613(1996)024<0067:eoapme>2.3.co;2
Frasca, G., Gueydan, F., & Brun, J.-P. (2015). Structural record of Lower Miocene westward motion of the Alboran Domain in the Western Betics, Spain. *Tectonophysics*, *657*, 1–20. https://doi.org/10.1016/j.tecto.2015.05.017
Frasca, G., Gueydan, F., Brun, J.-P., & Monié, P. (2016). Deformation mechanisms in a continental rift up to mantle exhumation. Field evidence from the western Betics, Spain. *Marine and Petroleum Geology*, *76*, 310–328. https://doi.org/10.1016/j.marpetgeo.2016.04.020
Frasca, G., Gueydan, F., Poujol, M., Brun, J.-P., Parat, F., Monié, P., et al. (2017). Fast switch from extensional exhumation to thrusting of the Ronda Peridotites (South Spain). *Terra Nova*, *29*, 117–126. https://doi.org/10.1111/ter.12255
Frizon de Lamotte, D., Andrieux, J. E. A. N., & Guezou, J. C. (1991). Cinematique des chevauchements neogenes dans l'Arc betico-rifain; discussion sur les modeles geodynamiques. *Bulletin de la Societe Geologique de France*, *162*(4), 611–626. https://doi.org/10.2113/gssgfbull.162.4.611
Gabalda, S., Beyssac, O., Jolivet, L., Agard, P., & Chopin, C. (2009). Thermal structure of a fossil subduction wedge in the Western Alps. *Terra Nova*, *21*, 28–34. https://doi.org/10.1111/j.1365-3121.2008.00849.x
Galindo-Zaldívar, J., Gonzalez-Lodeiro, F., & Jabaloy, A. (1989). Progressive extensional shear structures in a detachment contact in the Western Sierra Nevada (Betic Cordilleras, Spain). *Geodinamica Acta*, *3*, 73–85. https://doi.org/10.1080/09853111.1989.11105175
Garcia-Castellanos, D., Fernàndez, M., & Torne, M. (2002). Modeling the evolution of the Guadalquivir foreland basin (southern Spain). *Tectonics*, *21*, 91–917. https://doi.org/10.1029/2001tc001339
García-Dueñas, V., & Balanyá, J. C. (1986). Estructura y naturaleza del Arco de Gibraltar. *Maleo Bolletin Societa Geologica del Portugal*, *2*, 23.
García-Dueñas, V., Balanyá, J. C., & Martínez-Martínez, J. M. (1992). Miocene extensional detachments in the outcropping basement of the northern Alboran Basin (Betics) and their tectonic implications. *Geo-Marine Letters*, *12*, 88–95. https://doi.org/10.1007/bf02084917
García-Dueñas, V., Martínez, V., & Navarro-Vilá, F. (1986). *La zona de falla de Torres Cartas: Conjunto de fallas normales de bajo ángulo entre Nevado-Filabrides y Alpujarrides (Sierra Alhamilla, Béticas Orientales)*.
García-Hernández, M., López-Garrido, A. C., Rivas, P., Sanz de Galdeano, C., & Juan, A. (1980). Mesozoic palaeogeographic evolution of the external zones of the Betic Cordillera. *Geologie en Mijnbouw*, *59*, 155–168.
Garrido, C. J., & Bodinier, J.-L. (1999). Diversity of mafic rocks in the Ronda Peridotite: Evidence for pervasive melt-rock reaction during heating of subcontinental lithosphere by upwelling asthenosphere. *Journal of Petrology*, *40*, 729–754. https://doi.org/10.1093/petroj/40.5.729
Garrido, C. J., Gueydan, F., Booth-Rea, G., Précigout, J., Hidas, K., Padrón-Navarta, J. A., & Marchesi, C. (2011). Garnet lherzolite and garnet-spinel mylonite in the Ronda peridotite: Vestiges of Oligocene backarc mantle lithospheric extension in the western Mediterranean. *Geology*, *39*, 927–930. https://doi.org/10.1130/g31760.1
Gómez-Pugnaire, M. T., Nieto, F., Abad, I., Velilla, N., Garrido, C. J., Acosta-Vigil, A., et al. (2019). Alpine metamorphism in the Betic Internal Zones. In *The geology of Iberia: A geodynamic approach* (pp. 519–544). Cham: Springer. https://doi.org/10.1007/978-3-030-11295-0_13
González-Jiménez, J. M., Marchesi, C., Griffin, W. L., Gervilla, F., Belousova, E. A., Garrido, C. J., et al. (2017). Zircon recycling and crystallization during formation of chromite-and Ni-arsenide ores in the subcontinental lithospheric mantle (Serranía de Ronda, Spain). *Ore Geology Reviews*, *90*, 193–209. https://doi.org/10.1016/j.oregeorev.2017.02.012
Guerrera, F., Martín-Algarra, A., & Perrone, V. (1993). Late Oligocene-Miocene syn-/-late-orogenic successions in Western and Central Mediterranean Chains from the Betic Cordillera to the Southern Apennines. *Terra Nova*, *5*, 525–544. https://doi.org/10.1111/j.1365-3121.1993.tb00302.x
Guerrera, F., Martín-Martín, M., Perrone, V., & Tramontana, M. (2005). Tectono-sedimentary evolution of the southern branch of the Western Tethys (Maghrebian Flysch Basin and Lucanian Ocean): Consequences for Western Mediterranean geodynamics. *Terra Nova*, *17*, 358–367. https://doi.org/10.1111/j.1365-3121.2005.00621.x
Gueydan, F., Mazzotti, S., Tiberi, C., Cavin, R., & Villaseñor, A. (2019). Western Mediterranean subcontinental mantle emplacement by continental margin obduction. *Tectonics*, *38*(6), 2142–2157. https://doi.org/10.1029/2018tc005058
Gueydan, F., Pitra, P., Afiri, A., Poujol, M., Essaifi, A., & Paquette, J.-L. (2015). Oligo-Miocene thinning of the Beni Bousera peridotites and their Variscan crustal host rocks, Internal Rif, Morocco. *Tectonics*, *34*, 1244–1268. https://doi.org/10.1002/2014tc003769
Hernández-Pacheco, A. (1967). Estudio petrográfico y geoquímico del Macizo ultramáfico de Ojén (Málaga) 23. *Estudios Geológicos*.
Hidas, K., Booth-Rea, G., Garrido, C. J., Martínez-Martínez, J. M., Padrón-Navarta, J. A., Konc, Z., et al. (2013). Backarc basin inversion and subcontinental mantle emplacement in the crust: Kilometre-scale folding and shearing at the base of the proto-Alborán lithospheric mantle (Betic Cordillera, southern Spain). *Journal of the Geological Society*, *170*, 47–55. https://doi.org/10.1144/jgs2011-151
Homonnay, E., Corsini, M., Lardeaux, J. M., Romagny, A., Münch, P., Bosch, D., et al. (2018). Miocene crustal extension following thrust tectonic in the Lower Sebtides units (internal Rif, Ceuta Peninsula, Spain): Implication for the geodynamic evolution of the Alboran domain. *Tectonophysics*, *722*, 507–535. https://doi.org/10.1016/j.tecto.2017.11.028

Jabaloy, A., Galindo-Zaldívar, J., & González-Lodeiro, F. (1993). The Alpujárride-Nevado-Filábride extensional shear zone, Betic Cordillera, SE Spain. *Journal of Structural Geology*, *15*, 555–569. https://doi.org/10.1016/0191-8141(93)90148-4

Jabaloy-Sánchez, A., Gómez-Pugnaire, M. T., Padrón-Navarta, J. A., López Sánchez-Vizcaíno, V., & Garrido, C. J. (2015). Subduction- and exhumation-related structures preserved in metaserpentinites and associated metasediments from the Nevado–Filábride Complex (Betic Cordillera, SE Spain). *Tectonophysics*, *644–645*, 40–57. https://doi.org/10.1016/j.tecto.2014.12.022

Jammes, S., Manatschal, G., Lavier, L., & Masini, E. (2009). Tectonosedimentary evolution related to extreme crustal thinning ahead of a propagating ocean: Example of the western Pyrenees. *Tectonics*, *28*. https://doi.org/10.1029/2008tc002406

Johanesen, K., Platt, J. P., Kaplan, M. S., & Ianno, A. J. (2014). A revised thermal history of the Ronda peridotite, S. Spain: New evidence for excision during exhumation. *Earth and Planetary Science Letters*, *393*, 187–199. https://doi.org/10.1016/j.epsl.2014.01.024

Johanesen, K. E., & Platt, J. P. (2015). Rheology, microstructure, and fabric in a large scale mantle shear zone, Ronda Peridotite, southern Spain. *Journal of Structural Geology*, *73*, 1–17. https://doi.org/10.1016/j.jsg.2015.01.007

Jolivet, L., Augier, R., Faccenna, C., Negro, F., Rimmele, G., Agard, P., et al. (2008). Subduction, convergence and the mode of backarc extension in the Mediterranean region. *Bulletin de la Societe Geologique de France*, *179*, 525–550. https://doi.org/10.2113/gssgfbull.179.6.525

Jolivet, L., Faccenna, C., Goffé, B., Burov, E., & Agard, P. (2003). Subduction tectonics and exhumation of high-pressure metamorphic rocks in the Mediterranean orogens. *American Journal of Science*, *303*(5), 353–409. https://doi.org/10.2475/ajs.303.5.353

Kelemen, P. B., & Matter, J. (2008). In situ carbonation of peridotite for CO_2 storage. *Proceedings of the National Academy of Sciences*, *105*, 17295–17300. https://doi.org/10.1073/pnas.0805794105

Kirilova, M., Toy, V., Rooney, J. S., Giorgetti, C., Gordon, K. C., Collettini, C., & Takeshita, T. (2018). Structural disorder of graphite and implications for graphite thermometry. *Solid Earth*, *9*. https://doi.org/10.5194/se-9-223-2018

Klein, F., Bach, W., Humphris, S. E., Kahl, W.-A., Jons, N., Moskowitz, B., & Berquo, T. S. (2014). Magnetite in seafloor serpentinite–Some like it hot. *Geology*, *42*, 135–138. https://doi.org/10.1130/g35068.1

Klein, F., Bach, W., Jöns, N., McCollom, T., Moskowitz, B., & Berquó, T. (2009). Iron partitioning and hydrogen generation during serpentinization of abyssal peridotites from 15°N on the Mid-Atlantic Ridge. *Geochimica et Cosmochimica Acta*, *73*, 6868–6893. https://doi.org/10.1016/j.gca.2009.08.021

Klein, F., Bach, W., & McCollom, T. M. (2013). Compositional controls on hydrogen generation during serpentinization of ultramafic rocks. *Lithos*, *178*, 55–69. https://doi.org/10.1016/j.lithos.2013.03.008

Kornprobst, J. (1976). Signification structurale des peridotites dans l'orogene betico-rifain; arguments tires de l'etude des detritus observes dans les sediments paleozoiques. *Bulletin de la Societé géologique de France*, *7*, 607–618. https://doi.org/10.2113/gssgfbull.s7-xviii.3.607

Kornprobst, J., & Durand-Delga, M. (1985). *Carte géologique du Rif au 1: 50.000. Feuille de Tétouan*. Mém Serv Géol Maroc 292.

Kozur, H., Kampschuur, W., Mulder-Blanken, C. W. H., & Simon, O. J. (1974). Contribution to the Triassic ostracode faunas of the Betic Zone (southern Spain). *Scripta Geologica*, *23*, 1–56.

Lafuste, M. L. J., & Pavillon, M. J. (1976). Mise en evidence d'Eifélien daté au sein des terrains métamorphiques des zones internes des Cordillères Bétiques. Intérêt de ce nouveau repère stratigraphique. *Comptes Rendus de l'Académie des Sciences de Paris*, *283*, 1015–1018.

Lagabrielle, Y., & Bodinier, J.-L. (2008). Submarine reworking of exhumed subcontinental mantle rocks: Field evidence from the Lherz peridotites, French Pyrenees: Cretaceous exhumation of pyrenean mantle. *Terra Nova*, *20*, 11–21. https://doi.org/10.1111/j.1365-3121.2007.00781.x

Lagabrielle, Y., Labaume, P., & de Saint Blanquat, M. (2010). Mantle exhumation, crustal denudation, and gravity tectonics during Cretaceous rifting in the Pyrenean realm (SW Europe): Insights from the geological setting of the lherzolite bodies. *Tectonics*, *29*. https://doi.org/10.1029/2009tc002588

Lahfid, A., Beyssac, O., Deville, E., Negro, F., Chopin, C., & Goffé, B. (2010). Evolution of the Raman spectrum of carbonaceous material in low-grade metasediments of the Glarus Alps (Switzerland): RSCM in low-grade metasediments. *Terra Nova*, *22*, 354–360. https://doi.org/10.1111/j.1365-3121.2010.00956.x

Laurent, V., Lanari, P., Naïr, I., Augier, R., Lahfid, A., & Jolivet, L. (2018). Exhumation of eclogite and blueschist (Cyclades, Greece): Pressure–temperature evolution determined by thermobarometry and garnet equilibrium modelling. *Journal of Metamorphic Geology*, *36*(6), 769–798. https://doi.org/10.1111/jmg.12309

Lemoine, M., Tricart, P., & Boillot, G. (1987). Ultramafic and gabbroic ocean floor of the Ligurian Tethys (Alps, Corsica, Apennines): In search of a genetic imodel. *Geology*, *15*, 622. https://doi.org/10.1130/0091-7613(1987)15<622:uagofo>2.0.co;2

Lenoir, X. (2001). The recrystallization front of the Ronda Peridotite: Evidence for melting and thermal erosion of subcontinental lithospheric mantle beneath the Alboran Basin. *Journal of Petrology*, *42*, 141–158. https://doi.org/10.1093/petrology/42.1.141

Lonergan, L. (1993). Timing and kinematics of deformation in the Malaguide Complex, internal zone of the Betic Cordillera, southeast Spain. *Tectonics*, *12*, 460–476. https://doi.org/10.1029/92tc02507

Lonergan, L., & Platt, J. P. (1995). The Malaguide-Alpujarride boundary: A major extensional contact in the Internal Zone of the eastern Betic Cordillera, SE Spain. *Journal of Structural Geology*, *17*, 1655–1671. https://doi.org/10.1016/0191-8141(95)00070-t

Lonergan, L., & White, N. (1997). Origin of the Betic-Rif mountain belt. *Tectonics*, *16*, 504–522. https://doi.org/10.1029/96tc03937

Loomis, T. P. (1972). Contact metamorphism of Pelitic Rock by the Ronda ultramafic intrusion, Southern Spain. *The Geological Society of America Bulletin*, *83*, 2449. https://doi.org/10.1130/0016-7606(1972)83[2449:cmoprb]2.0.co;2

Loomis, T. P. (1975). Tertiary mantle diapirism, orogeny, and plate tectonics east of the Strait of Gibraltar. *American Journal of Science*, *275*, 1–30. https://doi.org/10.2475/ajs.275.1.1

Lundeen, M. T. (1978). Emplacement of the Ronda peridotite, Sierra Bermeja, Spain. *The Geological Society of America Bulletin*, *89*, 172. https://doi.org/10.1130/0016-7606(1978)89<172:eotrps>2.0.co;2

Malvoisin, B., Brunet, F., Carlut, J., Rouméjon, S., & Cannat, M. (2012). Serpentinization of oceanic peridotites: 2. Kinetics and processes of San Carlos olivine hydrothermal alteration. *Journal of Geophysical Research*, *117*, B04102. https://doi.org/10.1029/2011jb008842

Malvoisin, B., Carlut, J., & Brunet, F. (2012). Serpentinization of oceanic peridotites: 1. A high-sensitivity method to monitor magnetite production in hydrothermal experiments. *Journal of Geophysical Research*, *117*. https://doi.org/10.1029/2011jb008612

Manatschal, G., Sauter, D., Karpoff, A. M., Masini, E., Mohn, G., & Lagabrielle, Y. (2011). The Chenaillet Ophiolite in the French/Italian Alps: An ancient analogue for an Oceanic Core Complex? *Lithos*, *124*, 169–184. https://doi.org/10.1016/j.lithos.2010.10.017

Marchesi, C., Garrido, C. J., Bosch, D., Bodinier, J.-L., Hidas, K., Padrón-Navarta, J. A., & Gervilla, F. (2012). A late Oligocene suprasubduction setting in the westernmost Mediterranean revealed by intrusive pyroxenite dikes in the Ronda Peridotite (Southern Spain). *The Journal of Geology*, *120*, 237–247. https://doi.org/10.1086/663875

Martín-Algarra, A., O'Dogherty, L., Aguado, Merlo R., & Gursky, H. J. (1998). Estratigrafía, petrografía, y significado paleogeográfico de las radiolaritas jurásicas de tipo austroalpino de la unidad de las Nieves (Formación Parauta, Rondaides, Cordillera Bética Occidental). *Geogaceta*, 211–214.

Martín-Algarra, A. (1987). *Evolución geológica alpina del contacto entre las zonas Internas y las zonas externas de la Cordillera Bética*. (PhD Thesis). Universidad de Granada.
Martín-Algarra, A., & Estévez, A. (1984). La BrèChe de la Nava: DéPôT continental synchrone de la structuration pendant le MiocèNe inféRieur des zones internes de l'Ouest des CordillèRes Bétiques. *Comptes Rendus de l'AcadéMie de Sciences*, *299*, 463–466.
Martin, B., & Fyfe, W. S. (1970). Some experimental and theoretical observations on the kinetics of hydration reactions with particular reference to serpentinization. *Chemical Geology*, *6*, 185–202. https://doi.org/10.1016/0009-2541(70)90018-5
Martínez-Martínez, J. M., & Azañón, J. M. (1997). Mode of extensional tectonics in the southeastern Betics (SE Spain): Implications for the tectonic evolution of the peri-Alborán orogenic system. *Tectonics*, *16*, 205–225. https://doi.org/10.1029/97tc00157
Martínez-Martínez, J. M., Soto, J. I., & Balanyá, J. C. (2002). Orthogonal folding of extensional detachments: Structure and origin of the Sierra Nevada elongated dome (Betics, SE Spain). *Tectonics*, *21*. https://doi.org/10.1029/2001tc001283
Masini, E., Manatschal, G., Tugend, J., Mohn, G., & Flament, J.-M. (2014). The tectono-sedimentary evolution of a hyper-extended rift basin: The example of the Arzacq–Mauléon rift system (Western Pyrenees, SW France). *International Journal of Earth Sciences*, *103*, 1569–1596. https://doi.org/10.1007/s00531-014-1023-8
Massonne, H.-J. (2014). Wealth of P–T–t information in medium-high grade metapelites: Example from the Jubrique Unit of the Betic Cordillera, S Spain. *Lithos*, *208–209*, 137–157. https://doi.org/10.1016/j.lithos.2014.08.027
Mayhew, L. E., Ellison, E. T., McCollom, T. M., Trainor, T. P., & Templeton, A. S. (2013). Hydrogen generation from low-temperature water–rock reactions. *Nature Geoscience*, *6*, 478–484. https://doi.org/10.1038/ngeo1825
Mazzoli, S., & Martín-Algarra, A. (2011). Deformation partitioning during transpressional emplacement of a 'mantle extrusion wedge': The Ronda peridotites, western Betic Cordillera, Spain. *Journal of the Geological Society*, *168*, 373–382. https://doi.org/10.1144/0016-76492010-126
Mazzoli, S., Martín-Algarra, A., Reddy, S. M., Sánchez-Vizcaíno, V. L., Fedele, L., & Noviello, A. (2013). The evolution of the footwall to the Ronda subcontinental mantle peridotites: Insights from the Nieves Unit (western Betic Cordillera). *Journal of the Geological Society*, *170*, 385–402. https://doi.org/10.1144/jgs2012-105
McCollom, T. M., & Bach, W. (2009). Thermodynamic constraints on hydrogen generation during serpentinization of ultramafic rocks. *Geochimica et Cosmochimica Acta*, *73*, 856–875. https://doi.org/10.1016/j.gca.2008.10.032
McCollom, T. M., Klein, F., Robbins, M., Moskowitz, B., Berquó, T. S., Jöns, N., et al. (2016). Temperature trends for reaction rates, hydrogen generation, and partitioning of iron during experimental serpentinization of olivine. *Geochimica et Cosmochimica Acta*, *181*, 175–200. https://doi.org/10.1016/j.gca.2016.03.002
Mével, C. (2003). Serpentinization of abyssal peridotites at mid-ocean ridges. *Comptes Rendus Geoscience*, *335*, 825–852. https://doi.org/10.1016/j.crte.2003.08.006
Michard, A., Chalouan, A., Feinberg, H., Goffé, B., & Montigny, R. (2002). How does the Alpine belt end between Spain and Morocco. *Bulletin de la Societe Geologique de France*, *173*, 3–15. https://doi.org/10.2113/173.1.3
Michard, A., Negro, F., Saddiqi, O., Bouybaouene, M. L., Chalouan, A., Montigny, R., & Goffé, B. (2006). Pressure–temperature–time constraints on the Maghrebide mountain building: Evidence from the Rif–Betic transect (Morocco, Spain), Algerian correlations, and geodynamic implications. *Comptes Rendus Geoscience*, *338*(1–2), 92–114. https://doi.org/10.1016/j.crte.2005.11.011
Milliken, K. L., & Morgan, J. K. (1996). Chemical evidence for near-seafloor precipitation of calcite in serpentinites (site 897) and serpentinite breccias (site 899), Iberia Abyssal Plain. In Whitmarsh, R. B., Sawyer, D. S., Klaus, D. S., & Masson, D. G. (Eds.), *Proceedings of the Ocean Drilling Program. Scientific results*. https://doi.org/10.2973/odp.proc.sr.149.229.1996
Monie, P., Galindo-Zaldivar, J., Lodeiro, F. G., Goffe, B., & Jabaloy, A. (1991). 40Ar/39Ar geochronology of Alpine tectonism in the Betic Cordilleras (southern Spain). *Journal of the Geological Society*, *148*(2), 289–297.
Monié, P., Torres-Roldán, R. L., & García-Casco, A. (1994). Cooling and exhumation of the Western Betic Cordilleras, $^{40}Ar/^{39}Ar$ thermochronological constraints on a collapsed terrane. *Tectonophysics*, *238*, 353–379. https://doi.org/10.1016/0040-1951(94)90064-7
Moody, J. B. (1976). Serpentinization: A review. *Lithos*, *9*, 125–138. https://doi.org/10.1016/0024-4937(76)90030-x
Morishita, T., Arai, S., & Gervilla, F. (2001). High-pressure aluminous mafic rocks from the Ronda peridotite massif, southern Spain: Significance of sapphirine- and corundum-bearing mineral assemblages. *Lithos*, *57*, 143–161. https://doi.org/10.1016/s0024-4937(01)00036-6
Nakamura, Y., Oohashi, K., Toyoshima, T., Satish-Kumar, M., & Akai, J. (2015). Strain-induced amorphization of graphite in fault zones of the Hidaka metamorphic belt, Hokkaido, Japan. *Journal of Structural Geology*, *72*, 142–161. https://doi.org/10.1016/j.jsg.2014.10.012
Negro, F., Beyssac, O., Goffe, B., Saddiqi, O., & Bouybaouene, M. L. (2006). Thermal structure of the Alboran Domain in the Rif (northern Morocco) and the Western Betics (southern Spain). Constraints from Raman spectroscopy of carbonaceous material. *Journal of Metamorphic Geology*, *24*, 309–327. https://doi.org/10.1111/j.1525-1314.2006.00639.x
Obata, M. (1977). *Petrology and petrogenesis of the Ronda HT peridotite intrusion, southern Spain*. (PhD Thesis). MIT.
Obata, M. (1980). The Ronda Peridotite: Garnet-, Spinel-, and Plagioclase-Lherzolite facies and the P-T trajectories of a high-temperature mantle intrusion. *Journal of Petrology*, *21*, 533–572.
Obata, M., & Lundeen, M. (1979). *Geologic map of the Ronda ultramafic complex*. Geological Society of America Digital Maps and Chart Series.
O'Dogherty, L., Martín-Algarra, A., Gursky, H.-J., & Aguado, R. (2001). The Middle Jurassic radiolarites and pelagic limestones of the Nieves unit (Rondaide Complex, Betic Cordillera): Basin starvation in a rifted marginal slope of the western Tethys. *International Journal of Earth Sciences*, *90*, 831–846.
Osete, M. L., Freeman, R., & Vegas, R. (1988). Preliminary palaeomagnetic results from the Subbetic Zone (Betic Cordillera, southern Spain): Kinematic and structural implications. *Physics of the Earth and Planetary Interiors*, *52*(3–4), 283–300. https://doi.org/10.1016/0031-9201(88)90121-5
Pedrera, A., Luque-Espinar, J. A., Martos-Rosillo, S., Pardo-Igúzquiza, E., Durán-Valsero, J. J., Martínez-Moreno, F., & Guardiola-Albert, C. (2015). Structural controls on karstic conduits in a collisional orogen (Sierra de las Nieves, Betic Cordillera, S Spain). *Geomorphology*, *238*, 15–26. https://doi.org/10.1016/j.geomorph.2015.02.008
Pedrera, A., Ruiz-Constán, A., García-Senz, J., Azor, A., Marín-Lechado, C., Ayala, C., et al. (2020). Evolution of the South-Iberian paleomargin: From hyperextension to continental subduction. *Journal of Structural Geology*, *138*. https://doi.org/10.1016/j.jsg.2020.104122
Picazo, S., Cannat, M., Delacour, A., Escartín, J., Rouméjon, S., & Silantyev, S. (2012). Deformation associated with the denudation of mantle-derived rocks at the Mid-Atlantic Ridge 13°–15°N: The role of magmatic injections and hydrothermal alteration. *Geochemistry, Geophysics, Geosystems*, *13*. https://doi.org/10.1029/2012GC004121
Piles Mateo, E., Chamon Cobos, C., Estevez Gonzales, C., Crespo, V., Aguilar, M., & Reyes, K. L. (1973). *Marbella, Mapa Geologico de España, escala 1:50.000, 1065*. Instituto Geológico y Minero de España.

Platt, J. P. (1986). Dynamics of orogenic wedges and the uplift of high-pressure metamorphic rocks. *The Geological Society of America Bulletin*, *97*, 1037. https://doi.org/10.1130/0016-7606(1986)97<1037:doowat>2.0.co;2
Platt, J. P., Anczkiewicz, R., Soto, J. I., Kelley, S. P., & Thirlwall, M. (2006). Early Miocene continental subduction and rapid exhumation in the western Mediterranean. *Geology*, *34*(11), 981–984. https://doi.org/10.1130/g22801a.1
Platt, J. P., Argles, T. W., Carter, A., Kelley, S. P., Whitehouse, M. J., & Lonergan, L. (2003). Exhumation of the Ronda peridotite and its crustal envelope: Constraints from thermal modelling of a P–T–time array. *Journal of the Geological Society*, *160*, 655–676. https://doi.org/10.1144/0016-764902-108
Platt, J. P., Behr, W. M., Johanesen, K., & Williams, J. R. (2013). The Betic-Rif arc and its orogenic hinterland: A review. *Annual Review of Earth and Planetary Sciences*, *41*, 313–357. https://doi.org/10.1146/annurev-earth-050212-123951
Platt, J. P., & Behrmann, J. H. (1986). Structures and fabrics in a crustal-scale shear zone, Betic Cordillera, SE Spain. *Journal of Structural Geology*, *8*, 15–33. https://doi.org/10.1016/0191-8141(86)90014-3
Platt, J. P., Kelley, S. P., Carter, A., & Orozco, M. (2005). Timing of tectonic events in the Alpujárride Complex, Betic Cordillera, southern Spain. *Journal of the Geological Society*, *162*, 451–462. https://doi.org/10.1144/0016-764903-039
Platt, J. P., Soto, J. I., Whitehouse, M. J., Hurford, A. J., & Kelley, S. P. (1998). Thermal evolution, rate of exhumation, and tectonic significance of metamorphic rocks from the floor of the Alboran extensional basin, western Mediterranean. *Tectonics*, *17*(5), 671–689. https://doi.org/10.1029/98tc02204
Platt, J. P., & Vissers, R. L. M. (1989). Extensional collapse of thickened continental lithosphere: A working hypothesis for the Alboran Sea and Gibraltar arc. *Geology*, *17*, 540. https://doi.org/10.1130/0091-7613(1989)017<0540:ecotcl>2.3.co;2
Platt, J. P., & Whitehouse, M. J. (1999). Early Miocene HT metamorphism and rapid exhumation in the Betic Cordillera (Spain): Evidence from U–Pb zircon ages. *Earth and Planetary Science Letters*, *171*(4), 591–605. https://doi.org/10.1016/s0012-821x(99)00176-4
Platzman, E., & Lowrie, W. (1992). Paleomagnetic evidence for rotation of the Iberian Peninsula and the external Betic Cordillera, Southern Spain. *Earth and Planetary Science Letters*, *108*, 45–60. https://doi.org/10.1016/0012-821x(92)90059-5
Platzman, E. S., Platt, J. P., & Olivier, P. (1993). Palaeomagnetic rotations and fault kinematics in the Rif Arc of Morocco. *Journal of the Geological Society*, *150*, 707–718. https://doi.org/10.1144/gsjgs.150.4.0707
Plunder, A., Agard, P., Dubacq, B., Chopin, C., & Bellanger, M. (2012). How continuous and precise is the record of P-T paths? Insights from combined thermobarometry and thermodynamic modelling into subduction dynamics (Schistes Lustrés, W. Alps). *Journal of Metamorphic Geology*, *30*, 323–346. https://doi.org/10.1111/j.1525-1314.2011.00969.x
Précigout, J., Gueydan, F., Gapais, D., Garrido, C. J., & Essaifi, A. (2007). Strain localisation in the subcontinental mantle—A ductile alternative to the brittle mantle. *Tectonophysics*, *445*, 318–336. https://doi.org/10.1016/j.tecto.2007.09.002
Précigout, J., Gueydan, F., Garrido, C. J., Cogné, N., & Booth-Rea, G. (2013). Deformation and exhumation of the Ronda peridotite (Spain). *Tectonics*, *32*, 1011–1025. https://doi.org/10.1002/tect.20062
Priem, H. N. A., Boelrijk, N. A. I. M., Hebeda, E. H., Oen, I. S., Verdurmen, E. A. T., & Verschure, R. H. (1979). Isotopic dating of the emplacement of the ultramafic masses in the Serrania de Ronda, Southern Spain. *Contributions to Mineralogy and Petrology*, *70*, 103–109. https://doi.org/10.1007/bf00371876
Puga, E., Fanning, M., Díaz de Federico, A., Nieto, J. M., Beccaluva, L., Bianchini, G., & Díaz Puga, M. A. (2011). Petrology, geochemistry and U–Pb geochronology of the Betic Ophiolites: Inferences for Pangaea break-up and birth of the westernmost Tethys Ocean. *Lithos*, *124*, 255–272. https://doi.org/10.1016/j.lithos.2011.01.002
Reuber, I., Michard, A., Chalouan, A., Juteau, T., & Jermoumi, B. (1982). Structure and emplacement of the Alpine-type peridotites from Beni Bousera, Rif, Morocco: A polyphase tectonic interpretation. *Tectonophysics*, *82*, 231–251. https://doi.org/10.1016/0040-1951(82)90047-6
Rossetti, F., Lucci, F., Theye, T., Bouybaouenne, M., Gerdes, A., Opitz, J., et al. (2020). Hercynian anatexis in the envelope of the Beni Bousera peridotites (Alboran Domain, Morocco): Implications for the tectono-metamorphic evolution of the deep crustal roots of the Mediterranean region. *Gondwana Research*, *83*. https://doi.org/10.1016/j.gr.2020.01.020
Rossetti, F., Theye, T., Lucci, F., Bouybaouene, M. L., Dini, A., Gerdes, A., et al. (2010). Timing and modes of granite magmatism in the core of the Alboran Domain, Rif chain, northern Morocco: Implications for the Alpine evolution of the western Mediterranean. *Tectonics*, *29*. https://doi.org/10.1029/2009tc002487
Ruiz-Cruz, M. D., & Sanz de Galdeano, C. (2014). Garnet variety and zircon ages in UHP meta-sedimentary rocks from the Jubrique zone (Alpujárride Complex, Betic Cordillera, Spain): Evidence for a pre-Alpine emplacement of the Ronda peridotite. *International Geology Review*, *56*, 845–868. https://doi.org/10.1080/00206814.2014.904759
Sánchez-Rodríguez, L., & Gebauer, D. (2000). Mesozoic formation of pyroxenites and gabbros in the Ronda area (southern Spain), followed by Early Miocene subduction metamorphism and emplacement into the middle crust: U–Pb sensitive high-resolution ion microprobe dating of zircon. *Tectonophysics*, *316*, 19–44.
Sánchez-Vizcaíno, V. L., Rubatto, D., Gómez-Pugnaire, M. T., Trommsdorff, V., & Müntener, O. (2001). Middle Miocene high-pressure metamorphism and fast exhumation of the Nevado-Filábride Complex, SE Spain. *Terra Nova*, *13*(5), 327–332. https://doi.org/10.1046/j.1365-3121.2001.00354.x
Sanz de Galdeano, C., & Andreo, B. (1995). Structure of Sierra Blanca (Alpujarride Complex, west of the Betic Cordillera). *Estudios geológicos*, *51*(1–2), 43–55. https://doi.org/10.3989/egeol.95511-2282
Sanz de Galdeano, C., & Ruiz Cruz, M. (2016). Late Palaeozoic to Triassic formations unconformably deposited over the Ronda peridotites (Betic Cordilleras): Evidence for their Variscan time of crustal emplacement. *Estud. Geológicos*, *72*, e043. https://doi.org/10.3989/egeol.42046.368
Sanz de Galdeano, C., & Vera, J. A. (1992). Stratigraphic record and paleogeographical context of the Neogene basins in the Betic Cordillera, Spain. *Basin Research*, *4*, 21–36. https://doi.org/10.1111/j.1365-2117.1992.tb00040.x
Sanz de Galdeano, C. S. (2017). Implication of the geology of the Guadaiza and Verde valleys (Malaga Province, Betic Cordillera) on the position of the Ronda peridotites and the structure of the Alpujárride Complex. *Boletin Geologico y Minero*, *128*(4), 989–1006. https://doi.org/10.21701/bolgeomin.128.4.006
Schwarzenbach, E. M., Früh-Green, G. L., Bernasconi, S. M., Alt, J. C., & Plas, A. (2013). Serpentinization and carbon sequestration: A study of two ancient peridotite-hosted hydrothermal systems. *Chemical Geology*, *351*, 115–133. https://doi.org/10.1016/j.chemgeo.2013.05.016
Sosson, M., Morrillon, A. C., Bourgois, J., Féraud, G., Poupeau, G., & Saint-Marc, P. (1998). Late exhumation stages of the Alpujarride Complex (western Betic Cordilleras, Spain): New thermochronological and structural data on Los Reales and Ojen nappes. *Tectonophysics*, *285*(3–4), 253–273. https://doi.org/10.1016/s0040-1951(97)00274-6
Soustelle, V., Tommasi, A., Bodinier, J. L., Garrido, C. J., & Vauchez, A. (2009). Deformation and reactive melt transport in the mantle lithosphere above a large-scale partial melting domain: The Ronda Peridotite Massif, Southern Spain. *Journal of Petrology*, *50*, 1235–1266. https://doi.org/10.1093/petrology/egp032

Spakman, W., & Wortel, R. (2004). A tomographic view on western Mediterranean geodynamics. In *The TRANSMED atlas. The Mediterranean region from crust to mantle* (pp. 31–52). Berlin, Heidelberg: Springer. https://doi.org/10.1007/978-3-642-18919-7_2

Stampfli, G. M. (2000). Tethyan oceans. *Geological Society of London Special Publications*, *173*, 1–23. https://doi.org/10.1144/gsl.sp.2000.173.01.01

Streit, E., Kelemen, P., & Eiler, J. (2012). Coexisting serpentine and quartz from carbonate-bearing serpentinized peridotite in the Samail Ophiolite, Oman. *Contributions to Mineralogy and Petrology*, *164*, 821–837. https://doi.org/10.1007/s00410-012-0775-z

Torres-Roldán, R. L. (1979). The tectonic subdivision of the Betic Zone (Betic Cordilleras, southern Spain); its significance and one possible geotectonic scenario for the westernmost Alpine Belt. *American Journal of Science*, *279*, 19–51. https://doi.org/10.2475/ajs.279.1.19

Tubía, J. M. (1994). The Ronda peridotites (Los Reales nappe): An example of the relationship between lithospheric thickening by oblique tectonics and late extensional deformation within the Betic Cordillera (Spain). *Tectonophysics*, *238*, 381–398. https://doi.org/10.1016/0040-1951(94)90065-5

Tubía, J. M., & Cuevas, J. (1986). HT emplacement of the Los Reales peridotite nappe (Betic Cordillera, Spain). *Journal of Structural Geology*, *8*, 473–482. https://doi.org/10.1016/0191-8141(86)90064-7

Tubía, J. M., Cuevas, J., & Esteban, J. J. (2004). Tectonic evidence in the Ronda peridotites, Spain, for mantle diapirism related to delamination. *Geology*, *32*, 941. https://doi.org/10.1130/g20869.1

Tubía, J. M., Cuevas, J., & Esteban, J. J. (2013). Localization of deformation and kinematic shift during the hot emplacement of the Ronda peridotites (Betic Cordilleras, southern Spain). *Journal of Structural Geology*, *50*, 148–160. https://doi.org/10.1016/j.jsg.2012.06.010

Tubía, J. M., Cuevas, J., Esteban, J. J., & Ibarguchi, G. (2009). Remnants of a Mesozoic rift in a subducted terrane of the Alpujarride Complex (Betic Cordilleras, southern Spain). *The Journal of Geology*, *117*(1), 71–87. https://doi.org/10.1086/593322

Tubía, J. M., Cuevas, J., & Ibarguchi, J. G. (1997). Sequential development of the metamorphic aureole beneath the Ronda peridotites and its bearing on the tectonic evolution of the Betic Cordillera. *Tectonophysics*, *279*, 227–252. https://doi.org/10.1016/s0040-1951(97)00124-8

Tubía, J. M., Cuevas, J., Navarro-Vilá, F., Alvarez, F., & Aldaya, F. (1992). Tectonic evolution of the Alpujárride Complex (Betic Cordillera, southern Spain). *Journal of Structural Geology*, *14*, 193–203. https://doi.org/10.1016/0191-8141(92)90056-3

Tubía, J. M., Navarro Villa, F., & Cuevas, J. (1991). La evolución tectonometamórfica del Manto de Los Reales y el Maláguide, al oeste de Málaga. *Geogaceta*, *10*, 141–143.

Van der Wal, D., & Bodinier, J.-L. (1996). Origin of the recrystallisation front in the Ronda peridotite by km-scale pervasive porous melt flow. *Contributions to Mineralogy and Petrology*, *122*, 387–405. https://doi.org/10.1007/s004100050135

Van der Wal, D., & Vissers, R. L. M. (1993). Uplift and emplacement of upper mantle rocks in the western Mediterranean. *Geology*, *21*, 1119. https://doi.org/10.1130/0091-7613(1993)021<1119:uaeoum>2.3.co;2

Van der Wal, D., & Vissers, R. L. M. (1996). Structural Petrology of the Ronda Peridotite, SW Spain: Deformation History. *Journal of Petrology*, *37*, 23–43. https://doi.org/10.1093/petrology/37.1.23

van Hinsbergen, D. J. J., Vissers, R. L. M., & Spakman, W. (2014). Origin and consequences of western Mediterranean subduction, rollback, and slab segmentation. *Tectonics*, *33*, 393–419. https://doi.org/10.1002/2013tc003349

Varas-Reus, M. I., Garrido, C. J., Marchesi, C., Bosch, D., Acosta-Vigil, A., Hidas, K., et al. (2017). Sr-Nd-Pb isotopic systematics of crustal rocks from the western Betics (S. Spain): Implications for crustal recycling in the lithospheric mantle beneath the westernmost Mediterranean. *Lithos*, *276*, 45–61. https://doi.org/10.1016/j.lithos.2016.10.003

Vauchez, A., & Garrido, C. J. (2001). Seismic properties of an asthenospherized lithospheric mantle: Constraints from lattice preferred orientations in peridotite from the Ronda massif. *Earth and Planetary Science Letters*, *192*, 235–249. https://doi.org/10.1016/s0012-821x(01)00448-4

Vauchez, A., & Nicolas, A. (1991). Mountain building: Strike-parallel motion and mantle anisotropy. *Tectonophysics*, *185*, 183–201. https://doi.org/10.1016/0040-1951(91)90443-v

Villasante-Marcos, V., Osete, M. L., Gervilla, F., & García-Dueñas, V. (2003). Palaeomagnetic study of the Ronda peridotites (Betic Cordillera, Southern Spain). *Tectonophysics*, *377*, 119–141. https://doi.org/10.1016/j.tecto.2003.08.023

Vissers, R. L. (2012). André Dumont medallist lecture 2011: Extension in a convergent tectonic setting: A lithospheric view on the Alboran system of SW Europe. *Geologica Belgica*.

Vissers, R. L. M., Platt, J. P., & Van der Wal, D. (1995). Late orogenic extension of the Betic Cordillera and the Alboran Domain: A lithospheric view. *Tectonics*, *14*, 786–803. https://doi.org/10.1029/95tc00086

Vitale Brovarone, A., Beyssac, O., Malavieille, J., Molli, G., Beltrando, M., & Compagnoni, R. (2013). Stacking and metamorphism of continuous segments of subducted lithosphere in a high-pressure wedge: The example of Alpine Corsica (France). *Earth-Science Reviews*, *116*, 35–56. https://doi.org/10.1016/j.earscirev.2012.10.003

Weijermars, R. (1991). Geology and tectonics of the Betic Zone, SE Spain. *Earth-Science Reviews*, *31*, 153–236. https://doi.org/10.1016/0012-8252(91)90019-c

Weijermars, R., Roep, T. B., van dan Eeckhout, B., Postma, G., & Kleverlaan, K. (1985). Uplift history of a Betic fold nappe inferred from Neogene-Quaternary sedimentation and tectonics (in the Sierra Alhamilla and Almeria, Sorbas and Tabernas Basins of the Betic Cordilleras, SE Spain). *Geologie en Mijnbouw*, *64*, 397–411.

Whitehouse, M. J., & Platt, J. P. (2003). Dating high-grade metamorphism—Constraints from rare-earth elements in zircon and garnet. *Contributions to Mineralogy and Petrology*, *145*(1), 61–74. https://doi.org/10.1007/s00410-002-0432-z

Whitney, D. L., & Evans, B. W. (2010). Abbreviations for names of rock-forming minerals. *American Mineralogist*, *95*(1), 185–187. https://doi.org/10.2138/am.2010.3371

Williams, J. R., & Platt, J. P. (2018). A new structural and kinematic framework for the Alborán Domain (Betic–Rif arc, western Mediterranean orogenic system). *Journal of the Geological Society*, *175*(3), 465–496. https://doi.org/10.1144/jgs2017-086

Wopenka, B., & Pasteris, J. D. (1993). Structural characterization of kerogens to granulite-facies graphite: Applicability of Raman microprobe spectroscopy. *American Mineralogist*, *78*, 533–557.

Zeck, H., Albat, F., Hansen, B., Torres-Roldán, R., Garciá-Casco, A., & Martín-Algarra, A. (1989). A 21 ± 2 Ma age for the termination of the ductile alpine deformation in the internal zone of the betic cordilleras, South Spain. *Tectonophysics*, *169*, 215–220. https://doi.org/10.1016/0040-1951(89)90196-0

Zeck, H. P., Monié, P., Villa, I., & Hansen, B. T. (1990). Mantle diapirism in the W-Mediterranean and high rates of regional uplift, denudation and cooling. In *Symposium on diapirism* (pp. 403–422).

Zeck, H. P., & Williams, I. S. (2001). Hercynian metamorphism in nappe core complexes of the Alpine Betic–Rif belt, western Mediterranean—A SHRIMP zircon study. *Journal of Petrology*, *42*(7), 1373–1385. https://doi.org/10.1093/petrology/42.7.1373